JAERI-Research
2000-062

STUDY ON NATURAL CONVECTION HEAT TRANSFER IN VERTICAL ANNULAR SPACE OF A DOUBLE COAXIAL CYLINDER

February 2001

Yoshitomo INABA and Tetsuaki TAKEDA

日本原子力研究所
Japan Atomic Energy Research Institute

本レポートは，日本原子力研究所が不定期に公刊している研究報告書です。
入手の問合わせは，日本原子力研究所研究情報部研究情報課（〒319-1195　茨城県那珂郡東海村）あて，お申し越しください。なお，このほかに財団法人原子力弘済会資料センター（〒319-1195　茨城県那珂郡東海村日本原子力研究所内）で複写による実費頒布をおこなっております。

This report is issued irregularly.
Inquiries about availability of the reports should be addressed to Research Information Division, Department of Intellectual Resources, Japan Atomic Energy Research Institute, Tokai-mura, Naka-gun, Ibaraki-ken, 319-1195, Japan.

編集兼発行　　日本原子力研究所

JAERI-Research 2000-062

Study on Natural convection Heat Transfer in Vertical Annular Space of a Double Coaxial Cylinder

Yoshitomo INABA and Tetsuaki TAKEDA

Department of Advanced Nuclear Heat Technology
Oarai Research Establishment
Japan Atomic Energy Research Institute
Oarai-machi, Higashiibaraki-gun, Ibaraki-ken

(Received November 22, 2000)

Water cooling panels are adopted as a vessel cooling system of a high temperature-engineering test reactor (HTTR) to cool the reactor core indirectly by natural convection and thermal radiation. In this study, we carried out experiments on natural convection heat transfer coupled with thermal radiation in vertical annular space of a double coaxial cylinder in order to investigate heat transfer characteristics in vertical annular space between the reactor pressure vessel and the cooling panels of the HTTR. In the present experiments, Rayleigh number based on the width of the vertical space was set to be $6.8\times10^5<Ra<1.8\times10^6$ for helium and $4.2\times10^7<Ra<1.0\times10^8$ for nitrogen. This report described about the heat transfer coefficient of natural convection in the vertical space and the effect of thermal radiation on the transferred heat. As a result, a heat transfer coefficient of natural convection coupled with thermal radiation was obtained as functions of Rayleigh number, aspect ratio of the space, temperature and emissivities on the heated and cooled walls. In addition to the experiments, numerical analyses were performed on the combined phenomena of natural convection and thermal radiation in the space. The numerical results were in good agreement with the experimental ones regarding the temperature on the heated and cooled walls.

Keywords: Natural Convection, Thermal Radiation, Emissivity, Heat Transfer, Vertical Annular Space, Double Coaxial Cylinder, Experiment, Numerical Analysis, HTTR, Vessel Cooling System

同心二重円筒容器内の自然対流熱伝達に関する研究

日本原子力研究所大洗研究所核熱利用研究部
稲葉　良知・武田　哲明

(2000年11月22日受理)

高温ガス炉の炉容器冷却システムの1つに、水による冷却パネルを用い、自然対流と熱放射により間接的に炉心を冷却するシステムがある。高温工学試験研究炉（HTTR）においても、このシステムが採用されている。本研究では、HTTRの原子炉圧力容器－冷却パネル間の熱伝達特性を調べるため、内筒を加熱、外筒を水により冷却した同心二重円筒容器内の熱放射を伴う自然対流熱伝達に関する実験を行った。実験において、加熱壁面－冷却壁面間距離を代表長さとしたレイレー数は、ヘリウムに対して$6.8\times10^5<Ra<1.8\times10^6$、窒素に対して$4.2\times10^7<Ra<10^8$となった。試験空間内の自然対流と熱放射の効果について調べ、その結果熱放射を伴う自然対流熱伝達の相関式をレイレー数、試験空間のアスペクト比、加熱壁面・冷却壁面温度及び熱放射率の関数として得た。また実験を模擬した数値解析を行い、実験結果に対する解析の妥当性を評価したところ、両者は比較的良く一致した。

大洗研究所　〒311-1394　茨城県東茨城郡大洗町成田町新堀3607

Contents

目　次

1. Introduction

In Japan Atomic Energy Research Institute, the High Temperature-engineering Test Reactor (HTTR) was constructed to develop of High Temperature Gas-cooled Reactor (HTGR) technologies, to advance the HTGR and to study on advanced high temperature engineering and it went first critical in November 1998. The HTTR is the helium gas cooled reactor moderated by graphite, rated at thermal power of 30MW at reactor coolant outlet temperature of 850°C for case of rated operation or 950°C for case of high temperature test operation. A Vessel Cooling System (VCS) adopted for the HTTR is an indirect reactor core cooling system using water cooling panels and the system cools the reactor core indirectly by natural convection of air and thermal radiation. A Reactor Pressure Vessel (RPV) and a biological shielding concrete are cooled by the cooling panels during normal operation. The cooling panels also cool the reactor core under a no forced-cooling condition such as a primary pipe rupture accident. Therefore, it is important to clarify heat transfer characteristics in space between the RPV and the cooling panels. The RPV surface temperature rises 400°C in the rated operation. As a few gratings are installed between the RPV and the cooling panels, the heat transfer characteristics will be complicated in that space. A cross sectional view of the HTTR and the VCS is shown in Fig. 1.

In the HTTR design, an amount of heat removed by the VCS has been evaluated conservatively in terms of safety. However, it is necessary to evaluate quantitatively the amount of removed heat from the results obtained by the power-rise and the safety demonstration tests of the HTTR. Heat transfer characteristics in the space between the RPV and the cooling panels will be important in terms of the evaluation of the VCS performance. The RPV heated by the decay heat will be cooled by natural convection of air and thermal radiation. An amount of heat transported by thermal radiation increases with the temperature of the RPV and it depends not only on the geometry of the system but also on the emissivity of the wall surface. On the other hand, the amount of the heat transferred by natural convection depends on a flow in the vertical enclosure having one side heated wall and the other side cooled wall. Therefore, it is difficult to estimate quantitatively the amount of those heat.

We had already reported upon experiments on natural convection coupled with thermal radiation in a vertical enclosure of a double coaxial cylinder with an air cooling system in a previous report[1]. Maximum temperature in the experiments with the air cooling system was set to be lower than the present experiments with a water cooling system. In this study, we carry out experiments on natural convection heat transfer coupled with thermal radiation in vertical annular space of a double coaxial cylinder in order to investigate heat transfer characteristics in a vertical space between the RPV and the water cooling panels of the HTTR. This report describes a natural convection heat transfer in the vertical space, the effect of thermal radiation on the transferred heat, and the relationship between Nusselt number and Rayleigh number in that space. In addition to the

experiments, numerical analyses are performed on the combined phenomena of natural convection and thermal radiation in the space. The numerical results are compared with the experimental ones regarding the temperature on the heated and cooled walls.

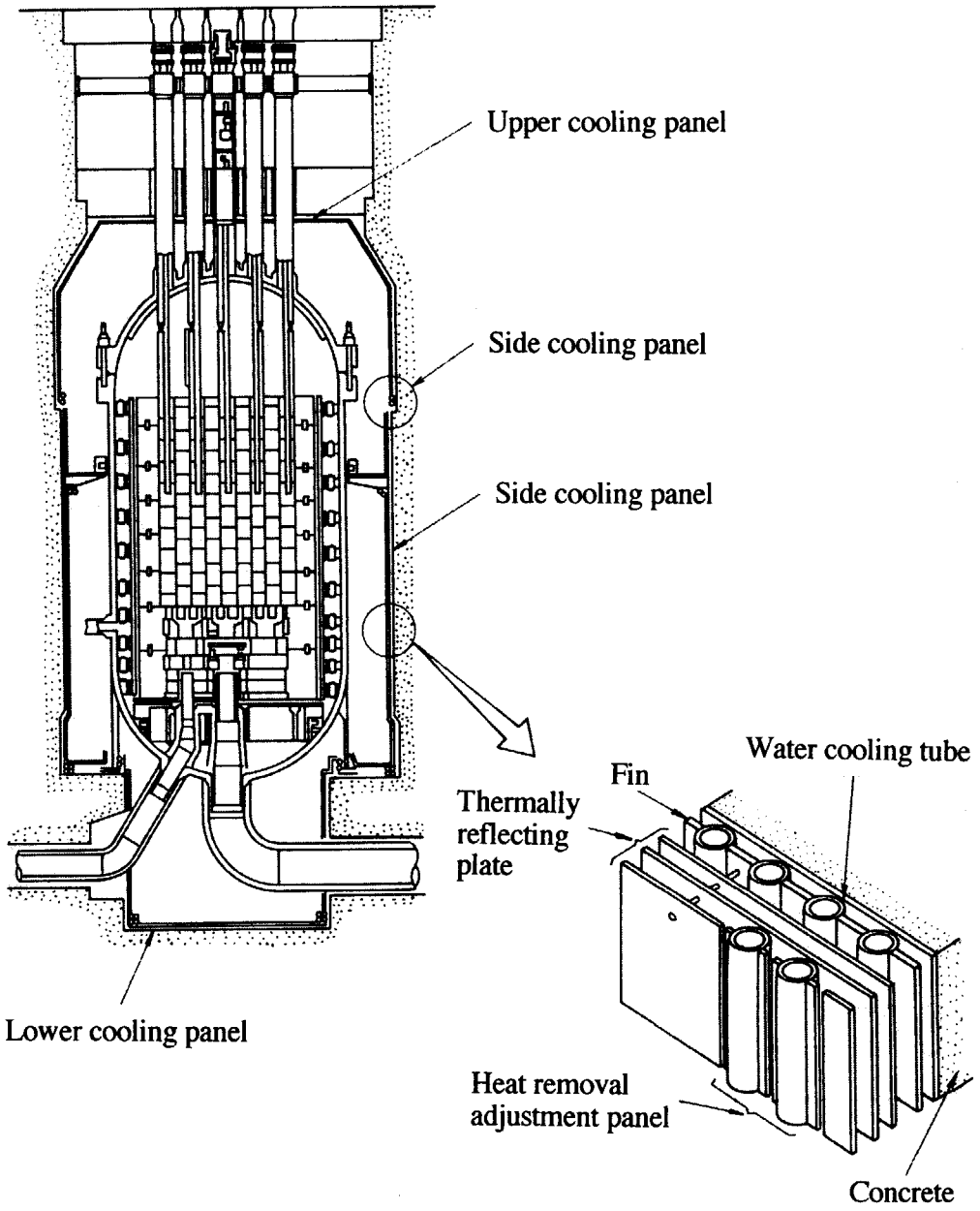

Fig. 1 Cross sectional view of the HTTR and the VCS.

2. Experiment on Natural Convection Coupled with Thermal Radiation

2.1 Purpose of Experiment

The object of the present experiments is to grasp the basic characteristics of heat transfer under the condition of natural convection coupled with thermal radiation in the vertical space. Main purposes of the experiments are listed as follows:

(1) Experiment on heat transfer by thermal radiation without natural convection.

(2) Experiment on heat transfer by natural convection coupled with thermal radiation.

(3) Investigations of relationship between the Nusselt number and the Rayleigh number of natural convection coupled with thermal radiation in the vertical space.

2.2 Experimental Apparatus

Figures 2 through 4 show schematic drawings of an experimental apparatus simulating the vertical space between the RPV and the water cooling panels of the HTTR. The experimental apparatus consists of a heating cylinder including electric heaters, a cooling cylinder and top and bottom disks. The heating and cooling cylinders are modeled on the RPV and the cooling panels. Height of heating section and the outer diameter of the heating cylinder are 1000mm and 318.5mm, respectively. Height of the cooling cylinder and the inner diameter are 1140mm and 900mm, respectively. Height of the test section is 998mm. The aspect ratio of the test section is 3.4. A test section is closed by the top and bottom disks. Specification of the experimental apparatus is described as below:

(1) Test section of experimental apparatus

The test section of the experimental apparatus is composed of the heating cylinder, the cooling cylinder and the top and bottom disks. The heating cylinder is made of stainless steel and ceramics, and it contains coiled heater lines. The heating section is divided into four parts. The central part of the heating section is heated by two main heaters having respectively 10kW capacity. The upper and lower part of the heating section is heated by two compensation heaters having respectively 3kW capacity. The surface temperature of the heating cylinder can be heated up to 700°C. The heating cylinder is hanged from the upper section to absorb a thermal expansion of the cylinder. The cooling cylinder is made of a stainless steel. Water cooling pipes made of copper are attached on the outside surface of the cooling cylinder, which is cooled by the cooling pipes. The outer diameter of the cooling pipe is 15.9mm and the number of cooling pipes is 175. The maximum flow rate of the cooling water is about 15*l*/s.

The test section is closed annular space and it is constructed by installing two disks for the top and bottom of the cooling cylinder. The top and bottom disks are made of stainless steel and its

diameter is about 1100mm. The top disk has flanges for taking out thermocouple lines and heater lines, and it has a pressure gauge and a Pirani gauge. A water cooling pipe is attached on the outer surface of the top disk. The bottom disk has flanges for taking out thermocouples and has entrances for vacuum and gases supply. Thermal insulation layers are fixed on the inside and outside of the top and bottom disks. The pressure in the test section can be set from vacuum to atmospheric pressure.

(2) Water cooling system

The water cooling system is divided into 5 loops. The cooling cylinder and the upper disk are cooled using 4 loops and 1 loop, respectively. The system for the cooling cylinder has inlet and outlet headers for each loop.

(3) Vacuum and gas supply system

The vacuum system consists of a vacuum pump, a pipe and valves assembled in the loop of vacuum system. This system is used to keep less than 0.1Torr in the test section when the experiment on radiation heat transfer is done at a vacuum condition. The gas supply system consists of a gas cylinder, a pipe and valves assembled in the loop of gas supply system. This system is used when the working fluid in the test section is exchanged.

(4) Power supply system

The power supply system is composed of voltage control and temperature–voltage conversion devices. The temperature of the heating cylinder is transformed into a voltage signal to draw out by this system.

(5) Measurement and control system

The temperature of the experimental apparatus is measured by K-type thermocouples, which are fixed to the walls by SUS bands, and temperature signals through a data logger are recorded by a personal computer. The pressure in the test section is measured by a mechanical pressure and a vacuum gauge. The thermocouples are attached to the test section symmetrically to evaluate the average heat transfer coefficient. Figures 5 through 8 indicate attached positions of the thermocouples in the experimental apparatus. Measurement positions and collection channel arrangement are shown in Table 1.

A schematic diagram of the experimental system is shown in Fig. 9.

2.3 Experimental Procedures and Conditions

The experimental procedures are described as follows:

(1) The pressure in the test section is kept lower than 0.1Torr.

(2) The test section is filled with He or N_2 gas up to the test condition. (This operation is not necessary for vacuum experiments.)

(3) While the water is flowed in the cooling pipes of the experimental apparatus, the heating cylinder is heated up to constant temperature.

(4) After the gas and wall temperature in the test section reaches at the steady state, the experimental data are measured.

The experimental conditions are shown in Table 2. For achieving constant heat flux on the surface of the heating cylinder, the electric current of the heater is kept at constant. The pressure in the test section is set at atmospheric pressure (0.1MPa) when it is filled with He or N_2.

Table 1 Measuring positions and collection channel arrangement (1/3)

Item	TAG No.	Measuring Position	Sensor	Range	Channel	Output	Remark
Temperature	TE-H01A	Inner surface of heating cylinder, side 0° -1	K-Type T/C	0～700 ℃	CH-102	DC mV	B(1)
	TE-H02A	Inner surface of heating cylinder, side 0° -2	〃	〃	CH-103	〃	B(2)
	TE-H03A	Inner surface of heating cylinder, side 0° -3	〃	〃	CH-104	〃	B(3)
	TE-H04A	Inner surface of heating cylinder, side 0° -4	〃	〃	CH-105	〃	B(4)
	TE-H05A	Outer surface of heating cylinder, side 0° -1	K-Type T/C	0～700 ℃	CH-106	DC mV	B(5)
	TE-H06A	Outer surface of heating cylinder, side 0° -2	〃	〃	CH-107	〃	B(6)
	TE-H07A	Outer surface of heating cylinder, side 0° -3	〃	〃	CH-108	〃	B(7)
	TE-H08A	Outer surface of heating cylinder, side 0° -4	〃	〃	CH-109	〃	B(8)
	TE-H09A	Outer surface of heating cylinder, side 0° -5	〃	〃	CH-110	〃	B(9)
	TE-H10A	Outer surface of heating cylinder, side 0° -6	〃	〃	CH-111	〃	B(10)
	TE-H11A	Outer surface of heating cylinder, side 0° -7	〃	〃	CH-112	〃	B(11)
	TE-H12A	Outer surface of heating cylinder, side 0° -8	〃	〃	CH-113	〃	B(12)
	TE-H13A	Outer surface of heating cylinder, side 0° -9	〃	〃	CH-114	〃	B(13)
	TE-H01B	Inner surface of heating cylinder, side 120° -1	K-Type T/C	0～700 ℃	CH-115	DC mV	B(14)
	TE-H02B	Inner surface of heating cylinder, side 120° -2	〃	〃	CH-116	〃	B(15)
	TE-H03B	Outer surface of heating cylinder, side 120° -1	K-Type T/C	0～700 ℃	CH-117	DC mV	B(16)
	TE-H04B	Outer surface of heating cylinder, side 120° -2	〃	〃	CH-118	〃	B(17)
	TE-H05B	Outer surface of heating cylinder, side 120° -3	〃	〃	CH-119	〃	B(18)
	TE-H06B	Outer surface of heating cylinder, side 120° -4	〃	〃	CH-120	〃	B(19)
	TE-H07B	Outer surface of heating cylinder, side 120° -5	〃	〃	CH-121	〃	B(20)
	TE-H01C	Inner surface of heating cylinder, side 240° -1	K-Type T/C	0～700 ℃	CH-122	DC mV	B(21)
	TE-H02C	Inner surface of heating cylinder, side 240° -2	〃	〃	CH-123	〃	B(22)
	TE-H03C	Outer surface of heating cylinder, side 240° -1	K-Type T/C	0～700 ℃	CH-124	DC mV	B(23)
	TE-H04C	Outer surface of heating cylinder, side 240° -2	〃	〃	CH-125	〃	B(24)
	TE-H05C	Outer surface of heating cylinder, side 240° -3	〃	〃	CH-126	〃	B(25)
	TE-H06C	Outer surface of heating cylinder, side 240° -4	〃	〃	CH-127	〃	B(26)
	TE-H07C	Outer surface of heating cylinder, side 240° -5	〃	〃	CH-128	〃	B(27)
	TE-H01D	Outer surface of heating cylinder, bottom center	K-Type T/C	0～700 ℃	CH-129	DC mV	B(28)
	TE-H02D	Outer surface of heating cylinder, bottom 0°	〃	〃	CH-130	〃	B(29)
	TE-H03D	Outer surface of heating cylinder, bottom 120°	〃	〃	CH-131	〃	B(30)
	TE-H04D	Outer surface of heating cylinder, bottom 240°	〃	〃	CH-132	〃	B(31)

Table 1 Measuring positions and collection channel arrangement (2/3)

Temperature	TE-H01E	Inner surface of cooling cylinder, bottom center	K-Type T/C	0～700 ℃	CH-133	DC mV	B(32)
	TE-H02E	Inner surface of cooling cylinder, bottom 0°	〃	〃	CH-134	〃	B(33)
	TE-H03E	Inner surface of cooling cylinder, bottom 120°	〃	〃	CH-135	〃	B(34)
	TE-H04E	Inner surface of cooling cylinder, bottom 240°	〃	〃	CH-136	〃	B(35)
Temperature	TE-H01F	Upside surface of lower thermal insulation plate, 0° outside	K-Type T/C	0～700 ℃	CH-137	DC mV	B(36)
	TE-H02F	Upside surface of lower thermal insulation plate, 0° center	〃	〃	CH-138	〃	B(37)
	TE-H03F	Upside surface of lower thermal insulation plate, 0° inside	〃	〃	CH-139	〃	B(38)
	TE-H04F	Upside surface of lower thermal insulation plate, 240°	〃	〃	CH-140	〃	B(39)
	TE-H05F	Upside surface of lower thermal insulation plate, 120°	〃	〃	CH-141	〃	B(40)
	TE-H01G	Downside surface of upper thermal insulation plate, 0° outside	K-Type T/C	0～700 ℃	CH-142	DC mV	B(41)
	TE-H02G	Downside surface of upper thermal insulation plate, 0° center	〃	〃	CH-143	〃	B(42)
	TE-H03G	Downside surface of upper thermal insulation plate, 0° inside	〃	〃	CH-144	〃	B(43)
	TE-H04G	Downside surface of upper thermal insulation plate, 240°	〃	〃	CH-145	〃	B(44)
	TE-H05G	Downside surface of upper thermal insulation plate, 120°	〃	〃	CH-146	〃	B(45)
Temperature	TE-L01A	Inner surface of cooling cylinder, side 0° -1	K-Type T/C	0～700 ℃	CH-147	DC mV	B(46)
	TE-L02A	Inner surface of cooling cylinder, side 0° -2	〃	〃	CH-148	〃	B(47)
	TE-L03A	Inner surface of cooling cylinder, side 0° -3	〃	〃	CH-149	〃	B(48)
	TE-L04A	Inner surface of cooling cylinder, side 0° -4	〃	〃	CH-150	〃	B(49)
	TE-L05A	Inner surface of cooling cylinder, side 0° -5	〃	〃	CH-151	〃	B(50)
	TE-L06A	Inner surface of cooling cylinder, side 0° -6	〃	〃	CH-152	〃	B(51)
	TE-L07A	Inner surface of cooling cylinder, side 0° -7	〃	〃	CH-153	〃	B(52)
	TE-L01B	Inner surface of cooling cylinder, side 120° -1	K-Type T/C	0～700 ℃	CH-154	DC mV	B(53)
	TE-L02B	Inner surface of cooling cylinder, side 120° -2	〃	〃	CH-155	〃	B(54)
	TE-L03B	Inner surface of cooling cylinder, side 120° -3	〃	〃	CH-156	〃	B(55)
	TE-L04B	Inner surface of cooling cylinder, side 120° -4	〃	〃	CH-157	〃	B(56)
	TE-L01C	Inner surface of cooling cylinder, side 240° -1	K-Type T/C	0～700 ℃	CH-158	DC mV	B(57)
	TE-L02C	Inner surface of cooling cylinder, side 240° -2	〃	〃	CH-159	〃	B(58)
	TE-L03C	Inner surface of cooling cylinder, side 240° -3	〃	〃	CH-160	〃	B(59)
	TE-L04C	Inner surface of cooling cylinder, side 240° -4	〃	〃	CH-161	〃	B(60)
	TE-L01E	Inner surface of cooling cylinder, bottom 0°	K-Type T/C	0～700 ℃	CH-162	DC mV	B(61)
	TE-L02E	Inner surface of cooling cylinder, bottom 120°	〃	〃	CH-163	〃	B(62)
	TE-L03E	Inner surface of cooling cylinder, bottom 240°	〃	〃	CH-164	〃	B(63)

Table 1 Measuring positions and collection channel arrangement (3/3)

Temperature	TE-L01I	Inner surface of top disk, 0° -1	K-Type T/C	0～700 ℃	CH-165	DC mV	B(64)
	TE-L02I	Inner surface of top disk, 0° -2	〃	〃	CH-166	〃	B(65)
	TE-L03I	Inner surface of top disk, 120° -1	K-Type T/C	0～700 ℃	CH-167	DC mV	B(66)
	TE-L04I	Inner surface of top disk, 120° -2	〃	〃	CH-168	〃	B(67)
	TE-L05I	Inner surface of top disk, 240° -1	K-Type T/C	0～700 ℃	CH-169	DC mV	B(68)
	TE-L06I	Inner surface of top disk, 240° -2	〃	〃	CH-170	〃	B(69)
Temperature	TE-W01A	Outer surface of cooling cylinder, side 0° -1	K-Type T/C	0～700 ℃	CH-171	DC mV	B(70)
	TE-W02A	Outer surface of cooling cylinder, side 0° -2	〃	〃	CH-172	〃	B(71)
	TE-W03A	Outer surface of cooling cylinder, side 0° -3	〃	〃	CH-173	〃	B(72)
	TE-W04A	Outer surface of cooling cylinder, side 0° -4	〃	〃	CH-174	〃	B(73)
	TE-W01K	Outer surface of cooling cylinder, bottom 0° center	K-Type T/C	0～700 ℃	CH-175	DC mV	B(74)
	TE-W02K	Outer surface of cooling cylinder, bottom 0° -1	K-Type T/C	0～700 ℃	CH-176	DC mV	B(75)
	TE-W03K	Outer surface of cooling cylinder, bottom 0° -2	〃	〃	CH-177	〃	B(76)
	TE-W04K	Outer surface of cooling cylinder, bottom 0° -3	〃	〃	CH-178	〃	B(77)
	TE-W05K	Outer surface of cooling cylinder, bottom 0° -4	〃	〃	CH-179	〃	B(78)
	TE-W06K	Outer surface of cooling cylinder, bottom 120° -1	K-Type T/C	0～700 ℃	CH-180	DC mV	B(79)
	TE-W07K	Outer surface of cooling cylinder, bottom 120° -2	〃	〃	CH-201	〃	B(80)
	TE-W08K	Outer surface of cooling cylinder, bottom 240° -1	K-Type T/C	0～700 ℃	CH-203	DC mV	B(81)
	TE-W09K	Outer surface of cooling cylinder, bottom 240° -2	〃	〃	CH-204	〃	B(82)
Temperature	TE-W01J	Outer surface of top disk, 0° -1	K-Type T/C	0～700 ℃	CH-205	DC mV	B(83)
	TE-W02J	Outer surface of top disk, 0° -2	〃	〃	CH-206	〃	B(84)
	TE-W03J	Outer surface of top disk, 0° -3	〃	〃	CH-207	〃	B(85)
	TE-W04J	Outer surface of top disk, 0° -4	〃	〃	CH-208	〃	B(86)
	TE-W05J	Outer surface of top disk, 120° -1	K-Type T/C	0～700 ℃	CH-209	DC mV	B(87)
	TE-W06J	Outer surface of top disk, 120° -2	〃	〃	CH-210	〃	B(88)
	TE-W07J	Outer surface of top disk, 120° -3	〃	〃	CH-211	〃	B(89)
	TE-W08J	Outer surface of top disk, 120° -4	〃	〃	CH-212	〃	B(90)
	TE-W09J	Outer surface of top disk, 240° -1	K-Type T/C	0～700 ℃	CH-213	DC mV	B(91)
	TE-W10J	Outer surface of top disk, 240° -2	〃	〃	CH-214	〃	B(92)
	TE-W11J	Outer surface of top disk, 240° -3	〃	〃	CH-215	〃	B(93)
	TE-W12J	Outer surface of top disk, 240° -4	〃	〃	CH-216	〃	B(94)
Temperature	TE-CW01B	Outer surface of cooling pipe, 120° -1	K-Type T/C	0～700 ℃	CH-217	DC mV	B(95)
	TE-CW02B	Outer surface of cooling pipe, 120° -2	〃	〃	CH-218	〃	B(96)
Pressure		Test section					

Table 2 Experimental conditions

Working Fluid	Pressure	Electric Power					
Vacuum	below 0.1Torr	6.5A (10.4kW)	7A (11.2kW)	8A (12.8kW)	10A (16kW)	12A (19.2kW)	14A (22.4kW)
He	0.1MPa	6.5A (10.4kW)		8A (12.8kW)	10A (16kW)	12A (19.2kW)	14A (22.4kW)
N_2	0.1MPa	6.5A (10.4kW)		8A (12.8kW)	10A (16kW)	12A (19.2kW)	14A (22.4kW)

Electric Power (W) = Electric Power (A) × 200 (V) × 8 (the number of heating systems)

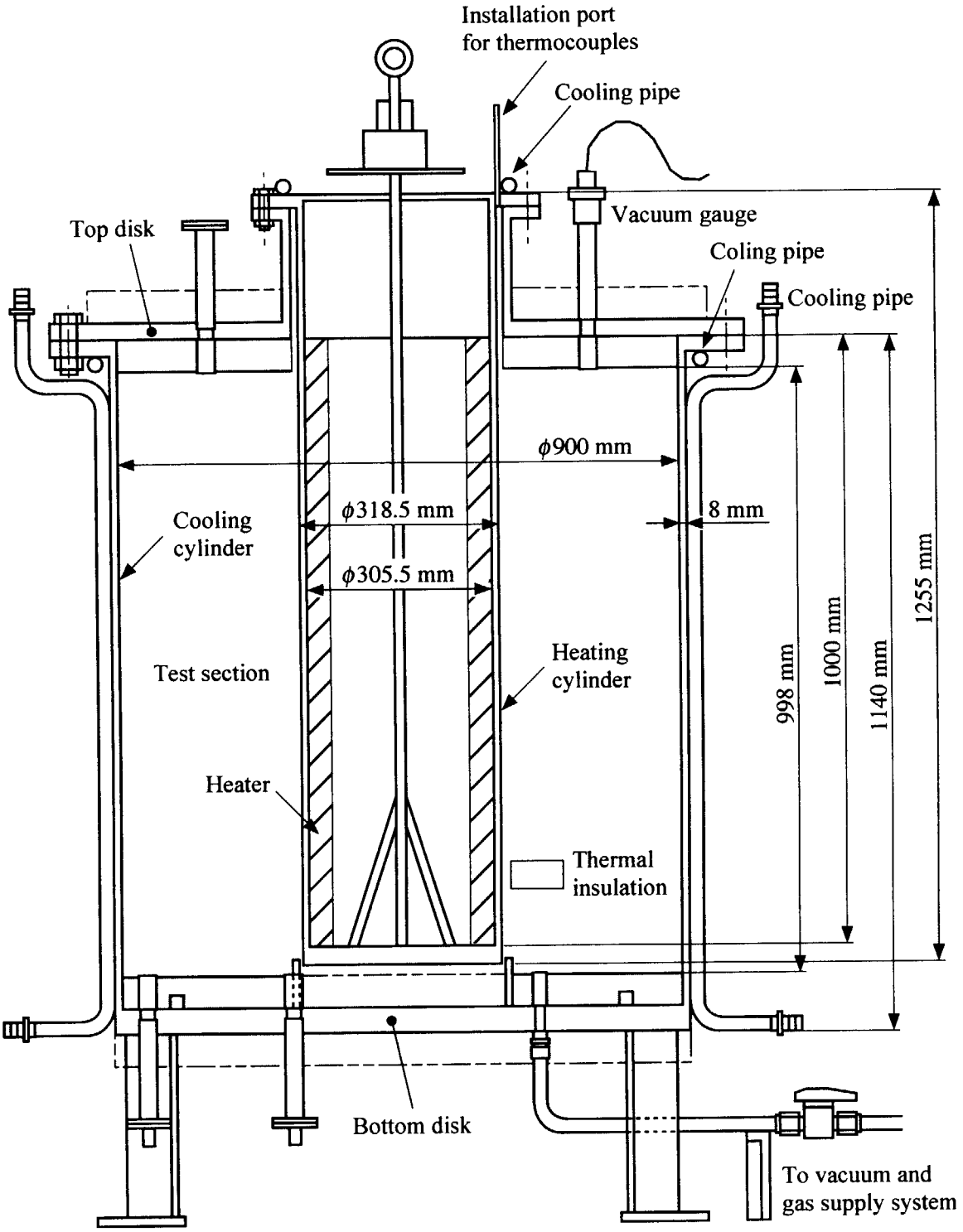

Fig. 2 Schematic of the experimental apparatus.

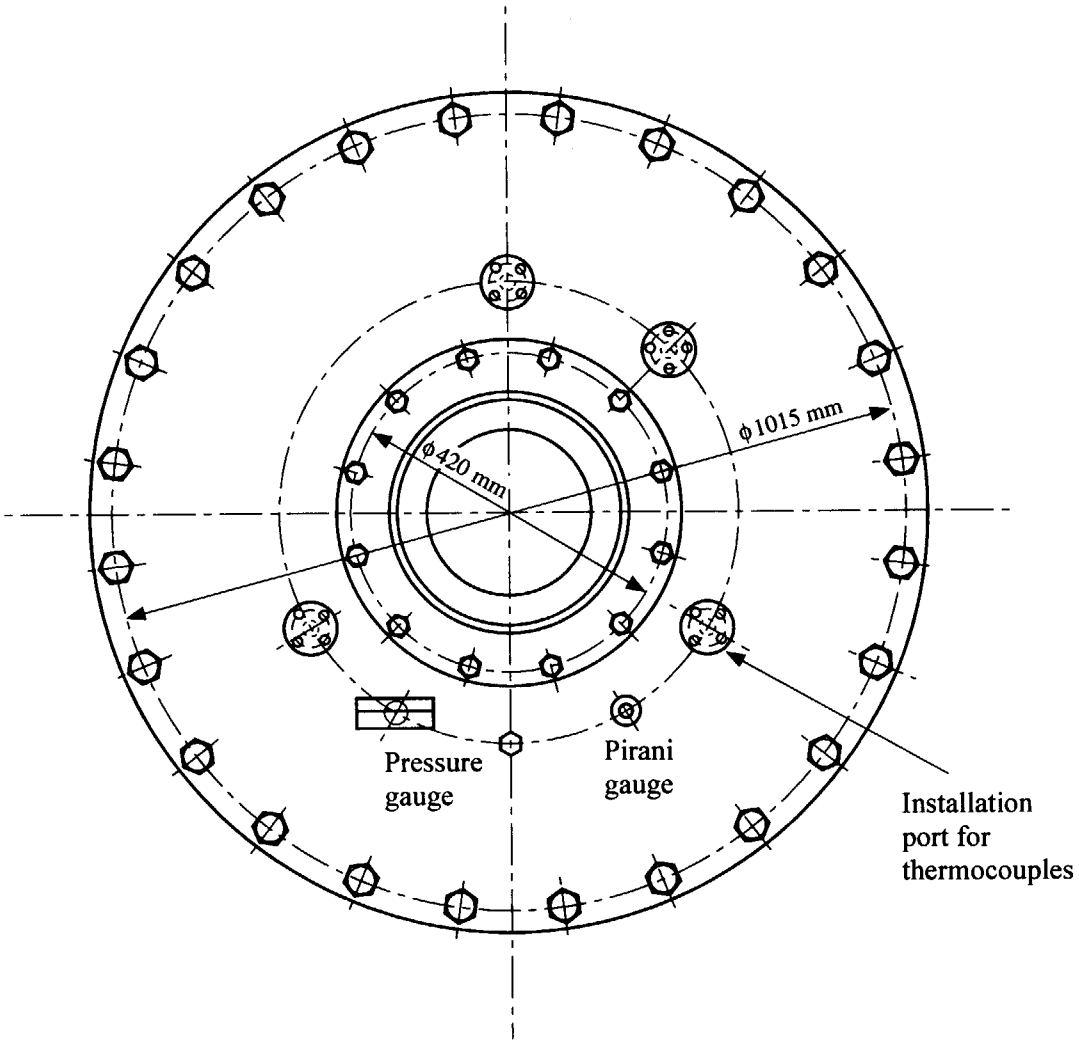

Fig. 3 Top side figure of the experimental apparatus.

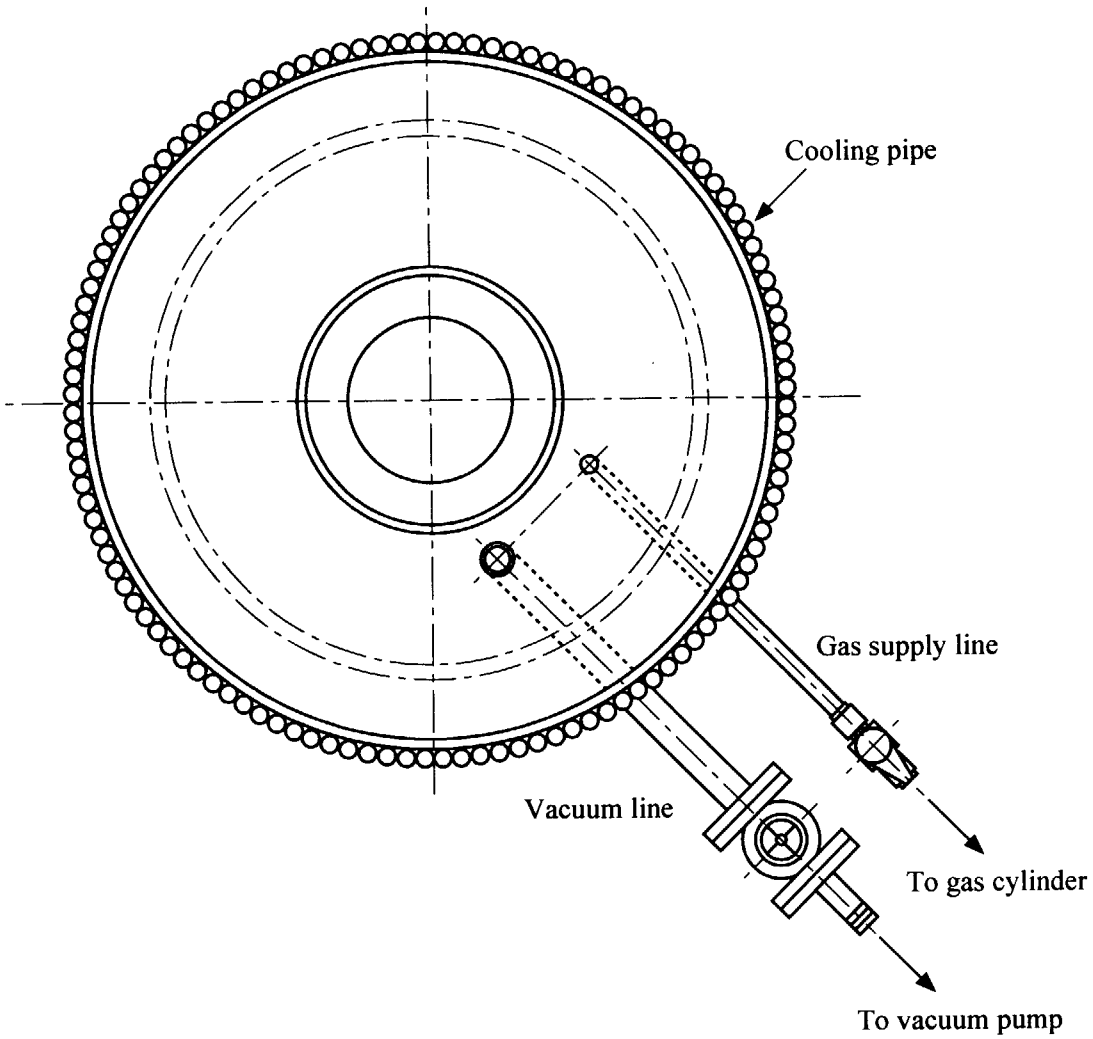

Fig. 4 Bottom side figure of the experimental apparatus.

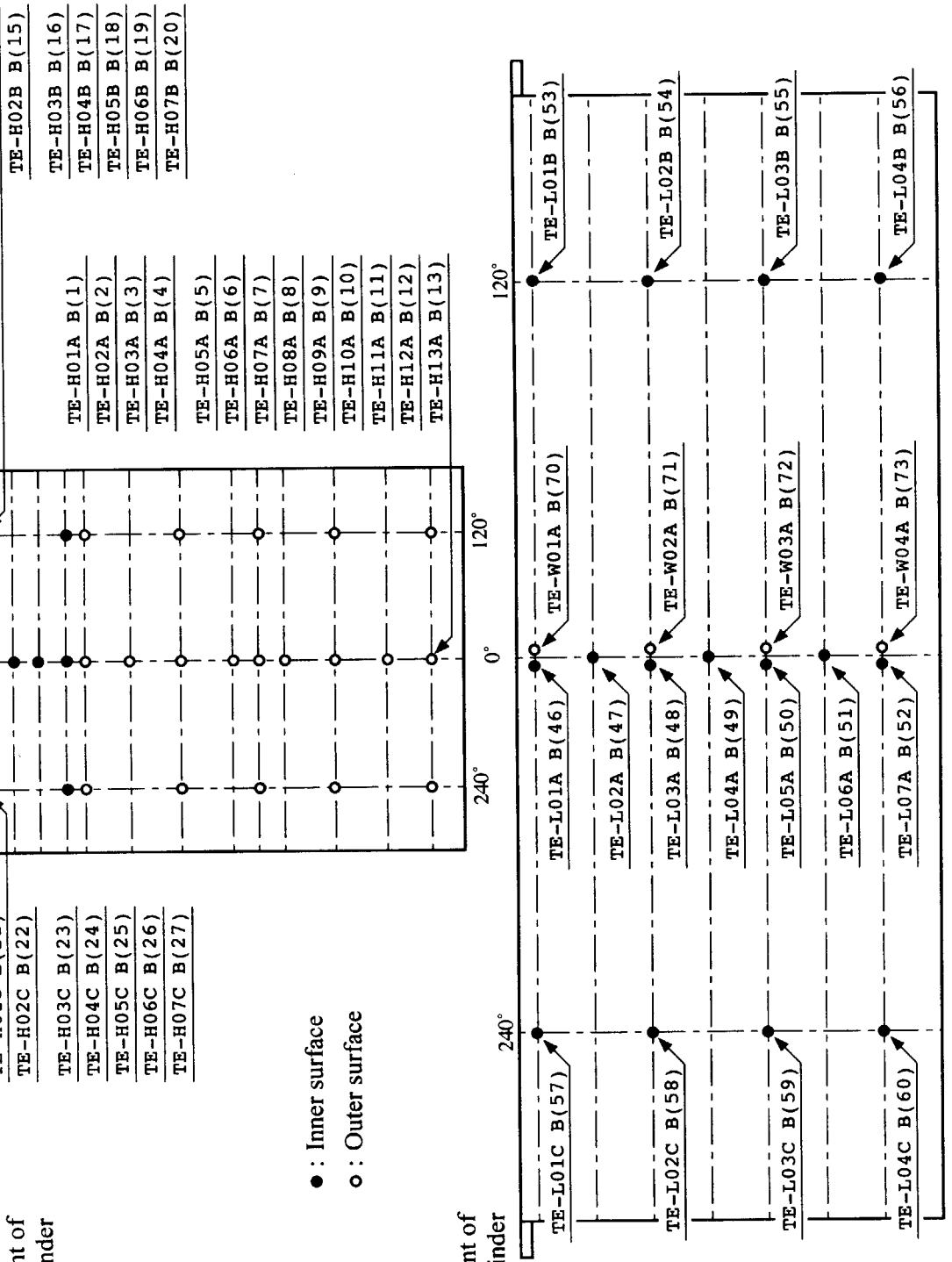

Fig. 5 Attached positions of thermocouples (side).

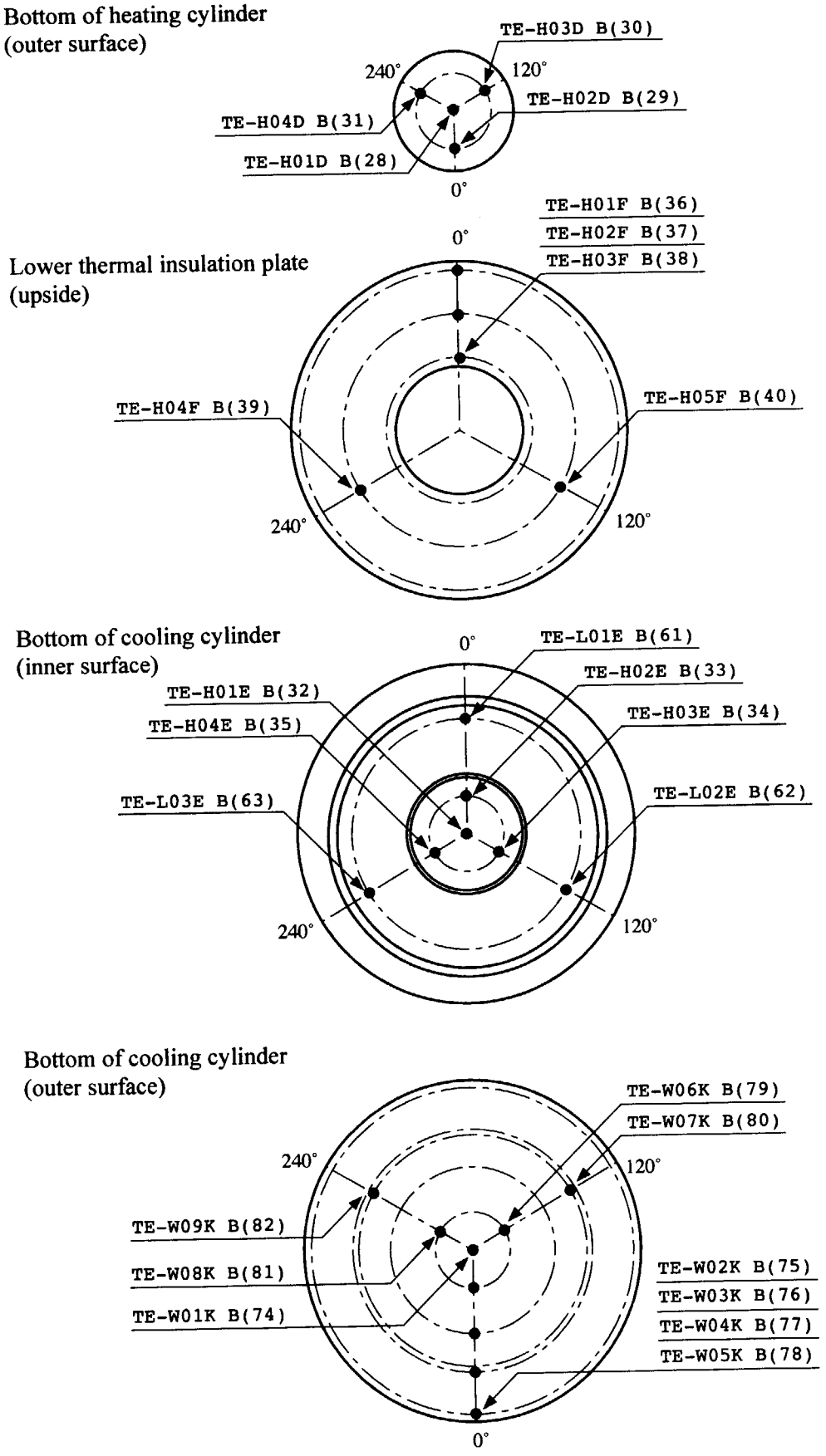

Fig. 6 Attached positions of thermocouples (top and bottom, a).

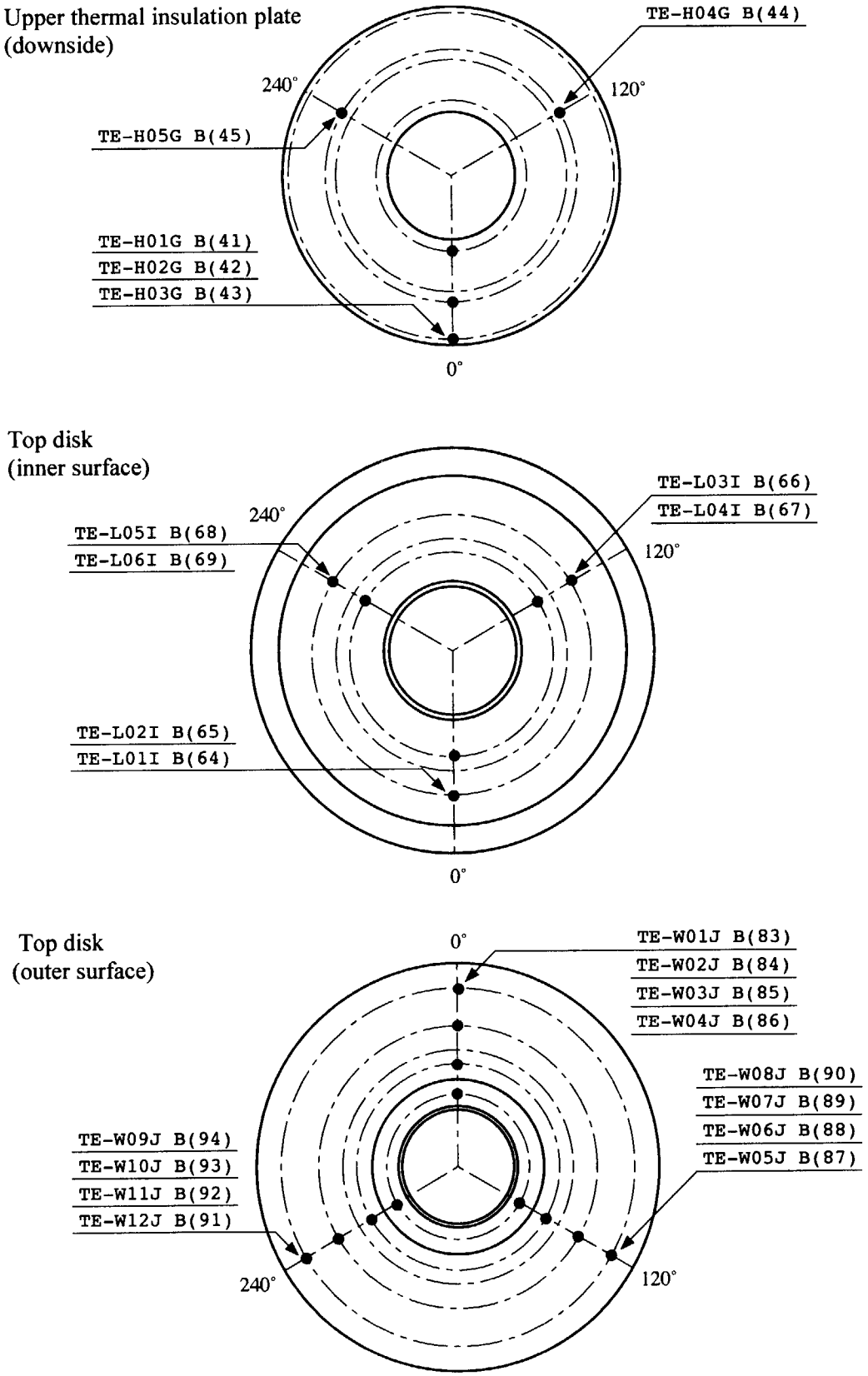

Fig. 7 Attached positions of thermocouples (top and bottom, b).

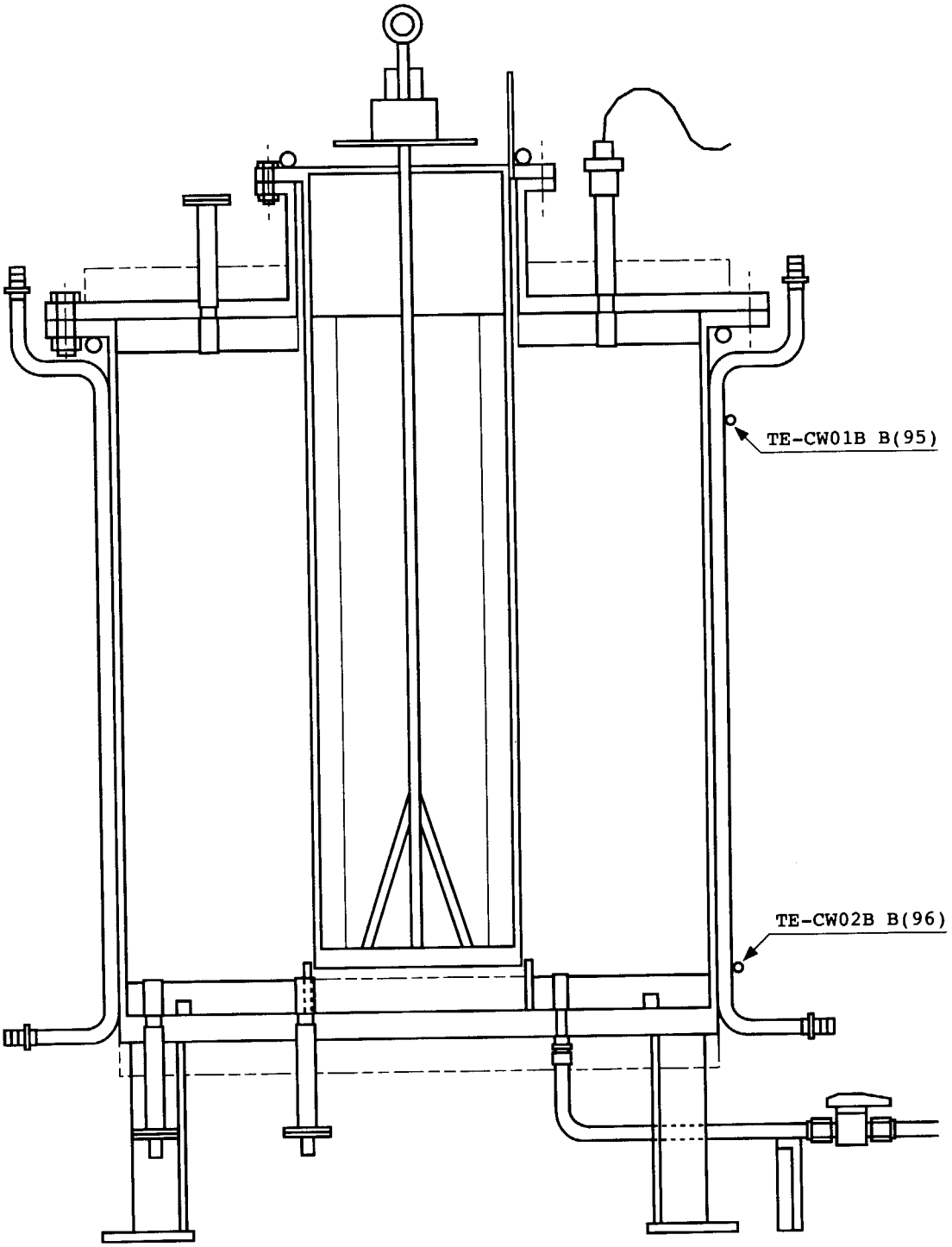

Fig. 8 Attached positions of thermocouples (cooling pipe).

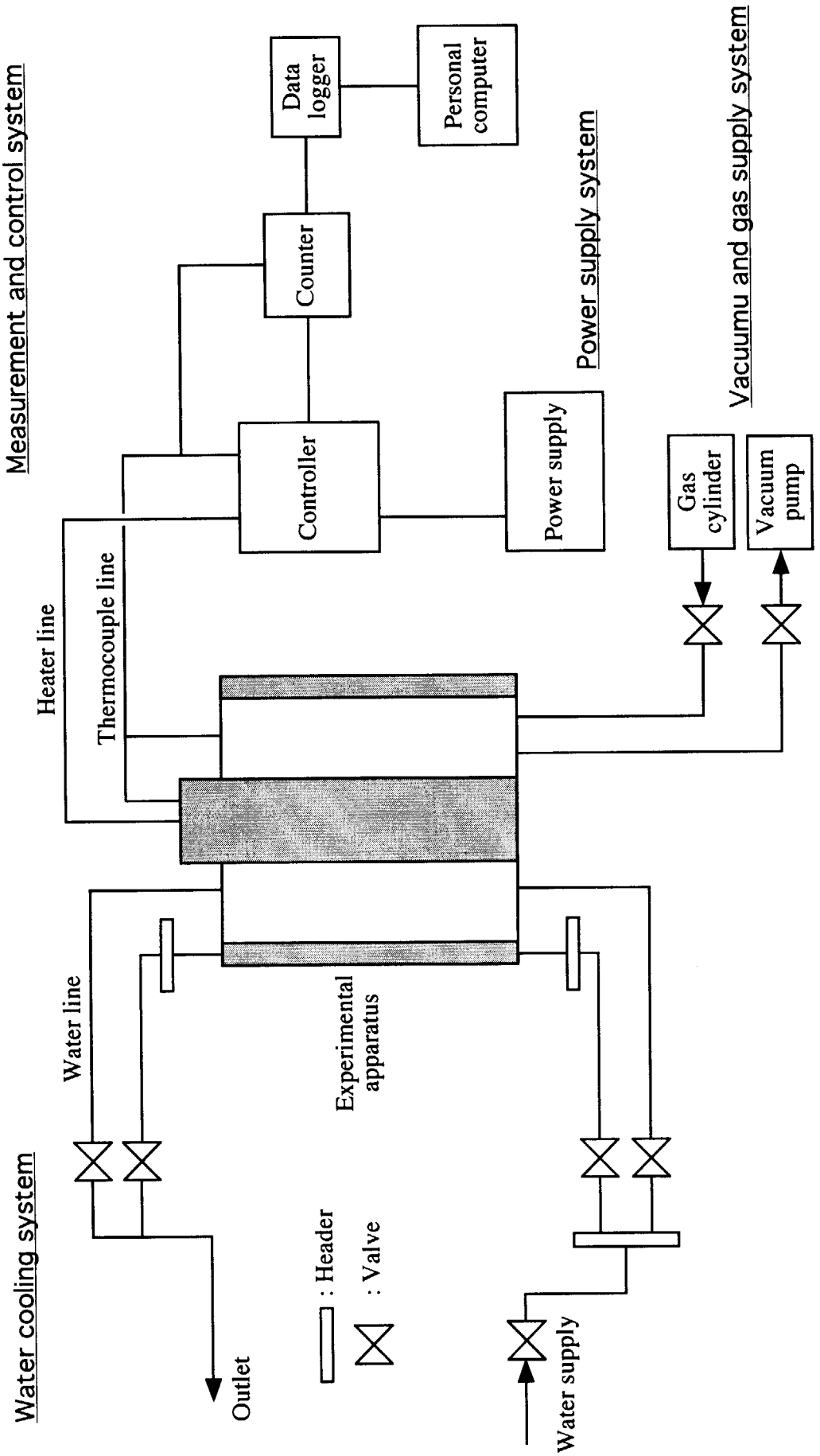

Fig. 9 Schematic diagram of the experimental system.

3. Experimental Results and Discussion

3.1 Experimental Results

The experimental results for vacuum condition and filling with He or N_2 of 0.1MPa are shown in Table 3, Table 4 and Table 5. The measured temperature distributions on the outer surface of the heating cylinder and on the inner surface of the cooling cylinder are shown in Figs. 10 through 14. In the experiments, temperature range of the heating cylinder surface is about 295.4°C～561.4°C at vacuum condition, and about 200.3～509.7°C for He and about 258.0～536.5°C for N_2 at atmosphere pressure. It was confirmed that the deviation of the measured temperature caused by the method of fixing the thermocouples to the walls was very small (cf. Appendix-1). As the electric power increases, each temperature distribution for vacuum, He and N_2 is more similar and approaches a constant temperature distribution along the wall surfaces because of the effect of thermal radiation.

We suppose that two-dimensional convection is generated mainly in the test section of the apparatus to evaluate the Nusselt number and the Rayleigh number using the experimental data. We use the experimental data in a middle zone of the cylinders because of little influence of the upper and the lower thermal insulation plates. The experimental data are arranged as below:

3.1.1 Equivalent heat transfer coefficient for thermal radiation

(1) Evaluation from experimental results for vacuum condition

As it is difficult to take into account of all factors such as a view-factor, emissivities and so on, an experimental correlation for estimating the radiative heat flux on the inner surface of the cooling cylinder is derived from the experimental results for the vacuum condition. The radiative heat flux q_r is

$$q_r = f_r \cdot \left(T_1^4 - T_2^4\right) \quad (\mathrm{W/m^2}) \tag{1}$$

where f_r is a coefficient, T is the absolute temperature of the wall surface and the subscripts "1" and "2" represent the value at the outer surface of the heating cylinder and the inner surface of the cooling cylinder, respectively. The coefficient $f_{r,exp.}$ evaluated from the experimental results for the vacuum condition is as follows (cf. Table 6):

$$f_{r,exp.} = 4.22 \times 10^{-2}\left(T_1^4 - T_2^4\right)^{-0.560} \quad (\mathrm{W/m^2K^4}). \tag{2}$$

Equation (2) is derived from the power approximation using the method of least squares. The comparison of the radiative heat flux given by the experimental results and Eqs. (1) and (2) for the vacuum condition is shown in Fig. 15.

(2) Evaluation from thermal radiation theory

In addition to Eq. (2), we adopt another equations based on calculations. The experimental

coefficient $f_{r,exp.}$ given by Eq. (2) is function of $(T_1^4 - T_2^4)$, but f_r is constant value essentially.

If the present experimental apparatus can be regarded as the infinite double coaxial cylinder, the radiative heat flux on the inner surface of the cooling cylinder is given by

$$q_r = h_r \times (T_1 - T_2)$$

$$= \frac{A_1}{A_2} \cdot \frac{1}{\frac{1}{\varepsilon_1} + \left(\frac{1}{\varepsilon_2} - 1\right)\frac{A_1}{A_2}} \cdot \sigma\left(T_1^4 - T_2^4\right) \quad (\mathrm{W/m^2}) \tag{3}$$

where h_r is the equivalent heat transfer coefficient for thermal radiation, A is the area, ε is the emissivity, σ is the Stefan-Boltzmann constant.

In the present experimental apparatus, the vertical annular test section is closed by the top and the bottom disks and it has finite length, and thus the view-factor from the outer surface of the heating cylinder to the inner surface of the cooling cylinder is not the same as the one of vertical annular space of the infinite double coaxial cylinder. In this case, the radiative heat flux on the surface of the cooling cylinder can be obtained as follows:

$$q_r = \frac{A_1}{A_2} \cdot \frac{F_{12}}{1 + F_{12}\left(\frac{1}{\varepsilon_1} - 1\right) + F_{21}\left(\frac{1}{\varepsilon_2} - 1\right)} \cdot \sigma\left(T_1^4 - T_2^4\right) \quad (\mathrm{W/m^2}) \tag{4}$$

where F_{ij} is the view-factor from i-surface to j-surface. The view-factor F_{12} and F_{21} can be obtained by the integration of infinitesimal surface in the cylindrical coordination.

The parameters of Eqs. (3) and (4) for the present geometry and the material are listed as follows:

$A_1 / A_2 = 0.3815 / 0.9$

$F_{12} = 0.4228$, $F_{21} = 0.18$

$\varepsilon_1 = 0.7$, $\varepsilon_2 = 0.5$

The comparison of the experimental results of the radiative heat flux with the calculated results given by Eqs. (3) and (4) for the vacuum condition is shown in Fig. 16. The calculated results are a little smaller than the experimental results and the calculated result by Eq. (3) is closer to the experimental results than the one by Eq. (4). The difference between the both is supposed to be caused by the following reasons:

- The radiative heat flux calculated by equations is the average value of the whole inner surface of the cylinder. However, the experimental one is the value of the middle zone of the cylinder.
- The heat transferred by thermal radiation from the upper and the lower thermal insulation plates to the surface of the cylinder is ignored in the calculations.
- The emissivities, ε_1 and ε_2 are value based on assuming the oxide nickel surface.

We adopt Eq. (3) as the calculated result of the radiative heat flux and so the coefficient $f_{r,calc.}$ evaluated from the thermal radiation theory is given by

$$f_{r,calc.} = \frac{A_1}{A_2} \cdot \frac{1}{\frac{1}{\varepsilon_1} + \left(\frac{1}{\varepsilon_2} - 1\right)\frac{A_1}{A_2}} \cdot \sigma = constant \quad (\mathrm{W/m^2K^4}). \tag{5}$$

Then the equivalent heat transfer coefficient for thermal radiation is

$$h_r = \frac{q_r}{(T_1 - T_2)} \quad (\mathrm{W/m^2K}). \tag{6}$$

3.1.2 Heat transfer coefficient on the cooling cylinder

The heat flux on the cooling cylinder will be obtained as follows:

$$q_{all} = \frac{\Delta T_{wall}}{R} \quad (\mathrm{W/m^2}). \tag{7}$$

in which ΔT_{wall} is the temperature difference between the inner and outer surface of the cooling cylinder, and R is the thermal resistance, which is evaluated from the heat balance of input heat and output heat.

The heat transfer coefficient on the cooling cylinder can be written as follows:

$$h_{all} = \frac{q_{all}}{T_1 - T_2} \quad (\mathrm{W/m^2K}). \tag{8}$$

Thus, the heat transfer coefficient by natural convection is given by

$$h_c = \frac{q_{all} - q_r}{T_1 - T_2} = h_{all} - h_r \quad (\mathrm{W/m^2K}). \tag{9}$$

3.1.3 Nusselt number and Rayleigh number

The Nusselt number for natural convection coupled with thermal radiation (the total Nusselt number, Nu_{all}) and for natural convection (the convective Nusselt number, Nu_c) is written by

$$Nu_{all}(l) = \frac{h_{all} l}{k_g} \tag{10}$$

$$Nu_c(l) = \frac{h_c l}{k_g} \tag{11}$$

$$Nu_{all}(d) = \frac{h_{all} d}{k_g} \tag{12}$$

$$Nu_c(d) = \frac{h_c d}{k_g} \tag{13}$$

where l is the height of the annular test section, d is the width of the annular test section and k_g is the thermal conductivity of the filled gas.

The Nusselt number for the vertical enclosure with an inside-heated and outside-cooled double coaxial cylinder[2][3] is given by

$$Nu = 0.364\{Ra(l)\, f(Pr)\}^{0.25}(r_o / r_i)^{0.5} \qquad 10^4 \leqq Ra(d) < 10^5 \tag{14}$$

in which

$$f(Pr) = \left\{1 + (0.5/Pr)^{9/16}\right\}^{-16/9} \qquad (Pr = 0 \sim \infty) \tag{15}$$

where Pr is the Prandtl number, r_o is the outer radius and r_i is the inner radius. Eq. (14) is derived from calculation based on $Pr = 1$, $l/(r_o - r_i) = 5, 10, 15$, $r_o/r_i = 1, 2$.

The Rayleigh number based on the height and the width of the test section is defined by

$$Ra(l) = \frac{Pr \cdot g\beta(T_1 - T_2)l^3}{\nu_g^2} \tag{16}$$

$$Ra(d) = \frac{Pr \cdot g\beta(T_1 - T_2)d^3}{\nu_g^2} \tag{17}$$

where g is the gravitational acceleration, β is the thermal expansion coefficient and ν_g is the kinematic viscosity of the filled gas.

3.1.4 Thermophysical properties

Polynomial fitting functions dependent on temperature are developed according to database of thermophysical properties of materials[4]. Average temperature in the test section is used in the polynomial fitting functions and it is defined as follows:

$$\bar{T} = \frac{(T_1 + T_2)}{2} \quad \text{(K)}. \tag{18}$$

Each value according to the above data arrangement is listed in Table 6 through Table 9. In Tables 8-1 and 8-2, $f_{r,exp.}$ is used for the evaluation of q_r, and in Tables 9-1 and 9-2, $f_{r,calc.}$ is used for the evaluation of q_r.

3.2 Discussion

Figures 17 and 18 show the relationship between the Nusselt number and the Rayleigh number on the inner surface of the cooling cylinder. Figure 17 is based on the $f_{r,exp.}$ and Fig. 18 is based on the $f_{r,calc.}$. The Nusselt number and the Rayleigh number in each figure are based on the height of the test section. Symbols (○ and □) represent the total Nusselt number $Nu_{all}(l)$ for natural convection coupled with thermal radiation and symbols (● and ■) represent the convective Nusselt number $Nu_c(l)$ for natural convection without thermal radiation. A solid line represents Eq. (14).

As shown in Fig. 17 and Fig. 18, $Nu_c(l)$ is in agreement with the one obtained from Eq. (14) and $Nu_c(l)$ increases with increasing $Ra(l)$ in the present experiments. $Ra(l)$ decreases with increasing the gas temperature because the kinematic viscosity of gas increases with the gas temperature, but the radiative Nusselt number $Nu_r(l)$ ($= Nu_{all}(l) - Nu_c(l)$) increases with decreasing $Ra(l)$ because

$Nu_r(l)$ increases with the gas temperature; therefore it is possible that $Nu_{all}(l)$ decreases with increasing $Ra(l)$ if $Nu_c(l)$ is in quantitative agreement with the conventional correlation about the Nusselt number such as Eq. (14), It is necessary to analyze the phenomenon of natural convection coupled with thermal radiation under the high temperature condition to obtain the relationship between Nu_{all} and Ra.

Figures 19 and 20 show the ratio of the heat transferred by thermal radiation to the heat transferred by convection and radiation. Horizontal axis in each figure represents the outer surface temperature of the heating cylinder. When the wall temperature is about 400°C, the ratio of thermal radiation becomes 79% for Fig. 19 based on $f_{r,exp.}$ and 45% for Fig. 20 based on $f_{r,calc.}$.

3.2.1 Nusselt number for natural convection heat transfer

A general expression form of the average Nusselt number for laminar flow in a vertical rectangular enclosure is

$$Nu = a \cdot Ra^{b}(l/d)^{c} \tag{19}$$

where a, b and c are constants. The constants for laminar flow in air were obtained by Eckert and Carlson[5], Elder[6], Newell and Schmidt[7] and so on. For the convection-dominated regime ($Ra(d) > 10^6$) in a vertical cavity, studied by Gill[8], the average Nusselt number was calculated by Bejan[9] as follows:

$$Nu = 0.364\, Ra^{0.25}(l/d)^{-0.25}. \tag{20}$$

In the present experiment, the Rayleigh number based on the width of the space depends not only on the gas temperature but also on the gas species, the aspect ratio l/d is 3.43 and $Ra(d)$ is varied from 6.8×10^5 to 1.0×10^8. Firstly, the average Nusselt number for each gas species is obtained from Eqs. (19) and (20). The average Nusselt numbers for laminar flow in He are

$$Nu_c(d) = 0.288\, Ra(d)^{0.25}(l/d)^{-0.25} \quad \text{based on } f_{r,exp.} \tag{21}$$

$$Nu_c(d) = 0.628\, Ra(d)^{0.25}(l/d)^{-0.25} \quad \text{based on } f_{r,calc.} \tag{22}$$

$$(6.8\times10^5 < Ra(d) < 1.8\times10^6)$$

, and the ones in N_2 are

$$Nu_c(d) = 0.272\, Ra(d)^{0.25}(l/d)^{-0.25} \quad \text{based on } f_{r,exp.} \tag{23}$$

$$Nu_c(d) = 0.863\, Ra(d)^{0.25}(l/d)^{-0.25} \quad \text{based on } f_{r,calc.} \tag{24}$$

$$(4.2\times10^7 < Ra(d) < 1.0\times10^8)\ .$$

The average Nusselt numbers in the present experiments are obtained as

$$Nu_c(d) = 0.280\, Ra(d)^{0.25}(l/d)^{-0.25} \quad \text{based on } f_{r,exp.} \tag{25}$$

$$Nu_c(d) = 0.745\, Ra(d)^{0.25}(l/d)^{-0.25} \quad \text{based on } f_{r,calc.} \tag{26}$$

$$(6.8\times10^5 < Ra(d) < 1.0\times10^8)\ .$$

Figure 21 shows the average Nusselt number for He and N_2 based on $f_{r,exp.}$ in the experiments. The solid and dotted lines in the figure indicate Eqs. (21), (23) and (25). Figure 22 shows the average Nusselt number for He and N_2 based on $f_{r,calc.}$ in the experiments. The solid and dotted lines in the figure indicate Eqs. (22), (24) and (26). According to these equations, the Nusselt number increases as the Rayleigh number increases in case of the natural convection.

3.2.2 Nusselt number for natural convection heat transfer coupled with thermal radiation

Figure 23 shows the ratio of the heat transferred by only thermal radiation to the heat transferred by convection and radiation as the function of the difference of the forth power of the heated and cooled wall surface temperature. Figure 23 is based on $f_{r,exp.}$. The ratio of the heat transferred by thermal radiation can be obtained as follows:

$$R_{r,exp.} = \frac{q_r}{q_{all}} = \frac{f_{r,exp.} \cdot \left(T_1^4 - T_2^4\right)}{q_{all}} = 3.204 \times 10^{-2} \left(T_1^4 - T_2^4\right)^{0.1235}. \tag{27}$$

Equation (27) is derived from the power approximation using the method of least squares. In addition to Eq. (27), an analytical equation based on $f_{r,calc.}$ for R_r is obtained by supposing that the wall of the cooling cylinder absorbs all input heat to the test section. The analytical equation for R_r is as below:

$$R_{r,calc.} = \frac{q_r}{q_{all}} = \frac{A_1}{A_2} \cdot \frac{1}{\frac{1}{\varepsilon_1} + \left(\frac{1}{\varepsilon_2} - 1\right)\frac{A_1}{A_2}} \cdot \sigma\left(T_1^4 - T_2^4\right) / \left(\frac{Q}{A_2}\right) = f_{r,calc.} \cdot \left(T_1^4 - T_2^4\right) / \left(\frac{Q}{A_2}\right)$$

$$= A_1 \cdot \frac{1}{\frac{1}{\varepsilon_1} + \left(\frac{1}{\varepsilon_2} - 1\right)\frac{A_1}{A_2}} \cdot \sigma\left(T_1^4 - T_2^4\right) / Q \tag{28}$$

where Q is the total heating power to the test section. Then the average Nusselt numbers for natural convection heat transfer coupled with thermal radiation are as follows:

$$Nu_{all}(d) = Nu_c(d) + Nu_r(d)$$

$$= Nu_c(d) + R_r\, Nu_{all}(d)$$

$$\therefore\ Nu_{all}(d) = \frac{Nu_c(d)}{1 - R_r}$$

$$= \frac{0.288\, Ra(d)^{0.25} (l/d)^{-0.25}}{1 - R_{r,exp.}} \quad \text{based on Eqs. (21) and (27)} \tag{29}$$

$$(6.8 \times 10^5 < Ra(d) < 1.8 \times 10^6)$$

$$= \frac{0.272\, Ra(d)^{0.25} (l/d)^{-0.25}}{1 - R_{r,exp.}} \quad \text{based on Eqs. (23) and (27)} \tag{30}$$

$$(4.2 \times 10^7 < Ra(d) < 1.0 \times 10^8)$$

$$= \frac{0.280\, Ra(d)^{0.25} (l/d)^{-0.25}}{1 - R_{r,exp.}} \quad \text{based on Eqs. (25) and (27)} \tag{31}$$

$$(6.8 \times 10^5 < Ra(d) < 1.0 \times 10^8)$$

$$= \frac{0.628\, Ra(d)^{0.25} (l/d)^{-0.25}}{1 - R_{r,calc.}} \quad \text{based on Eqs. (22) and (28)} \tag{32}$$

$$(6.8 \times 10^5 < Ra(d) < 1.8 \times 10^6)$$

$$= \frac{0.863\, Ra(d)^{0.25} (l/d)^{-0.25}}{1 - R_{r,calc.}} \quad \text{based on Eqs. (24) and (28)} \tag{33}$$

$$(4.2 \times 10^7 < Ra(d) < 1.0 \times 10^8)$$

$$= \frac{0.745\, Ra(d)^{0.25} (l/d)^{-0.25}}{1 - R_{r,calc.}} \quad \text{based on Eqs. (26) and (28)} \tag{34}$$

$$(6.8 \times 10^5 < Ra(d) < 1.0 \times 10^8) \ .$$

Figure 24 shows the average Nusselt number coupled with thermal radiation for He and N_2 based on $f_{r,exp.}$ and $R_{r,exp.}$ in the experiments. The solid and dotted lines in the figure indicate Eqs. (29), (30) and (31). Figure 25 shows the average Nusselt number coupled with thermal radiation for He and N_2 based on $f_{r,calc.}$ and $R_{r,calc.}$ in the experiments. The solid and dotted lines in the figure indicate Eqs. (32), (33) and (34). According to these equations, the Nusselt number decreases as the Rayleigh number increases in case of the natural convection coupled with thermal radiation.

Comparison of Eqs. (31) and (34) with the correlation suggested in Ref. (1) is shown in Appendix-2.

Table 3 Experimental results for vacuum condition (1/3)

Measuring Position					Measured Temperature (℃)					
Section		Angle	Position (mm)	Channel	6.5A	7A	8A	10A	12A	14A
Heating Cylinder	Inner surface	0°	1310	B(1)	36.8	70.2	57.4	90.6	107.1	78.7
〃	(Side)	〃	1240	B(2)	80.8	140.3	153.6	182.7	213.5	216.8
〃	〃	〃	1170	B(3)	126.3	207.4	237.4	271.4	315.6	340.8
〃	〃	〃	1100	B(4)	198.5	283.2	322.8	375.2	438	486.2
〃	Outer surface	0°	1049	B(5)	270.3	338.8	382	455.2	535	601.5
〃	(Side)	〃	932	B(6)	304.7	341.7	379.7	448.2	516.4	575.5
〃	〃	〃	799	B(7)	306.3	334.2	368.6	436	501.2	557
〃	〃	〃	666	B(8)	300	330.3	364.1	431.3	496.5	553.5
〃	〃	〃	599.5	B(9)	300.8	329.4	361.5	424.7	484.1	534.1
〃	〃	〃	533	B(10)	301.6	329.8	364	430.5	496.2	552.8
〃	〃	〃	400	B(11)	299.4	329.4	364.5	432.5	499.1	557.3
〃	〃	〃	267	B(12)	289.5	325.4	358.8	427	491.5	546.8
〃	〃	〃	150	B(13)	292.9	342.4	378	451.1	521.8	582.1
〃	Inner surface	120°	1310	B(14)	38.2	71.1	58.8	91.5	107.8	81.4
〃	(Side)	〃	1100	B(15)	186.9	257.9	294.8	341.7	398.4	440.7
〃	Outer surface	120°	1050	B(16)	266.9	322.7	363.2	433.2	507.2	568.2
〃	(Side)	〃	800	B(17)	310.8	338.3	372.4	441.3	506.5	562.7
〃	〃	〃	600	B(18)	306	335.7	367.9	433.9	495.5	547.4
〃	〃	〃	400	B(19)	312.2	343.1	377.6	448.7	516.1	574.1
〃	〃	〃	150	B(20)	289.3	337.7	373.1	443.2	511.1	569.6
〃	Inner surface	240°	1310	B(21)	39.1	75.4	64.2	97.4	115.1	91.5
〃	(Side)	〃	1100	B(22)	191.2	275.6	313.9	365.9	427.6	473.7
〃	Outer surface	240°	1050	B(23)	255.9	319.2	359.1	426.6	498.6	557
〃	(Side)	〃	800	B(24)	302.7	328.7	361.4	426.4	487.7	540.2
〃	〃	〃	600	B(25)	303.1	332	363.8	429.2	490.6	543.2
〃	〃	〃	400	B(26)	301.4	330.4	364.7	432.1	496.8	552.4
〃	〃	〃	150	B(27)	298.3	348.1	384.3	458.2	530.2	592.1
〃	Outer surface	Center	0	B(28)	317	386	430	520	604.5	680.6
〃	(Bottom)	0°	100	B(29)	312.1	378.8	421.7	507.1	587.9	659.8
〃	〃	120°	100	B(30)	309.4	375.1	417	500.9	579.2	648.8
〃	〃	240°	100	B(31)	311.1	376.8	418.8	503.3	582.7	652.8

Table 3 Experimental results for vacuum condition (2/3)

Cooling Cylinder	Inner surface	Center	0	B(32)	36.6	51.4	62.4	85.2	111.3	136.6
〃	(Bottom)	0°	100	B(33)	37.6	53.1	65.2	87.7	113.5	138.8
〃	〃	120°	100	B(34)	37.5	52.1	62.9	85.5	111.3	135.3
〃	〃	240°	100	B(35)	36.8	51.3	62.2	84.5	110.9	136.7
Lower Thermal	Upside surface	0°	424	B(36)	154.7	191.1	227.1	264.3	310.8	348.7
Insulation Plate	〃	〃	309	B(37)	182.2	219.5	249.2	302.9	356.5	402.3
〃	〃	〃	194	B(38)	186.8	227.3	259.2	315	374.4	427.3
〃	〃	240°	309	B(39)	183.1	218.9	248.7	303.6	358.3	404.7
〃	〃	120°	309	B(40)	180.3	216.9	247.1	299.3	352.4	398.5
Upper Thermal	Downside surface	0°	200	B(41)	217.6	257.5	287.3	352.7	416.6	472.4
Insulation Plate	〃	〃	334	B(42)	180.8	214.3	245.3	293.3	345.4	389.1
〃	〃	〃	432	B(43)	157.2	187.2	221.3	248	293.8	327.1
〃	〃	120°	338.5	B(44)	181.2	214.6	245.5	294.2	346	390.4
〃	〃	240°	338.5	B(45)	181.1	214	244.9	293.7	345.9	390.1
Cooling Cylinder	Inner surface	0°	1050	B(46)	47.3	58.5	67.9	89.6	114.8	135.6
〃	(Side)	〃	900	B(47)	50.3	59.9	71	91.4	116.4	140
〃	〃	〃	750	B(48)	45	52.6	63.2	80.5	105.1	127.9
〃	〃	〃	600	B(49)	43.2	49.9	59.8	75.6	98.7	120.2
〃	〃	〃	450	B(50)	49.2	55.8	65.8	83.4	107.7	131.5
〃	〃	〃	300	B(51)	54.2	62.2	73	90.8	115.1	139
〃	〃	〃	150	B(52)	54.6	64.7	77.2	95.5	118.2	140.5
〃	〃	120°	1050	B(53)	53.2	64.1	72.8	95.2	120.3	143
〃	〃	〃	750	B(54)	49.1	49.7	53.8	60.1	73.4	86.4
〃	〃	〃	450	B(55)	43.8	44.9	50.7	57.9	71.4	85
〃	〃	〃	150	B(56)	53.5	61.4	72.4	85.2	105.6	127
〃	〃	240°	1050	B(57)	48.4	58.7	67.8	86.7	109.7	127.3
〃	〃	〃	750	B(58)	42.2	46	52.7	60.3	74.4	88.9
〃	〃	〃	450	B(59)	35.9	39.4	45.9	54.9	69.2	82.2
〃	〃	〃	150	B(60)	48.8	56.8	69	82.9	106.2	128.8
〃	Inner surface	0°	305	B(61)	32.7	43.9	53.2	68.5	87.7	106.9
〃	(Bottom)	120°	305	B(62)	33.4	44.5	53.6	69	88.7	106.7
〃	〃	240°	305	B(63)	32.2	43.2	52.5	67.7	88.3	107.9

Table 3 Experimental results for vacuum condition (3/3)

Top Disk	Inner surface	0°	370	B(64)	34.6	48.4	53.5	73.8	96.3	107
〃	〃	〃	270	B(65)	38.5	56.5	60.3	88.9	117.2	130.6
〃	〃	120°	370	B(66)	36.3	49.8	55.4	74.7	96.6	112.7
〃	〃	〃	270	B(67)	39.8	56.6	61.2	87.7	114.3	133.6
〃	〃	240°	370	B(68)	34.4	47.4	54.3	72.4	94	100.8
〃	〃	〃	270	B(69)	38.1	55.1	60.7	86.2	113.2	123.2
Cooling Cylinder	Outer surface	0°	1050	B(70)	46.8	57.8	67	88.4	113	133.3
〃	(Side)	〃	750	B(71)	40.8	46.6	58.6	69.2	93.2	113.8
〃	〃	〃	450	B(72)	43.9	49.4	58.5	76	97.6	117.1
〃	〃	〃	150	B(73)	45.1	53.1	63.5	75.3	89.6	107.9
〃	Outer surface	Center	0	B(74)	36.4	51	61.8	84	109.7	134.5
〃	(Bottom)	0°	100	B(75)	37.3	51.7	62.2	84.7	109.5	133.9
〃	〃	〃	210	B(76)	35.7	48.7	58.6	78.1	100.5	122.9
〃	〃	〃	320	B(77)	32.4	43.3	52.3	66.9	85.6	104.1
〃	〃	〃	430	B(78)	32.5	42	50.5	62.6	79.3	95.6
〃	〃	120°	100	B(79)	37.4	51.5	62.1	84.4	109.9	133.9
〃	〃	〃	305	B(80)	33.4	44.4	53.3	68.4	87.8	105.6
〃	〃	240°	100	B(81)	36.8	51.1	61.9	84	110.1	135.6
〃	〃	〃	305	B(82)	32	42.9	52.1	67.1	87.5	106.9
Top Disk	Outer surface	0°	470	B(83)	32.9	43.3	48.8	63	80.7	89.4
〃	〃	〃	370	B(84)	34.5	48.4	53.4	73.7	96.2	106.7
〃	〃	〃	270	B(85)	38.1	56.1	59.6	87.8	115.8	128.8
〃	〃	〃	190	B(86)	40.1	65	66.8	102.8	135.4	150.6
〃	〃	120°	470	B(87)	35	45.8	51.7	66	84.1	97.3
〃	〃	〃	370	B(88)	35.9	49.2	54.7	73.8	95.3	111.1
〃	〃	〃	270	B(89)	39.5	56.1	60.7	86.8	113.1	132.1
〃	〃	〃	190	B(90)	41.1	61.5	65.5	97	127.6	139.9
〃	〃	240°	470	B(91)	32.8	42.9	50	62.9	79.9	85.4
〃	〃	〃	370	B(92)	33.9	46.9	53.8	71.8	93.2	99.9
〃	〃	〃	270	B(93)	37.6	54.3	59.9	84.9	111.4	121.1
〃	〃	〃	190	B(94)	43.6	63.1	66.3	98.9	129.2	150.2
Cooling Pipe	Outer surface-1	120°	919.94	B(95)	23.8	25.5	28.6	28.4	31.7	33.2
〃	Outer surface-2	120°	67.94	B(96)	23.3	23.3	26	24.4	26.2	26.1

Table 4 Experimental results for filling with He of 0.1MPa (1/3)

Measuring Position					Measured Temperature (℃)				
Section		Angle	Position (mm)	Channel	6.5A	8A	10A	12A	14A
Heating Cylinder	Inner surface	0°	1310	B(1)	32.7	66	79.2	97.3	110.2
〃	(Side)	〃	1240	B(2)	61.4	106.7	132.6	166	191.7
〃	〃	〃	1170	B(3)	86	154.9	193.8	241.4	280
〃	〃	〃	1100	B(4)	114.3	236	294.7	360.4	416
〃	Outer surface	0°	1049	B(5)	163.9	318.8	399.5	485.6	559.9
〃	(Side)	〃	932	B(6)	222.8	322.1	396.9	475.1	541.1
〃	〃	〃	799	B(7)	224.3	305.6	378	453.9	517.5
〃	〃	〃	666	B(8)	212.8	293.1	366.6	444.1	510.2
〃	〃	〃	599.5	B(9)	211.2	285.6	354.4	424.4	484
〃	〃	〃	533	B(10)	211.3	286.5	359.9	436.1	503.3
〃	〃	〃	400	B(11)	203.1	276.9	352	428.2	499.4
〃	〃	〃	267	B(12)	189.3	267.7	344	422	492.8
〃	〃	〃	150	B(13)	178.3	265.8	347.7	433.7	512.6
〃	Inner surface	120°	1310	B(14)	34	66.9	80.3	97.9	109.7
〃	(Side)	〃	1100	B(15)	110.5	209.7	263.1	320	368.7
〃	Outer surface	120°	1050	B(16)	170.8	299.6	375.7	456.1	525.5
〃	(Side)	〃	800	B(17)	228.1	306.9	379.6	455.5	520
〃	〃	〃	600	B(18)	216.2	290.3	359.5	430.8	491.9
〃	〃	〃	400	B(19)	217.1	289.8	364.7	440.7	513
〃	〃	〃	150	B(20)	171.6	252.5	328.1	407.5	480.8
〃	Inner surface	240°	1310	B(21)	35	69.3	82.9	103.8	119.2
〃	(Side)	〃	1100	B(22)	113.2	227.9	284.1	351.5	408.3
〃	Outer surface	240°	1050	B(23)	160.5	297	371.3	451.9	520.6
〃	(Side)	〃	800	B(24)	223.6	302.8	374	447.6	509.5
〃	〃	〃	600	B(25)	213.8	289.2	359.3	431.9	493.8
〃	〃	〃	400	B(26)	206.2	279	353.4	429.1	500.4
〃	〃	〃	150	B(27)	181.7	267.2	347.3	430.9	507.5
〃	Outer surface	Center	0	B(28)	192.9	291	383.5	479.6	564.9
〃	(Bottom)	0°	100	B(29)	184.9	279.1	367.1	458.7	540
〃	〃	120°	100	B(30)	184.4	276	361.8	450.7	529.5
〃	〃	240°	100	B(31)	185.1	277.9	364.5	454.3	534.2

Table 4 Experimental results for filling with He of 0.1MPa (2/3)

Cooling Cylinder	Inner surface	Center	0	B(32)	54.3	87.4	122.2	163.1	204.3
〃	(Bottom)	0°	100	B(33)	53.6	86.3	120.6	161	201.9
〃	〃	120°	100	B(34)	52.8	85	118.6	158.3	198.2
〃	〃	240°	100	B(35)	52.7	84.7	118.2	158.1	198.2
Lower Thermal	Upside surface	0°	424	B(36)	42.9	66.5	91.8	125.5	162.1
Insulation Plate	〃	〃	309	B(37)	53.4	85.3	119.2	163.3	210.4
〃	〃	〃	194	B(38)	70.6	115.2	162.9	223.2	285.9
〃	〃	240°	309	B(39)	51.3	80.3	111.4	151.9	194.9
〃	〃	120°	309	B(40)	52.4	81.5	111.6	151.6	194.4
Upper Thermal	Downside surface	0°	200	B(41)	162.4	255.8	317.9	382.5	440.3
Insulation Plate	〃	〃	334	B(42)	124.3	182	230.6	286.2	335
〃	〃	〃	432	B(43)	92.4	134.7	170.2	211.8	248.2
〃	〃	120°	338.5	B(44)	122.7	176.3	225.2	278.7	325.2
〃	〃	240°	338.5	B(45)	123.2	175.4	219.6	273.8	322
Cooling Cylinder	Inner surface	0°	1050	B(46)	61.2	87.5	109.3	135.5	158.6
〃	(Side)	〃	900	B(47)	59.4	84.3	103.6	128	151.6
〃	〃	〃	750	B(48)	47.5	67.9	85.1	106.7	128.6
〃	〃	〃	600	B(49)	40	56.9	71.3	90.2	110
〃	〃	〃	450	B(50)	38.8	55.2	68.5	87.3	107.9
〃	〃	〃	300	B(51)	38.5	55.5	68.7	86.8	106.5
〃	〃	〃	150	B(52)	37.8	56.1	71.8	91.2	112.2
〃	〃	120°	1050	B(53)	66.6	94.7	117.8	147.1	170.9
〃	〃	〃	750	B(54)	41.8	53.3	61.1	72.4	84.1
〃	〃	〃	450	B(55)	33	43.9	48.9	58.2	68.9
〃	〃	〃	150	B(56)	36.8	53.5	66.3	83.5	101.8
〃	〃	240°	1050	B(57)	62.8	84.3	102	131.3	157.7
〃	〃	〃	750	B(58)	40.7	52.2	60.6	73.1	86.3
〃	〃	〃	450	B(59)	29.6	39.4	45.1	53.6	63.5
〃	〃	〃	150	B(60)	34.5	50.1	62	78	94.9
〃	Inner surface	0°	305	B(61)	40.2	62.8	85.8	114.2	144.3
〃	(Bottom)	120°	305	B(62)	39.8	61.5	83.6	111	139.3
〃	〃	240°	305	B(63)	39.4	60.9	83	111	139.9

Table 4 Experimental results for filling with He of 0.1MPa (3/3)

Top Disk	Inner surface	0°	370	B(64)	58.5	84.9	109.1	140.8	165.4
〃	〃	〃	270	B(65)	67.6	105.4	135.5	176.6	209.3
〃	〃	120°	370	B(66)	61.1	92.3	116.8	146	167.6
〃	〃	〃	270	B(67)	69.4	110.1	140.6	176	204.8
〃	〃	240°	370	B(68)	59.1	76.3	91.4	133.2	164.8
〃	〃	〃	270	B(69)	67.4	96.2	118.8	166.7	204.7
Cooling Cylinder	Outer surface (Side)	0°	1050	B(70)	60.4	86.4	107.8	133.7	156.5
〃	〃	〃	750	B(71)	43.8	62.5	77.8	96.5	115.7
〃	〃	〃	450	B(72)	36	50.5	63.2	78.5	95.7
〃	〃	〃	150	B(73)	33.2	49.4	60.6	74.2	87.8
〃	Outer surface (Bottom)	Center	0	B(74)	53.2	85.7	119.8	160.1	200.7
〃	〃	0°	100	B(75)	52.4	84.4	117.8	157.6	197.7
〃	〃	〃	210	B(76)	46.4	73.8	102.3	137.1	172.6
〃	〃	〃	320	B(77)	39.2	61	82.9	110.1	139
〃	〃	〃	430	B(78)	35.7	54	71.5	93.1	116.5
〃	〃	120°	100	B(79)	51.6	83	116	155.7	195.3
〃	〃	〃	305	B(80)	39.7	60.9	82.5	109.6	137.5
〃	〃	240°	100	B(81)	51.8	83	115.8	155	194.6
〃	〃	〃	305	B(82)	39.2	60.4	82.3	109.9	138.5
Top Disk	Outer surface	0°	470	B(83)	49.2	67.9	85.5	106.9	123.6
〃	〃	〃	370	B(84)	58.4	84.7	108.8	140.5	165.2
〃	〃	〃	270	B(85)	66.7	103.6	133.3	174	206.3
〃	〃	〃	190	B(86)	71.3	119.9	153.4	199.8	237.2
〃	〃	120°	470	B(87)	52.8	75.8	94.2	117.5	133.1
〃	〃	〃	370	B(88)	60.1	90.7	114.8	143.6	165
〃	〃	〃	270	B(89)	68.4	108.6	138.6	173.4	201.7
〃	〃	〃	190	B(90)	70.1	109.2	136.6	186.4	227
〃	〃	240°	470	B(91)	50.6	61.8	72.1	103.2	127
〃	〃	〃	370	B(92)	58.4	74	88.3	130.9	162.9
〃	〃	〃	270	B(93)	66.2	93.7	115.7	162.9	200.3
〃	〃	〃	190	B(94)	72.8	121.1	154.9	194.4	227.4
Cooling Pipe	Outer surface-1	120°	919.94	B(95)	24.1	29	30	31	32.5
〃	Outer surface-2	120°	67.94	B(96)	22.1	25.7	25.4	25	24.9

Table 5 Experimental results for filling with N_2 of 0.1MPa (1/3)

Measuring Position					Measured Temperature (℃)				
Section		Angle	Position (mm)	Channel	6.5A	8A	10A	12A	14A
Heating Cylinder	Inner surface	0°	1310	B(1)	39.5	49.7	84.9	102.6	116.9
〃	(Side)	〃	1240	B(2)	90.2	125.2	168	201.9	230
〃	〃	〃	1170	B(3)	148	197.5	250	297.9	338.1
〃	〃	〃	1100	B(4)	217.7	282.5	350.8	417.1	473.5
〃	Outer surface	0°	1049	B(5)	269.1	347.7	431.8	515.9	588.3
〃	(Side)	〃	932	B(6)	279	343.8	419.8	494.6	559.3
〃	〃	〃	799	B(7)	271.1	328.7	401.8	474.5	536.3
〃	〃	〃	666	B(8)	257.6	318.2	392.1	466.7	528.6
〃	〃	〃	599.5	B(9)	254.9	311.8	380.5	448.9	505.3
〃	〃	〃	533	B(10)	255.4	314.5	387.3	462.7	525.5
〃	〃	〃	400	B(11)	253.1	314.2	387.6	463.9	528.8
〃	〃	〃	267	B(12)	245.6	312.5	386	460.8	522.8
〃	〃	〃	150	B(13)	242.4	319.6	399	480.1	547.8
〃	Inner surface	120°	1310	B(14)	40.7	52	86	104	119.4
〃	(Side)	〃	1100	B(15)	193.8	253.8	316	376.4	427.9
〃	Outer surface	120°	1050	B(16)	254.1	327.1	406.8	486.2	553.9
〃	(Side)	〃	800	B(17)	273.7	330.6	404.7	478.2	540.8
〃	〃	〃	600	B(18)	259.4	316.8	386.9	457	515.5
〃	〃	〃	400	B(19)	267.4	326.9	401	477.7	542.2
〃	〃	〃	150	B(20)	238.2	310.2	386.5	463.8	529.2
〃	Inner surface	240°	1310	B(21)	45.5	57.1	92.5	112.4	127.2
〃	(Side)	〃	1100	B(22)	210.7	275.9	343.1	408.3	463.3
〃	Outer surface	240°	1050	B(23)	252.1	325.5	404	481.8	547.3
〃	(Side)	〃	800	B(24)	268.7	325.3	396.8	467.3	527.1
〃	〃	〃	600	B(25)	257.6	316.1	386.4	457.1	516.1
〃	〃	〃	400	B(26)	254.6	314.4	387.5	462.9	525.9
〃	〃	〃	150	B(27)	247.2	323.6	403.5	484.8	552.3
〃	Outer surface	Center	0	B(28)	273.6	358.7	452.5	546.4	628
〃	(Bottom)	0°	100	B(29)	266	348.9	438.5	528	605.2
〃	〃	120°	100	B(30)	264	344.4	432	519.3	594.2
〃	〃	240°	100	B(31)	265.2	346.7	435	523.1	599

Table 5 Experimental results for filling with N_2 of 0.1MPa (2/3)

Cooling Cylinder	Inner surface	Center	0	B(32)	49.4	71.1	96.5	126.1	155.3
〃	(Bottom)	0°	100	B(33)	49.6	71.4	96.8	126.4	155.5
〃	〃	120°	100	B(34)	48.9	70.2	95.1	124.3	153
〃	〃	240°	100	B(35)	48.5	69.5	94.4	123.7	152.5
Lower Thermal	Upside surface	0°	424	B(36)	71.6	100.4	138.8	185.8	230
Insulation Plate	〃	〃	309	B(37)	91.6	129.4	179.8	240.5	295.7
〃	〃	〃	194	B(38)	97.7	139.7	195.3	262.3	323.8
〃	〃	240°	309	B(39)	90.2	126.4	175.6	233.7	288.9
〃	〃	120°	309	B(40)	90.5	125.6	173.4	230.9	284.5
Upper Thermal	Downside surface	0°	200	B(41)	199.4	254.3	318.6	384.8	445.1
Insulation Plate	〃	〃	334	B(42)	162.6	207	260.5	315.6	364.9
〃	〃	〃	432	B(43)	144.8	183.1	228.5	272.4	309.6
〃	〃	120°	338.5	B(44)	159.5	203.2	256.4	311.9	361.1
〃	〃	240°	338.5	B(45)	160.6	205	257.9	312.9	361.4
Cooling Cylinder	Inner surface	0°	1050	B(46)	62.9	80.8	101.6	126.2	148.9
〃	(Side)	〃	900	B(47)	60.8	76.1	95	120.5	144.8
〃	〃	〃	750	B(48)	50.4	64.5	82.4	106.2	129.5
〃	〃	〃	600	B(49)	45	57.8	73.9	95.7	117.2
〃	〃	〃	450	B(50)	46.4	59.9	76.3	99	121.2
〃	〃	〃	300	B(51)	47.8	63.1	80.1	102.2	124
〃	〃	〃	150	B(52)	47.4	65.3	84	105	125
〃	〃	120°	1050	B(53)	68.6	87.2	108.7	135.2	161.6
〃	〃	〃	750	B(54)	44.1	50.9	58.7	72.7	84.6
〃	〃	〃	450	B(55)	38	44.5	52.3	64.8	77.1
〃	〃	〃	150	B(56)	45.7	59.2	73.7	91.6	110.1
〃	〃	240°	1050	B(57)	63.7	81.5	100.1	122.8	145.6
〃	〃	〃	750	B(58)	42.9	51.3	59.5	73.9	87.8
〃	〃	〃	450	B(59)	33.7	40.6	48.5	60.4	71.6
〃	〃	〃	150	B(60)	42.7	55.6	69.2	88	106.3
〃	Inner surface	0°	305	B(61)	40.7	57	75	96.4	117.6
〃	(Bottom)	120°	305	B(62)	40.6	55.8	73.3	94.2	115.1
〃	〃	240°	305	B(63)	39.8	55	72.7	94.1	115.8

Table 5 Experimental results for filling with N_2 of 0.1MPa (3/3)

Top Disk	Inner surface	0°	370	B(64)	53.4	71.9	91.3	113.8	132.5
〃	〃	〃	270	B(65)	61.2	84.2	109.4	138.4	162.4
〃	〃	120°	370	B(66)	55.2	72	90.6	114.4	136.2
〃	〃	〃	270	B(67)	61.5	81.9	105.4	134.7	160.9
〃	〃	240°	370	B(68)	53.4	71.7	90.4	112.5	131.6
〃	〃	〃	270	B(69)	60.1	82.5	106.6	134.8	158.4
Cooling Cylinder	Outer surface	0°	1050	B(70)	62.1	79.7	100.2	124.2	146.7
〃	(Side)	〃	750	B(71)	45.2	60.1	75.8	93.2	115.6
〃	〃	〃	450	B(72)	42.2	55.6	70.1	89.1	110.1
〃	〃	〃	150	B(73)	40.6	57.5	69	82.4	97.7
〃	Outer surface	Center	0	B(74)	48.5	69.8	94.8	123.9	152.7
〃	(Bottom)	0°	100	B(75)	48.5	69.8	94.6	123.6	152.1
〃	〃	〃	210	B(76)	45	64	85.9	111.5	137
〃	〃	〃	320	B(77)	40	55.7	73	93.5	113.9
〃	〃	〃	430	B(78)	37.7	51.6	66.1	83.5	100.2
〃	〃	120°	100	B(79)	48.1	68.8	93.4	122.3	151.1
〃	〃	〃	305	B(80)	40.4	55.3	72.6	93	113.6
〃	〃	240°	100	B(81)	47.9	68.6	93.1	121.9	150.3
〃	〃	〃	305	B(82)	39.5	54.4	72	93.1	114.5
Top Disk	Outer surface	0°	470	B(83)	47.1	60.9	75.5	92.3	106.1
〃	〃	〃	370	B(84)	53.3	71.7	91.2	113.6	132.2
〃	〃	〃	270	B(85)	60.5	83.1	108	136.6	160.3
〃	〃	〃	190	B(86)	67	92.9	122.8	156	184.5
〃	〃	120°	470	B(87)	49.9	63.4	78	96.8	114.7
〃	〃	〃	370	B(88)	54.3	70.8	89.1	112.5	134
〃	〃	〃	270	B(89)	60.8	80.9	104	133	158.7
〃	〃	〃	190	B(90)	63.9	88.5	116.4	148.3	175
〃	〃	240°	470	B(91)	47.9	62.4	76.5	93	108
〃	〃	〃	370	B(92)	52.9	70.9	89.4	111.2	130
〃	〃	〃	270	B(93)	59.1	81	104.6	132.2	155.2
〃	〃	〃	190	B(94)	65.5	88.3	115.5	148.4	177.8
Cooling Pipe	Outer surface-1	120°	919.94	B(95)	24.9	27.6	29.3	31.4	33.1
〃	Outer surface-2	120°	67.94	B(96)	22.8	24.6	25.1	25.5	25.6

Table 6 Results of experimental data arrangement for vacuum condition

Angle Height Gas	Electric Power (A)	Electric Power (kW)	T_1 (℃)	T_1 (K)	T_2 (℃)	T_2 (K)	$T_1^4-T_2^4$ (K^4)	$T_{outer\ wall}$ (℃)	$\overline{T}_{wall}$ (℃)	$\overline{T}_{wall}$ (K)	ΔT_{wall} (K)
0° 750mm Vacuum	6.5	10.4	304.0	577.13	45.0	318.15	1.007E+11	40.8	42.9	316.05	4.2
	7	11.2	332.8	605.91	52.6	325.75	1.235E+11	46.6	49.6	322.75	6.0
	8	12.8	366.9	640.09	63.2	336.35	1.551E+11	58.6	60.9	334.05	4.6
	10	16	434.3	707.42	80.5	353.65	2.348E+11	69.2	74.9	348.00	11.3
	12	19.2	499.5	772.62	105.1	378.25	3.359E+11	93.2	99.2	372.30	11.9
	14	22.4	555.7	828.86	127.9	401.05	4.461E+11	113.8	120.9	394.00	14.1
0° 450mm Vacuum	6.5	10.4	300.8	573.94	49.2	322.35	9.729E+10	43.9	46.6	319.70	5.3
	7	11.2	329.7	602.80	55.8	328.95	1.202E+11	49.4	52.6	325.75	6.4
	8	12.8	364.2	637.33	65.8	338.95	1.519E+11	58.5	62.2	335.30	7.3
	10	16	431.2	704.39	83.4	356.55	2.307E+11	76.0	79.7	352.85	7.4
	12	19.2	497.3	770.42	107.7	380.85	3.326E+11	97.6	102.7	375.80	10.1
	14	22.4	554.5	827.61	131.5	404.65	4.449E+11	117.1	124.3	397.45	14.4

Angle Height Gas	Electric Power (A)	Electric Power (kW)	k_{wall} (W/mK)	R (m^2K/W)	q_{all} (W/m^2)	f_r (W/m^2K^4)
0° 750mm Vacuum	6.5	10.4	16.0	0.00160171	2622.19	2.6041E-08
	7	11.2	16.1	0.00188564	3181.94	2.5759E-08
	8	12.8	16.1	0.00176833	2601.33	1.6775E-08
	10	16	16.2	0.00214497	5268.15	2.2437E-08
	12	19.2	16.3	0.00233381	5098.95	1.5181E-08
	14	22.4	16.4	0.00241972	5827.11	1.3062E-08
0° 450mm Vacuum	6.5	10.4	16.0	0.00160139	3309.62	3.4019E-08
	7	11.2	16.1	0.00188534	3394.61	2.8232E-08
	8	12.8	16.1	0.00176817	4128.55	2.7174E-08
	10	16	16.2	0.00214423	3451.12	1.4957E-08
	12	19.2	16.3	0.00233314	4328.94	1.3015E-08
	14	22.4	16.5	0.00241894	5953.02	1.3379E-08

Table 7 Results of experimental data arrangement for He and N_2 of 0.1MPa－Part 1－

Angle Height Gas	Electric Power	T_1		T_2		$\overline{T}_{12}$		ΔT_{12}	$T_1^4-T_2^4$	$T_{outer\ wall}$	$\overline{T}_{wall}$		ΔT_{wall}
	(A)	(℃)	(K)	(℃)	(K)	(℃)	(K)	(K)	(K^4)	(℃)	(℃)	(K)	(K)
	6.5	220.1	493.25	47.5	320.65	133.8	406.95	172.6	4.860E+10	43.8	45.7	318.80	3.7
0°	8	301.0	574.15	67.9	341.05	184.5	457.60	233.1	9.513E+10	62.5	65.2	338.35	5.4
750mm	10	373.8	646.95	85.1	358.25	229.5	502.60	288.7	1.587E+11	77.8	81.5	354.60	7.3
He	12	450.3	723.45	106.7	379.85	278.5	551.65	343.6	2.531E+11	96.5	101.6	374.75	10.2
	14	514.8	787.95	128.6	401.75	321.7	594.85	386.2	3.594E+11	115.7	122.2	395.30	12.9
	6.5	206.2	479.35	38.8	311.95	122.5	395.65	167.4	4.332E+10	36.0	37.4	310.55	2.8
0°	8	280.5	553.65	55.2	328.35	167.9	441.00	225.3	8.234E+10	50.5	52.9	326.00	4.7
450mm	10	355.0	628.15	68.5	341.65	211.8	484.90	286.5	1.420E+11	63.2	65.9	339.00	5.3
He	12	431.2	704.35	87.3	360.45	259.3	532.40	343.9	2.292E+11	78.5	82.9	356.05	8.8
	14	500.9	774.05	107.9	381.05	304.4	577.55	393.0	3.378E+11	95.7	101.8	374.95	12.2
	6.5	266.1	539.25	50.4	323.55	158.3	431.40	215.7	7.362E+10	45.2	47.8	320.95	5.2
0°	8	324.8	597.95	64.5	337.65	194.7	467.80	260.3	1.149E+11	60.1	62.3	335.45	4.4
750mm	10	398.2	671.35	82.4	355.55	240.3	513.45	315.8	1.872E+11	75.8	79.1	352.25	6.6
N_2	12	471.6	744.75	106.2	379.35	288.9	562.05	365.4	2.870E+11	93.2	99.7	372.85	13.0
	14	533.5	806.65	129.5	402.65	331.5	604.65	404.0	3.970E+11	115.6	122.6	395.70	13.9
	6.5	254.0	527.15	46.4	319.55	150.2	423.35	207.6	6.677E+10	42.2	44.3	317.45	4.2
0°	8	314.3	587.45	59.9	333.05	187.1	460.25	254.4	1.068E+11	55.6	57.8	330.90	4.3
450mm	10	387.5	660.65	76.3	349.45	231.9	505.05	311.2	1.756E+11	70.1	73.2	346.35	6.2
N_2	12	463.4	736.55	99.0	372.15	281.2	554.35	364.4	2.752E+11	89.1	94.1	367.20	9.9
	14	527.6	800.75	121.2	394.35	324.4	597.55	406.4	3.869E+11	110.1	115.7	388.80	11.1

Table 8-1 Results of experimental data arrangement for He and N_2 of 0.1MPa－Part 2－
(Case of using $f_{r,exp.}$)

Angle Height Gas	Electric Power (A)	k_{wall} (W/mK)	R (m^2K/W)	q_{all} (W/m^2)	$f_{r,exp.}$ (W/m^2K^4)	q_r (W/m^2)	q_c (W/m^2)	q_r/q_{all} (%)	h_{all} (W/m^2K)	h_r (W/m^2K)	h_c (W/m^2K)
	6.5	16.0	0.00096587	3830.74	4.3514E-08	2114.94	1715.81	55.2	22.20	12.26	9.94
0°	8	16.1	0.00119401	4522.59	2.9870E-08	2841.71	1680.88	62.8	19.40	12.19	7.21
750mm	10	16.2	0.00135018	5406.68	2.2425E-08	3559.04	1847.64	65.8	18.73	12.33	6.40
He	12	16.3	0.00167937	6073.71	1.7266E-08	4369.95	1703.77	71.9	17.68	12.72	4.96
	14	16.5	0.00196325	6570.73	1.4186E-08	5098.98	1471.75	77.6	17.01	13.20	3.81
	6.5	16.0	0.00096654	2896.94	4.6412E-08	2010.54	886.40	69.4	17.31	12.01	5.30
0°	8	16.1	0.00119545	3931.58	3.2387E-08	2666.82	1264.75	67.8	17.45	11.84	5.61
450mm	10	16.1	0.00135245	3918.82	2.3864E-08	3389.45	529.37	86.5	13.68	11.83	1.85
He	12	16.2	0.00168271	5229.66	1.8252E-08	4183.47	1046.19	80.0	15.21	12.17	3.04
	14	16.3	0.00196754	6200.63	1.4687E-08	4961.85	1238.78	80.0	15.78	12.63	3.15
	6.5	16.1	0.00138493	3754.70	3.4484E-08	2538.63	1216.06	67.6	17.40	11.77	5.64
0°	8	16.1	0.00116406	3779.86	2.6877E-08	3087.32	692.54	81.7	14.52	11.86	2.66
750mm	10	16.2	0.00155089	4255.63	2.0445E-08	3827.04	428.59	89.9	13.47	12.12	1.36
N_2	12	16.3	0.00210571	6173.68	1.6093E-08	4618.22	1555.46	74.8	16.89	12.64	4.26
	14	16.5	0.00207446	6700.54	1.3417E-08	5326.96	1373.58	79.5	16.59	13.19	3.40
	6.5	16.0	0.00138525	3031.95	3.6422E-08	2432.00	599.95	80.2	14.61	11.72	2.89
0°	8	16.1	0.00116460	3692.24	2.7996E-08	2989.99	702.25	81.0	14.51	11.75	2.76
450mm	10	16.2	0.00155177	3995.43	2.1192E-08	3720.65	274.78	93.1	12.84	11.96	0.88
N_2	12	16.3	0.00210677	4699.14	1.6475E-08	4533.97	165.17	96.5	12.89	12.44	0.45
	14	16.4	0.00207599	5346.84	1.3613E-08	5266.59	80.26	98.5	13.16	12.96	0.20

Table 8-2 Results of experimental data arrangement for He and N_2 of 0.1MPa－Part 3－
(Case of using $f_{r,exp.}$)

Angle Height Gas	Electric Power (A)	β (1/K)	k_g (mW/mK)	ν_g (mm²/s)	Pr (－)	$Ra\ (d)$ (－)	$Nu_{all}\ (d)$ (－)	$Nu_c\ (d)$ (－)	$Ra\ (l)$ (－)	$Nu\ (l)$ Eq.(14) (－)	$Nu_{all}\ (l)$ (－)	$Nu_c\ (l)$ (－)
0° 750mm He	6.5	0.002457	191.14	205.01	0.66966	1.627E+06	33.77	15.13	6.582E+07	41.85	115.91	51.92
	8	0.002185	207.93	249.91	0.66756	1.311E+06	27.13	10.08	5.304E+07	39.63	93.13	34.61
	10	0.001990	222.20	292.96	0.66592	1.074E+06	24.51	8.37	4.342E+07	37.69	84.12	28.75
	12	0.001813	237.09	343.19	0.66417	8.460E+05	21.68	6.08	3.421E+07	35.50	74.41	20.87
	14	0.001681	249.67	390.24	0.66309	6.809E+05	19.81	4.44	2.754E+07	33.62	68.01	15.23
0° 450mm He	6.5	0.002528	187.29	195.53	0.67023	1.786E+06	26.87	8.22	7.224E+07	42.84	92.23	28.22
	8	0.002268	202.51	234.78	0.66819	1.492E+06	25.05	8.06	6.033E+07	40.93	85.99	27.66
	10	0.002062	216.65	275.66	0.66656	1.248E+06	18.36	2.48	5.048E+07	39.14	63.02	8.51
	12	0.001878	231.32	323.06	0.66484	9.911E+05	19.12	3.82	4.008E+07	36.94	65.61	13.13
	14	0.001732	244.69	371.07	0.66342	7.897E+05	18.75	3.75	3.194E+07	34.89	64.36	12.86
0° 750mm N_2	6.5	0.002318	34.59	29.70	0.72498	9.901E+07	146.30	47.38	4.004E+09	117.92	502.16	162.64
	8	0.002138	36.81	34.05	0.73610	8.509E+07	114.69	21.01	3.441E+09	113.73	393.67	72.13
	10	0.001948	39.48	39.84	0.75753	7.070E+07	99.24	9.99	2.859E+09	108.93	340.65	34.31
	12	0.001779	42.19	46.41	0.78950	5.741E+07	116.42	29.33	2.322E+09	103.88	399.61	100.68
	14	0.001654	44.48	52.48	0.82526	4.822E+07	108.43	22.23	1.950E+09	99.93	372.18	76.30
0° 450mm N_2	6.5	0.002362	34.09	28.76	0.72323	1.032E+08	124.60	24.65	4.175E+09	119.13	427.67	84.63
	8	0.002173	36.35	33.13	0.73336	8.897E+07	116.07	22.08	3.598E+09	114.96	398.40	75.77
	10	0.001980	38.99	38.75	0.75295	7.443E+07	95.74	6.58	3.010E+09	110.27	328.61	22.60
	12	0.001804	41.77	45.34	0.78382	6.038E+07	89.75	3.15	2.442E+09	105.11	308.06	10.83
	14	0.001674	44.10	51.44	0.81879	5.068E+07	86.75	1.30	2.050E+09	101.09	297.75	4.47

Table 9-1 Results of experimental data arrangement for He and N_2 of 0.1MPa－Part 2－
(Case of using $f_{r,calc.}$)

Angle Height Gas	Electric Power (A)	k_{wall} (W/mK)	R (m^2K/W)	q_{all} (W/m^2)	$f_{r,calc.}$ (W/m^2K^4)	q_r (W/m^2)	q_c (W/m^2)	q_r/q_{all} (%)	h_{all} (W/m^2K)	h_r (W/m^2K)	h_c (W/m^2K)
0° 750mm He	6.5	16.0	0.00096587	3830.74	1.1255E-08	547.02	3283.73	14.3	22.20	3.17	19.03
	8	16.1	0.00119401	4522.59	1.1255E-08	1070.70	3451.89	23.7	19.40	4.59	14.81
	10	16.2	0.00135018	5406.68	1.1255E-08	1786.19	3620.49	33.0	18.73	6.19	12.54
	12	16.3	0.00167937	6073.71	1.1255E-08	2848.45	3225.26	46.9	17.68	8.29	9.39
	14	16.5	0.00196325	6570.73	1.1255E-08	4045.39	2525.33	61.6	17.01	10.47	6.54
0° 450mm He	6.5	16.0	0.00096654	2896.94	1.1255E-08	487.55	2409.39	16.8	17.31	2.91	14.39
	8	16.1	0.00119545	3931.58	1.1255E-08	926.73	3004.85	23.6	17.45	4.11	13.34
	10	16.1	0.00135245	3918.82	1.1255E-08	1598.53	2320.30	40.8	13.68	5.58	8.10
	12	16.2	0.00168271	5229.66	1.1255E-08	2579.58	2650.09	49.3	15.21	7.50	7.71
	14	16.3	0.00196754	6200.63	1.1255E-08	3802.25	2398.38	61.3	15.78	9.68	6.10
0° 750mm N_2	6.5	16.1	0.00138493	3754.70	1.1255E-08	828.53	2926.17	22.1	17.40	3.84	13.56
	8	16.1	0.00116406	3779.86	1.1255E-08	1292.79	2487.08	34.2	14.52	4.97	9.55
	10	16.2	0.00155089	4255.63	1.1255E-08	2106.76	2148.86	49.5	13.47	6.67	6.80
	12	16.3	0.00210571	6173.68	1.1255E-08	3229.78	2943.90	52.3	16.89	8.84	8.06
	14	16.5	0.00207446	6700.54	1.1255E-08	4468.39	2232.15	66.7	16.59	11.06	5.53
0° 450mm N_2	6.5	16.0	0.00138525	3031.95	1.1255E-08	751.51	2280.44	24.8	14.61	3.62	10.99
	8	16.1	0.00116460	3692.24	1.1255E-08	1201.98	2490.26	32.6	14.51	4.72	9.79
	10	16.2	0.00155177	3995.43	1.1255E-08	1975.96	2019.47	49.5	12.84	6.35	6.49
	12	16.3	0.00210677	4699.14	1.1255E-08	3097.38	1601.76	65.9	12.89	8.50	4.40
	14	16.4	0.00207599	5346.84	1.1255E-08	4354.08	992.76	81.4	13.16	10.71	2.44

Table 9-2 Results of experimental data arrangement for He and N_2 at 0.1MPa－Part 3－
(Case of using $f_{r,calc.}$)

Angle Height Gas	Electric Power (A)	β (1/K)	k_g (mW/mK)	ν_g (mm²/s)	Pr (－)	$Ra\ (d)$ (－)	$Nu_{all}\ (d)$ (－)	$Nu_c\ (d)$ (－)	$Ra\ (l)$ (－)	$Nu\ (l)$ Eq.(14) (－)	$Nu_{all}\ (l)$ (－)	$Nu_c\ (l)$ (－)
	6.5	0.002457	191.14	205.01	0.66966	1.627E+06	33.77	28.95	6.582E+07	41.85	115.91	99.36
0°	8	0.002185	207.93	249.91	0.66756	1.311E+06	27.13	20.71	5.304E+07	39.63	93.13	71.08
750mm	10	0.001990	222.20	292.96	0.66592	1.074E+06	24.51	16.41	4.342E+07	37.69	84.12	56.33
He	12	0.001813	237.09	343.19	0.66417	8.460E+05	21.68	11.51	3.421E+07	35.50	74.41	39.51
	14	0.001681	249.67	390.24	0.66309	6.809E+05	19.81	7.61	2.754E+07	33.62	68.01	26.14
	6.5	0.002528	187.29	195.53	0.67023	1.786E+06	26.87	22.35	7.224E+07	42.84	92.23	76.71
0°	8	0.002268	202.51	234.78	0.66819	1.492E+06	25.05	19.15	6.033E+07	40.93	85.99	65.72
450mm	10	0.002062	216.65	275.66	0.66656	1.248E+06	18.36	10.87	5.048E+07	39.14	63.02	37.31
He	12	0.001878	231.32	323.06	0.66484	9.911E+05	19.12	9.69	4.008E+07	36.94	65.61	33.25
	14	0.001732	244.69	371.07	0.66342	7.897E+05	18.75	7.25	3.194E+07	34.89	64.36	24.89
	6.5	0.002318	34.59	29.70	0.72498	9.901E+07	146.30	114.01	4.004E+09	117.92	502.16	391.35
0°	8	0.002138	36.81	34.05	0.73610	8.509E+07	114.69	75.46	3.441E+09	113.73	393.67	259.03
750mm	10	0.001948	39.48	39.84	0.75753	7.070E+07	99.24	50.11	2.859E+09	108.93	340.65	172.01
N_2	12	0.001779	42.19	46.41	0.78950	5.741E+07	116.42	55.51	2.322E+09	103.88	399.61	190.55
	14	0.001654	44.48	52.48	0.82526	4.822E+07	108.43	36.12	1.950E+09	99.93	372.18	123.98
	6.5	0.002362	34.09	28.76	0.72323	1.032E+08	124.60	93.71	4.175E+09	119.13	427.67	321.67
0°	8	0.002173	36.35	33.13	0.73336	8.897E+07	116.07	78.28	3.598E+09	114.96	398.40	268.71
450mm	10	0.001980	38.99	38.75	0.75295	7.443E+07	95.74	48.39	3.010E+09	110.27	328.61	166.10
N_2	12	0.001804	41.77	45.34	0.78382	6.038E+07	89.75	30.59	2.442E+09	105.11	308.06	105.01
	14	0.001674	44.10	51.44	0.81879	5.068E+07	86.75	16.11	2.050E+09	101.09	297.75	55.28

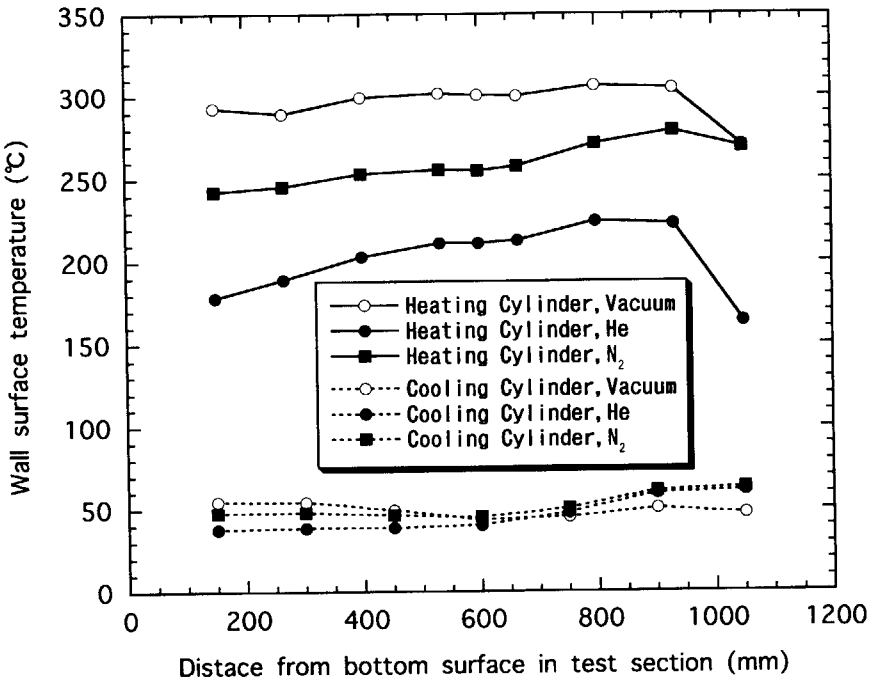

Fig. 10 Temperature distributions on wall surfaces for the experiments of 6.5A-heat input.

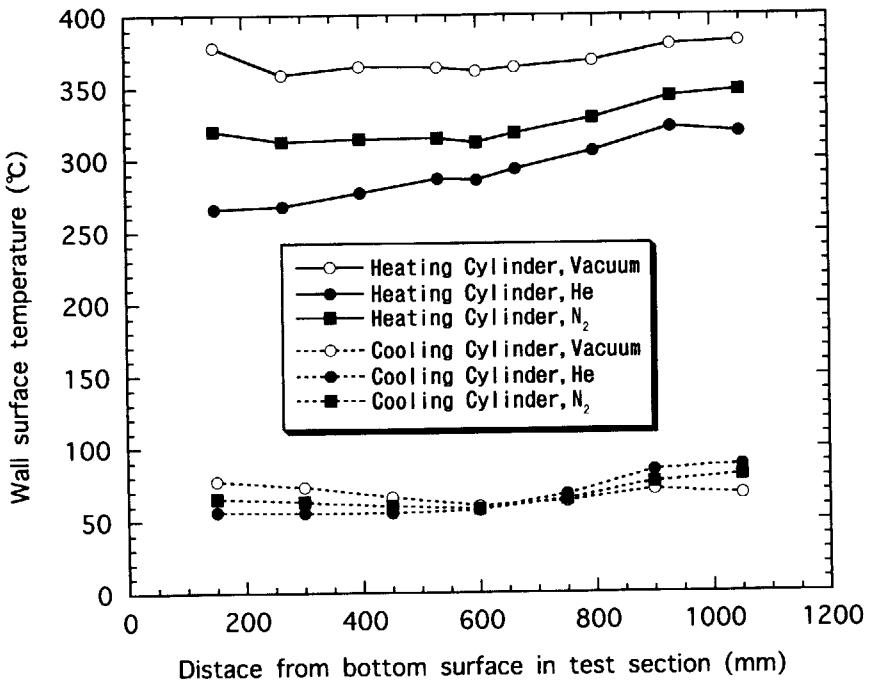

Fig. 11 Temperature distributions on wall surfaces for the experiments of 8A-heat input.

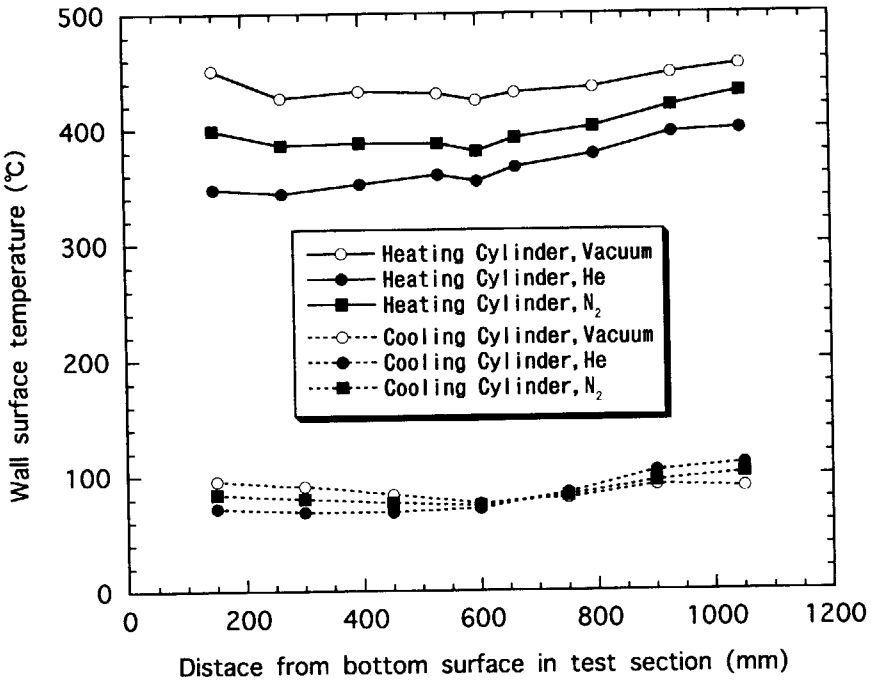

Fig. 12 Temperature distributions on wall surfaces for the experiments of 10A-heat input.

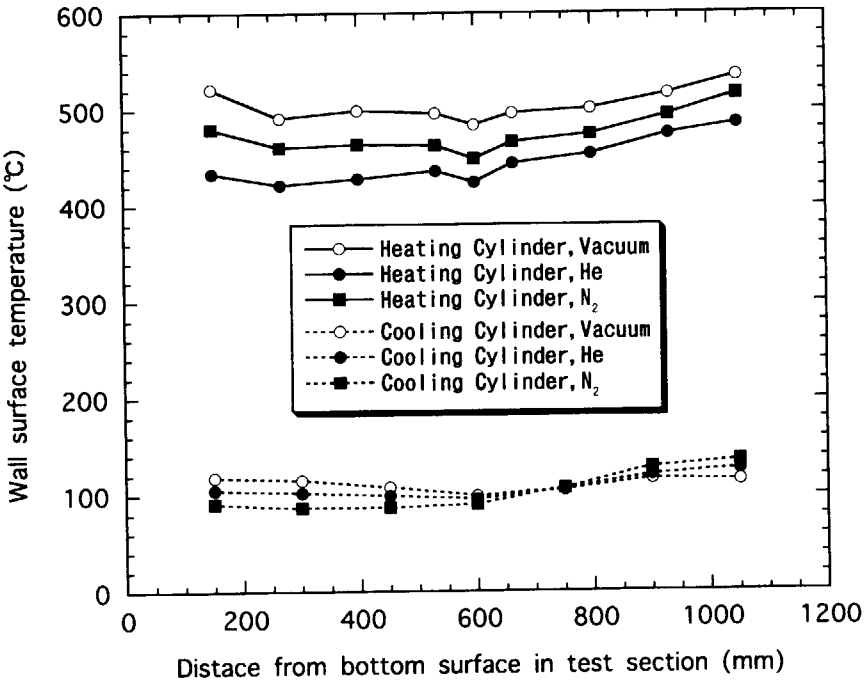

Fig. 13 Temperature distributions on wall surfaces for the experiments of 12A-heat input.

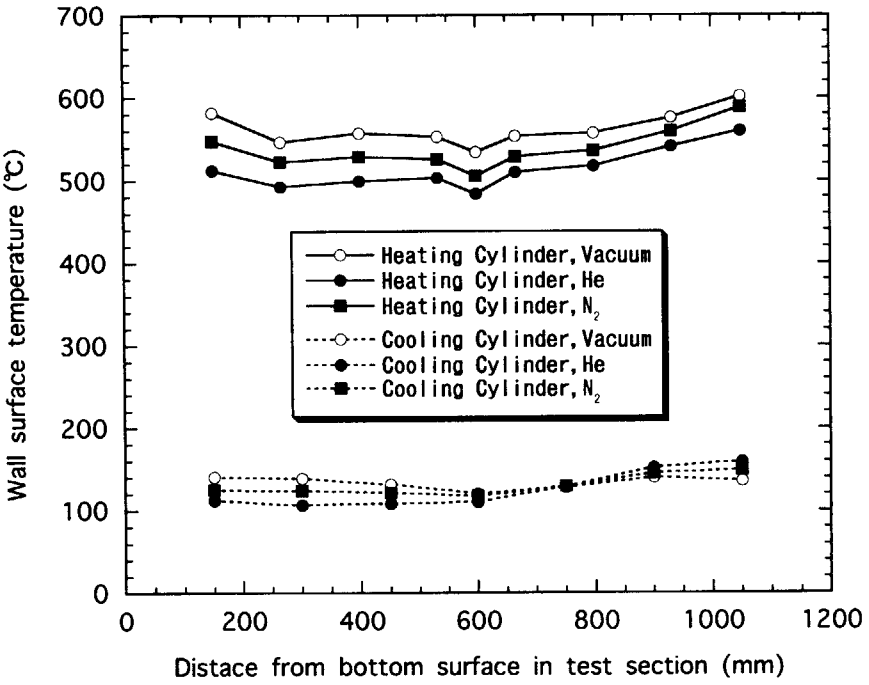

Fig. 14 Temperature distributions on wall surfaces for the experiments of 14A-heat input.

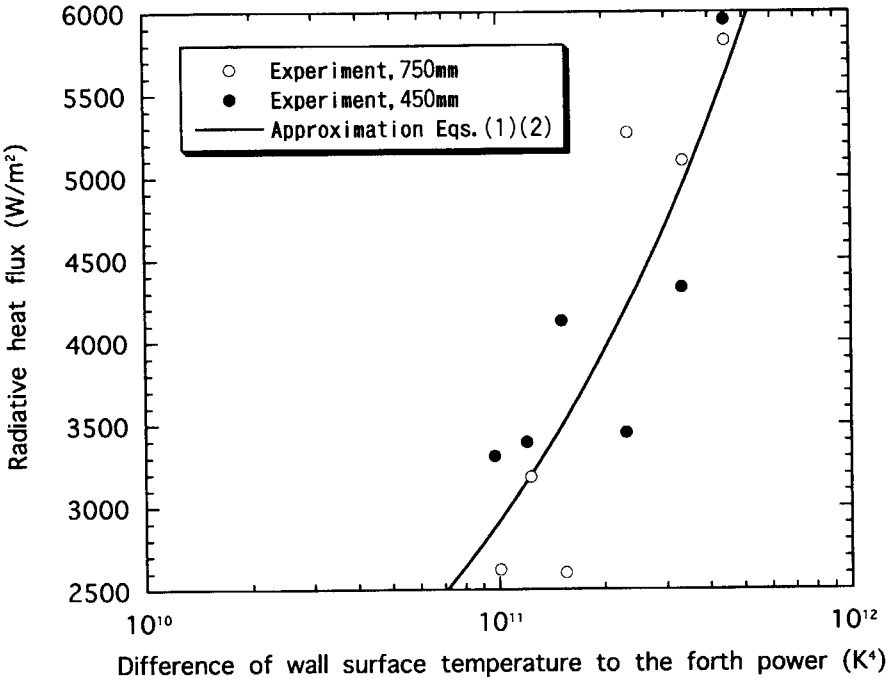

Fig. 15 Comparison of the radiative heat flux based on the experiments with the one based on Eqs. (1) and (2) for the vacuum condition.

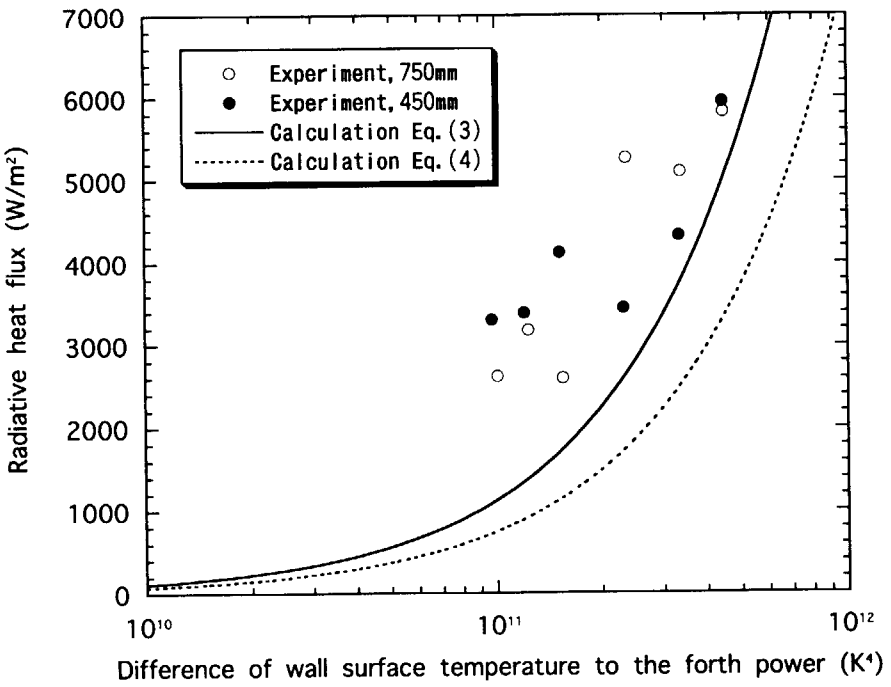

Fig. 16 Comparison of the radiative heat flux based on the experiments with the one based on Eqs. (3) and (4) for the vacuum condition.

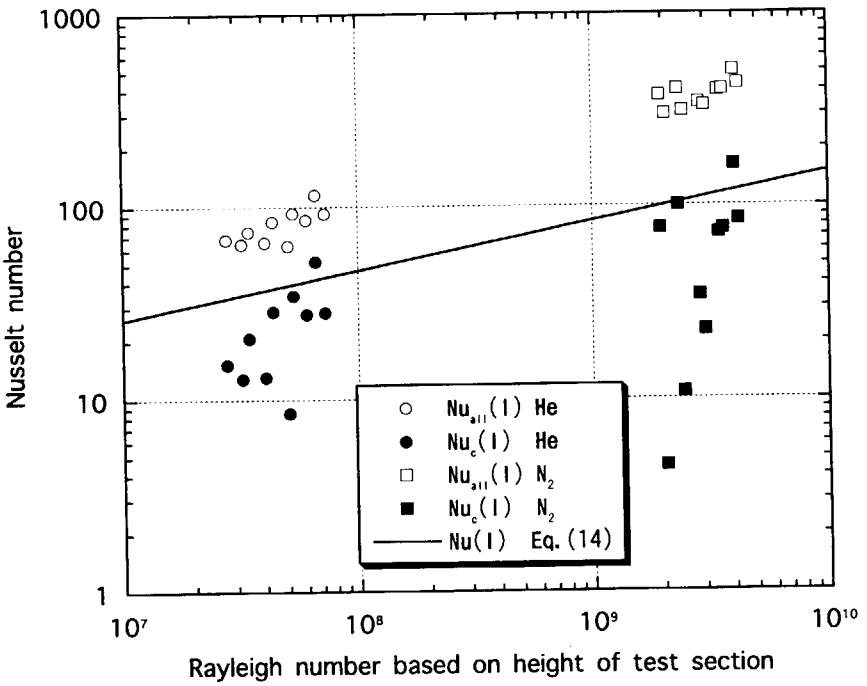

Fig. 17 Comparison of the Nusselt number based on the experiments using Eq. (2) with the one based on Eq. (14).

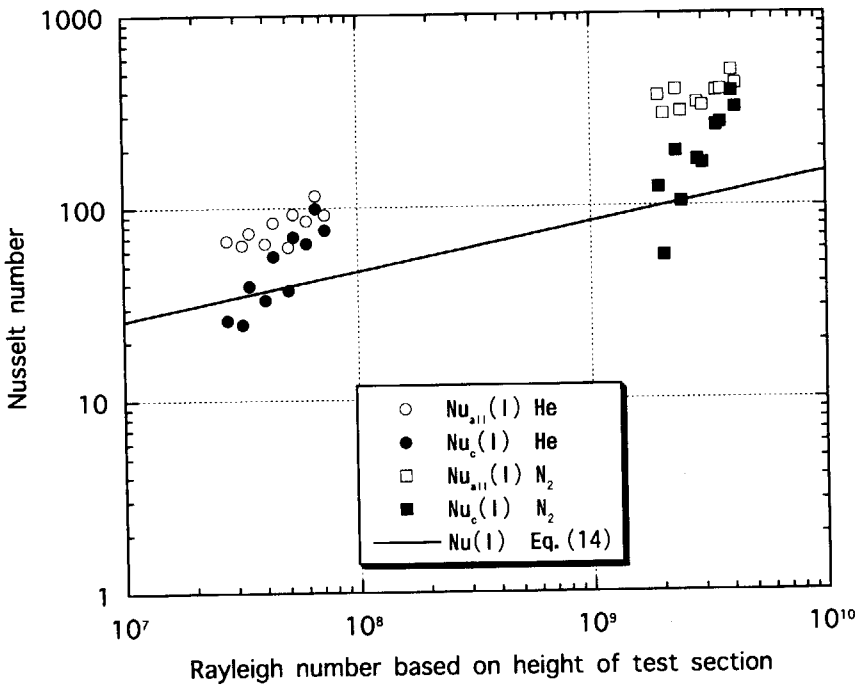

Fig. 18 Comparison of the Nusselt number based on the experiments using Eq. (5) with the one based on Eq. (14).

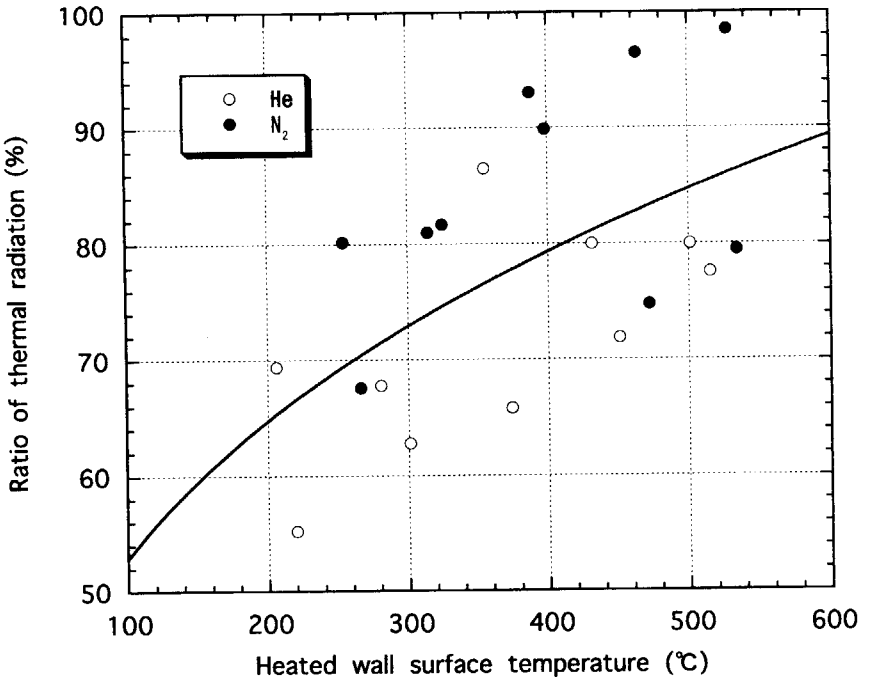

Fig. 19 Ratio of the heat transferred by thermal radiation to the heat transferred by convection and radiation using Eq. (2).

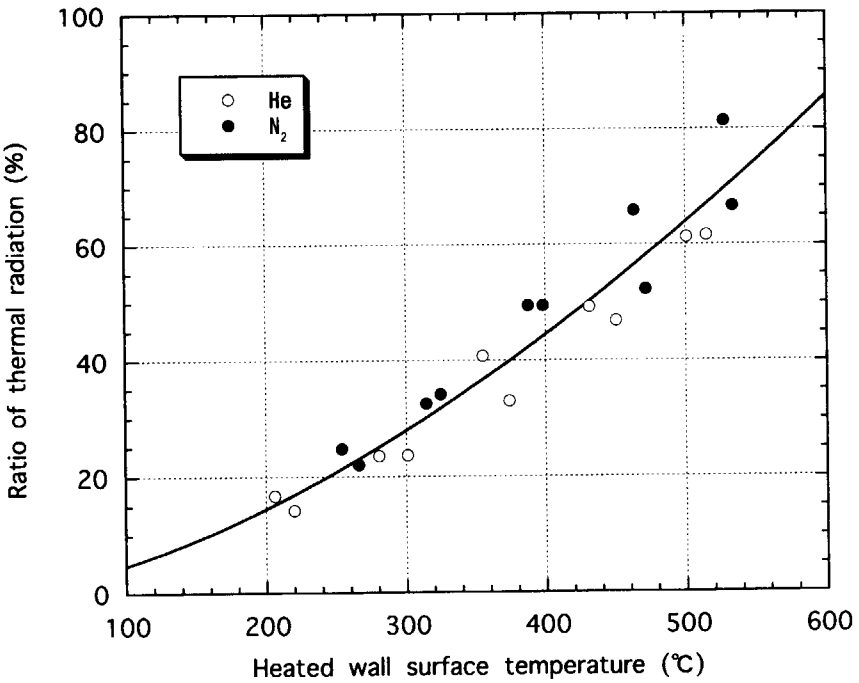

Fig. 20 Ratio of the heat transferred by thermal radiation to the the heat transferred by convection and radiation using Eq. (5).

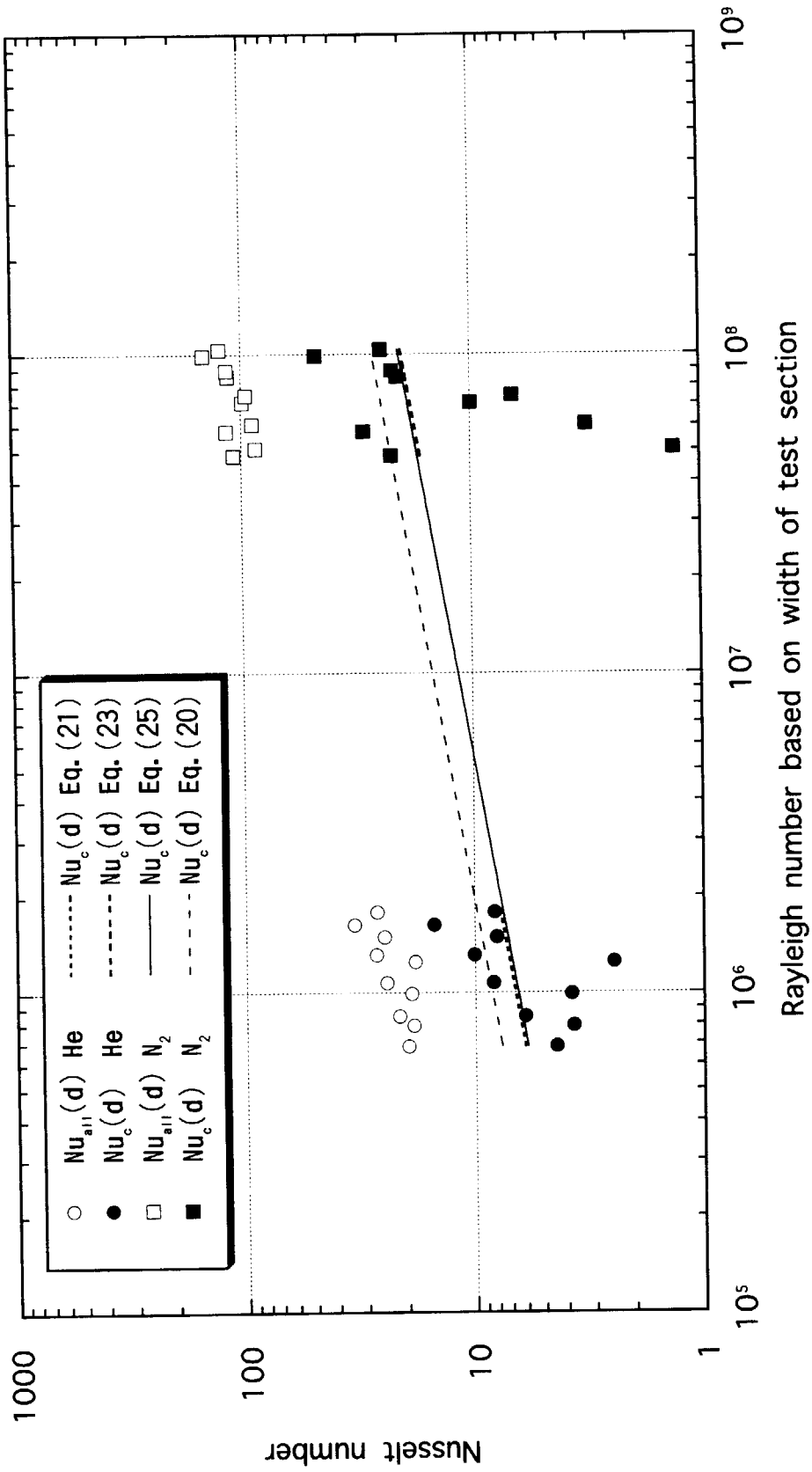

Fig. 21 Relationship between the Nusselt number and the Rayleigh number by Eqs. (21), (23) and (25).

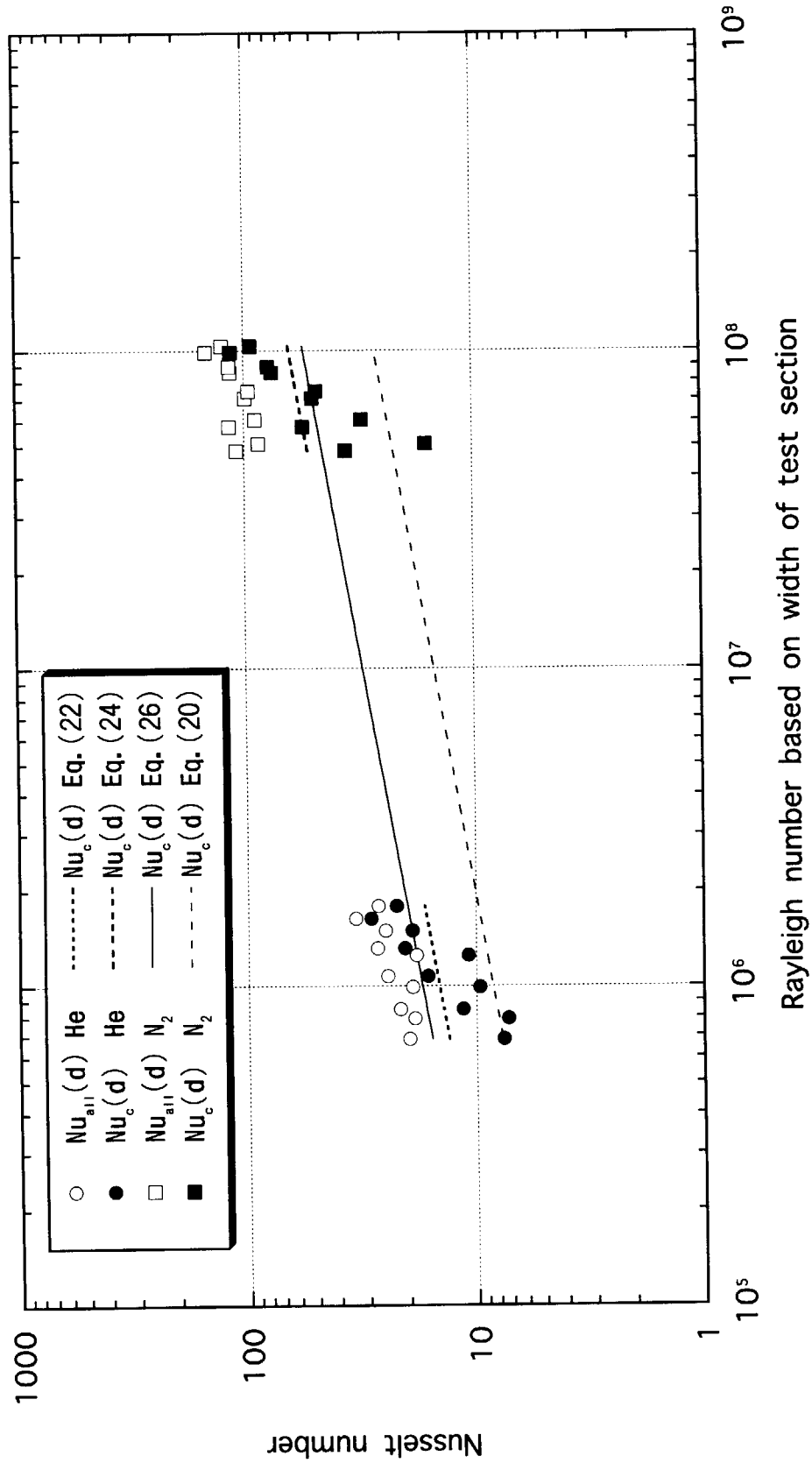

Fig. 22 Relationship between the Nusselt number and the Rayleigh number by Eqs. (22), (24) and (26).

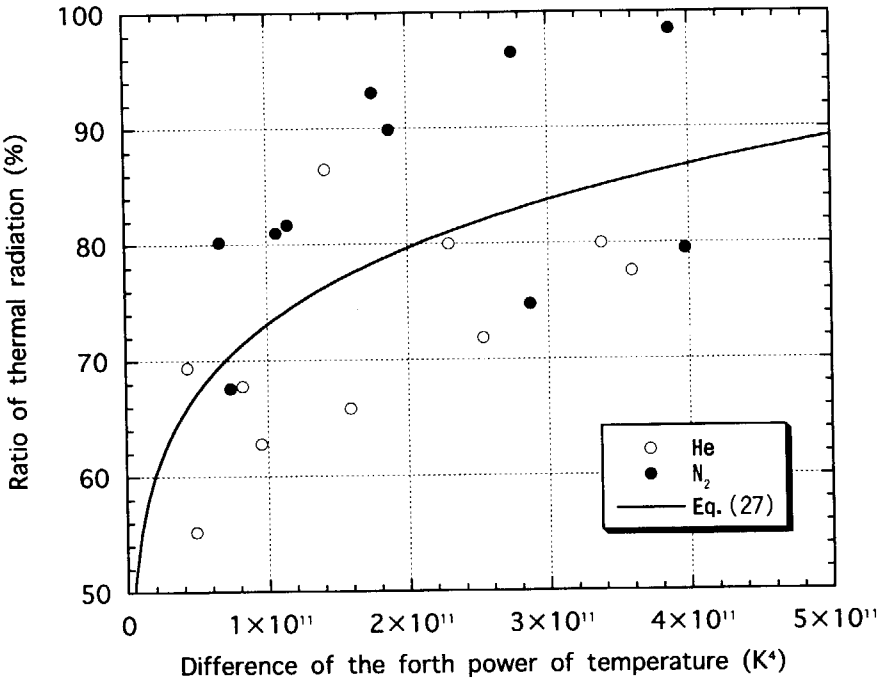

Fig. 23 Ratio of the heat transferred by thermal radiation to the heat transferred by convection and radiation shown as the function of the defference of the forth power of the heated and cooled wall surface temperature.

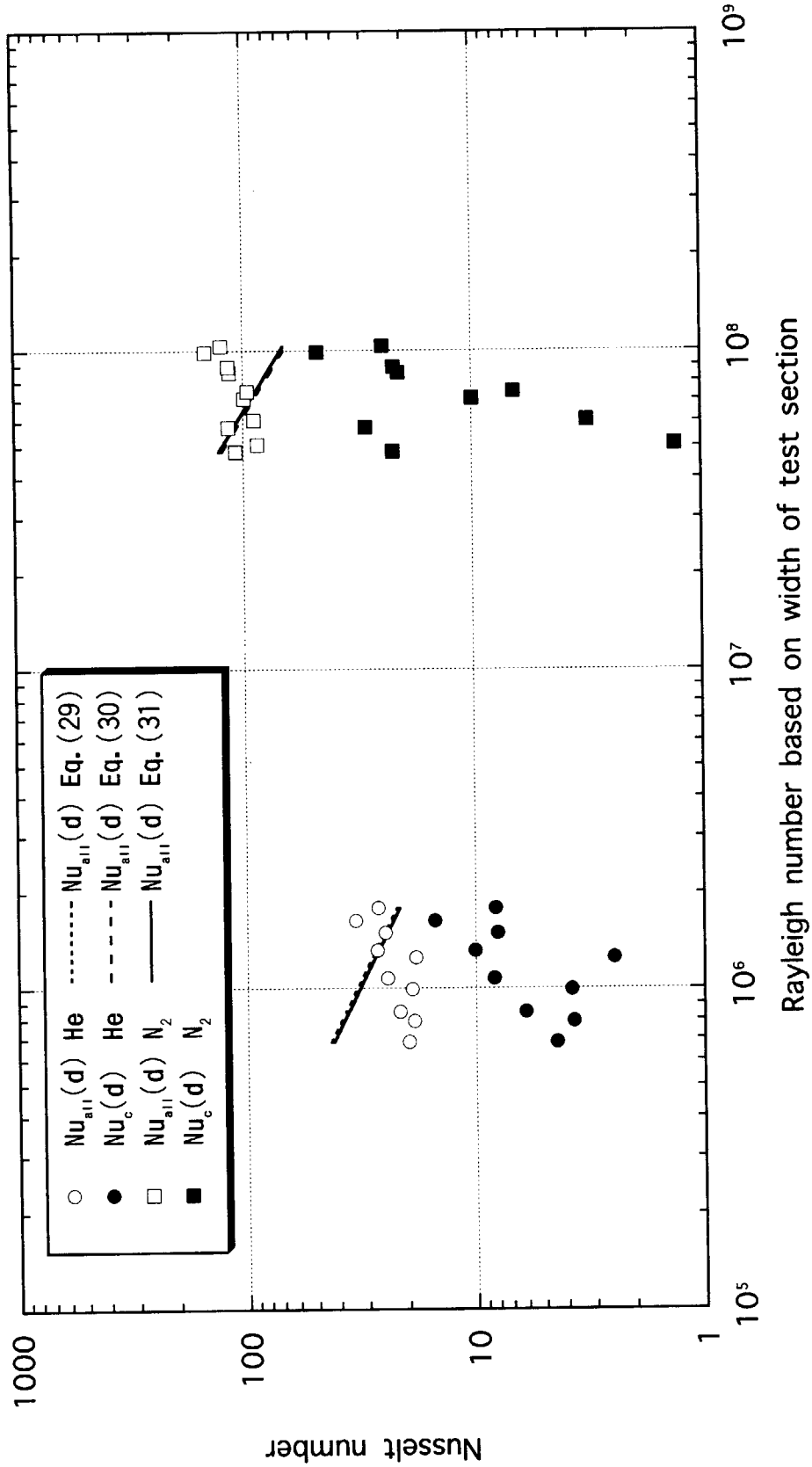

Fig. 24 Relationship between the Nusselt number and the Rayleigh number by Eqs. (29), (30) and (31).

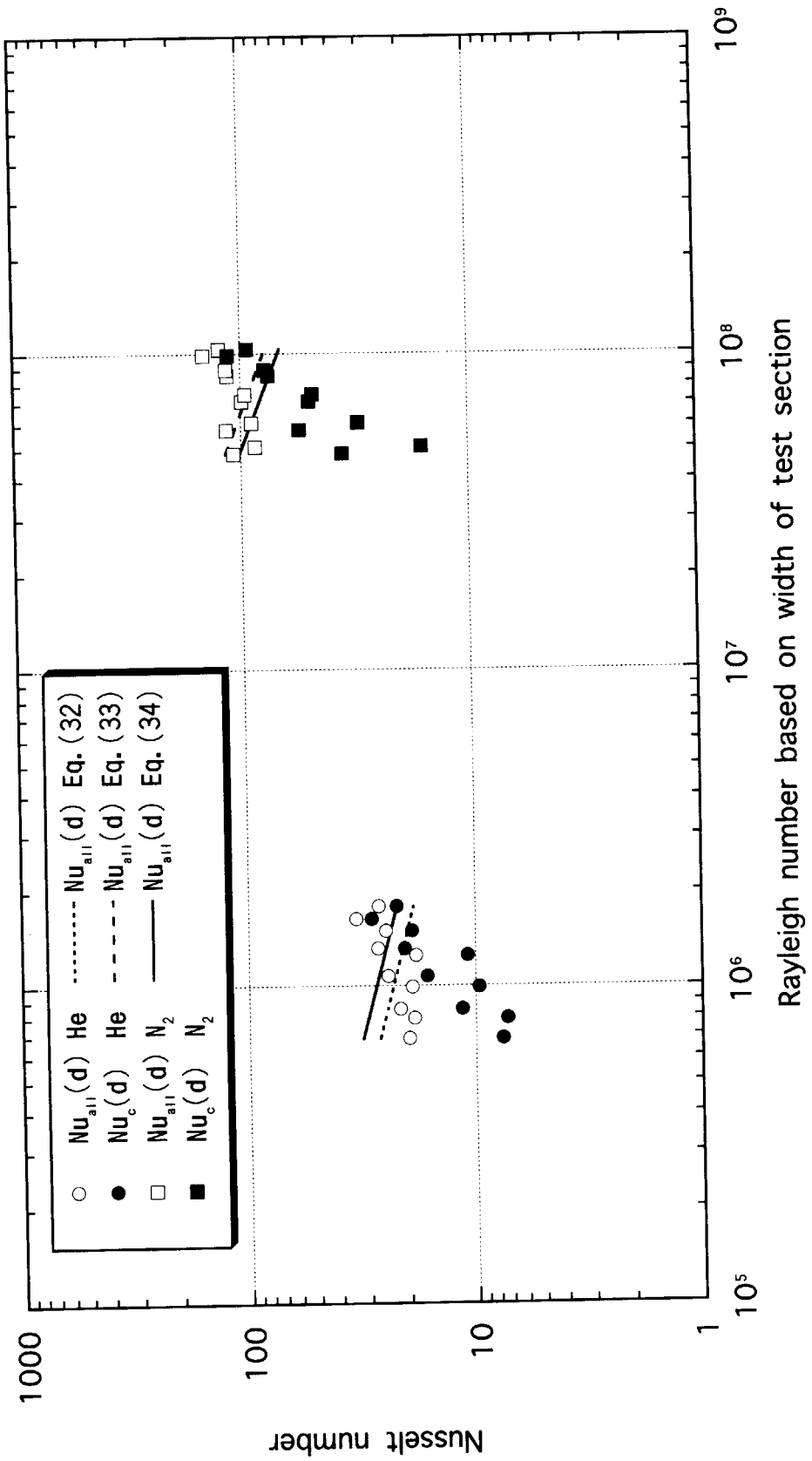

Fig. 25 Relationship between the Nusselt number and the Rayleigh number by Eqs. (32), (33) and (34).

4. Numerical Analysis

In addition to the experiments, we carry out numerical analyses by modeling of the experimental apparatus.

In the present numerical analysis, the CFD code FLUENT/UNS is used. FLUENT/UNS solves the governing differential equations for the conservation of mass, momentum and scalars such as energy, turbulence and chemical species in integral form. A control-volume based technique is used.

4.1 Basic Equations

The basic equations for the laminar flow under steady state conditions are summarized as follows:

Mass conservation

$$\frac{\partial}{\partial x_i}\left(\rho u_i\right)=0 \tag{35}$$

Momentum conservation

$$\frac{\partial}{\partial x_i}\left(\rho u_i u_j\right)=-\frac{\partial p}{\partial x_i}+\frac{\partial \tau_{ij}}{\partial x_j}+\rho g_i \tag{36}$$

with

$$\tau_{ij}=\mu\left(\frac{\partial u_i}{\partial x_j}+\frac{\partial u_j}{\partial x_i}\right)-\frac{2}{3}\mu\frac{\partial u_k}{\partial x_k}\delta_{ij} \tag{37}$$

Energy conservation

$$\frac{\partial}{\partial x_i}\left(\rho u_i h\right)=\frac{\partial}{\partial x_i}k\frac{\partial T}{\partial x_i}+\tau_{ij}\frac{\partial u_i}{\partial x_j}+Q_h \tag{38}$$

In above equations, x is the axial coordinate, ρ is the density, u is the velocity, p is the static pressure, τ_{ij} is the stress tensor given by Eq. (37), μ is the viscosity, δ is the delta function, g is the gravitational acceleration, h is the enthalpy, k is the thermal conductivity, T is the absolute temperature and Q_h is the source term.

4.2 Thermal Radiation Model

The thermal radiation is considered only for the surface to surface radiation. The Fluent code has some models for thermal radiation. The discrete transfer radiation model (DTRM) of these is used in this analysis. The main assumption of the DTRM is that the radiation leaving the surface element in a certain range of solid angles can be approximated by a single ray. The DTRM has the following limitations: (1) The DTRM assumes that all surfaces are diffuse. This means that the

reflection of incident radiation at the surface is isotropic with respect to solid angle. (2) The effect of scattering is not included.

4.2.1 The DTRM equations

The equation of thermal radiation for the change of radiant intensity dI, along a path ds when the DTRM is used, can be written as

$$\frac{dI}{ds} + aI = \frac{a\sigma T^4}{\pi} \tag{39}$$

where a is the gas absorption coefficient, I is the total hemispherical intensity, T is the gas local temperature and σ is the Stefan-Boltzmann constant. The DTRM integrates Eq. (39) along a series of rays emanating from boundary faces in each discrete control volume. If a is constant along the ray, then $I(s)$ can be estimated as

$$I(s) = \frac{\sigma T^4}{\pi}\left(1 - \exp\left[-as\right]\right) + I_0 \exp\left[-as\right] \tag{40}$$

where I_0 is the radiant intensity at the start of the incremental path, which is determined by the appropriate boundary condition. The energy source in the fluid due to radiation is then computed by summing the change in intensity along the path of each ray that is traced through the fluid control volume.

The ray tracing technique used in the DTRM can provide a prediction of radiation heat transfer between surfaces without explicit view-factor calculations. The accuracy of the models is limited mainly by the number of rays traced and the computational grid.

4.2.2 Boundary condition treatment for the DTRM at walls

The boundary condition treatment for the DTRM at walls is as follows: The radiation intensity approaching a point on a wall surface is integrated to yield the incident radiation heat flux, q_{rad}^-, as

$$q_{rad}^- = \int I^- d\Omega \tag{41}$$

where Ω is the hemispherical solid angle and I^- is the intensity of the incoming ray. The net radiation heat flux from the surface, q_{rad}^+ is then computed as a sum of the reflected portion of q_{rad}^- and the emissive power of the surface:

$$q_{rad}^+ = \left(1 - \varepsilon_w\right) q_{rad}^- + \varepsilon_w \sigma T_w^4 \tag{42}$$

where T_w is the surface temperature of the point P on the surface and ε_w is the wall emissivity, which is inputted as a boundary condition. FLUENT/UNS incorporates the radiation heat flux Eq. (42) in the prediction of the wall surface temperature. Equation (42) also provides the surface boundary condition for the radiation intensity I_0 of a ray emanating from the point P, as

$$I_0 = q_{rad}^+ / \pi \ . \tag{43}$$

4.3 Analytical model and boundary conditions

Figure 26 shows the analytical model and the boundary conditions in this analysis. The analytical model has two-dimension and symmetrical axis. The model consists of the heating cylinder, the test section and the cooling cylinder.

The top and bottom ends are adiabatic walls and heat from the heating cylinder to the test section is given as volumetric heat source that is input data for each analysis in the model. The cooling pipes attached on the outer surface of the cooling cylinder is not modeled. Instead of it, a heat transfer coefficient on the surface, h_0 is given as

$$h_0 = \frac{k}{d_0} Nu \tag{44}$$

where k is the thermal conductivity of water, d_0 is the inner diameter of the cooling pipes (=13.8mm) and Nu is the Nusselt number, which is equal to 4.36, supposed to developed laminar flow in a tube.

The flow regime of He and N_2 gases in the test section is supposed to the laminar flow for all analytical cases.

About grid size of the model, a constant bunching law is adopted for the fluid region and an ends bunching law is adopted for the solid region. The constant bunching law provides equal spacing of the nodes along a subedge. The ends bunching law provides symmetrical node placement with regard to the middle of the subedge. The node spacing is tight at the ends of the subedge, and becomes wider towards the middle of the subedge. The number of grids measures 60 grids in the x-direction and 63 grids in the y-direction. Figure 27 shows the grids of the model.

Polynomial fitting functions dependent on temperature are used for thermophysical properties of materials[4]. The emissivities on the heated and cooled walls are constant ($\varepsilon_1 = 0.7, \varepsilon_2 = 0.5$).

The numerical analyses are conducted for all the experimental conditions of He and N_2. The analytical conditions are shown in Table 10.

4.4 Numerical results and discussion

Figures 28 and 29 compare the calculated temperature on the heated and cooled wall surfaces with the experimental results for filling with He or N_2 and the heat input of 12A, respectively. A good agreement between the numerical and experimental results has been found. The cause of the difference between the numerical and experimental results may be the heat leak from the top and bottom disks, a measurement error of the heater power and the simplification of the analytical model. See Appendix-3 about the other calculated temperature on the heated and cooled wall surfaces.

Figures 30 and 31 show the contours of static temperature and the velocity vectors colored by the

velocity magnitude for filling with He in the analytical model. These figures have the same parameters as Fig. 28. Figures 32 and 33 show the contours of static temperature and the velocity vectors colored by the velocity magnitude for filling with N_2 in the analytical model. These figures have the same parameters as Fig. 29. According to the figures, flow patterns of He and N_2 are not same and the maximum temperature of N_2 is higher than the one of He, because of the difference of their thermophysical properties.

Table 10 Analytical conditions

Working Fluid	Pressure	Electric Power (W/m^3)	h_0 (W/m^2K)
He	0.1MPa	260746.4 (6.5A)	191.0
		322780.8 (8A)	193.1
		403476.0 (10A)	193.2
		484171.2 (12A)	193.4
		564866.4 (14A)	193.7
N_2	0.1MPa	261502.9 (6.5A)	191.4
		322780.8 (8A)	192.5
		403476.0 (10A)	193.0
		484171.2 (12A)	193.6
		564866.4 (14A)	194.0

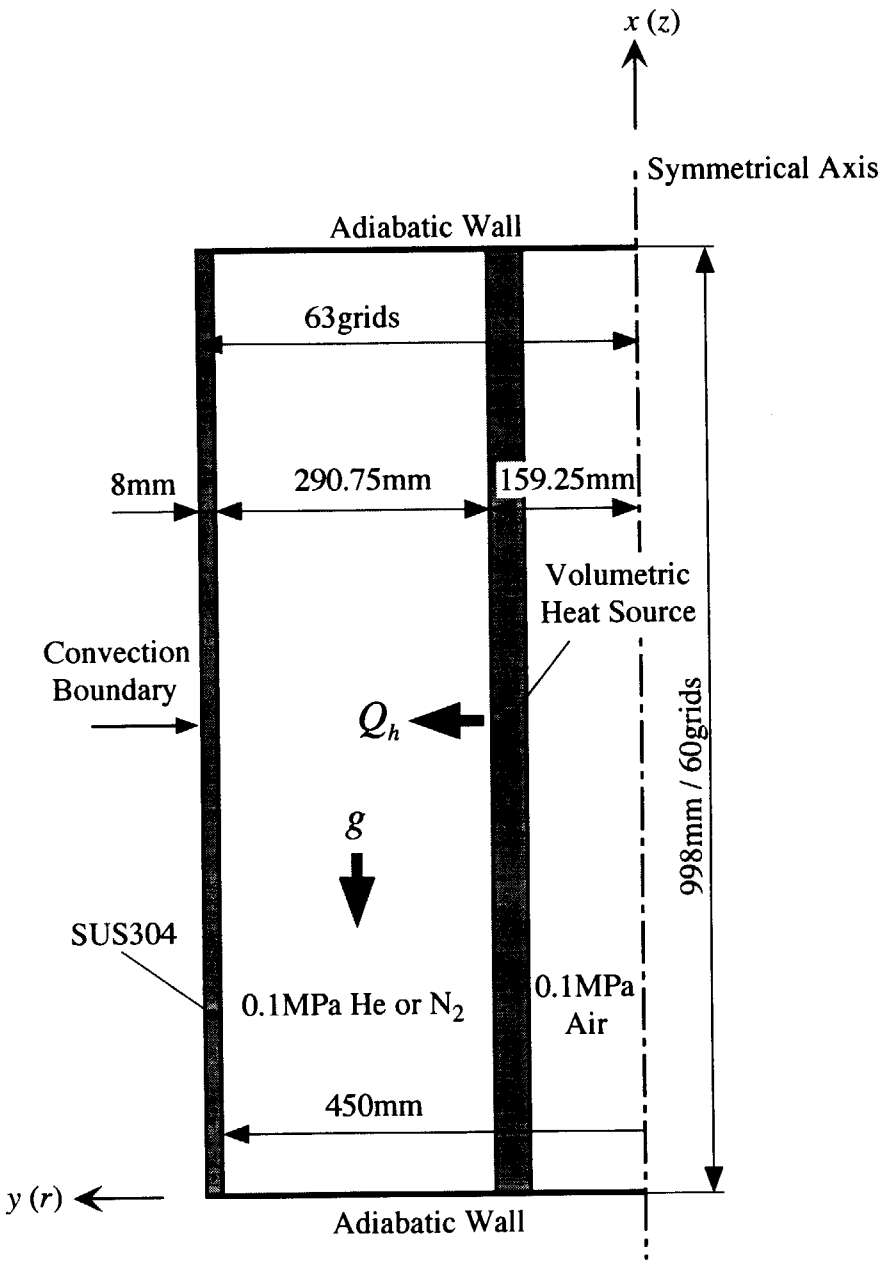

Fig. 26 Analytical model and baoundary conditions.

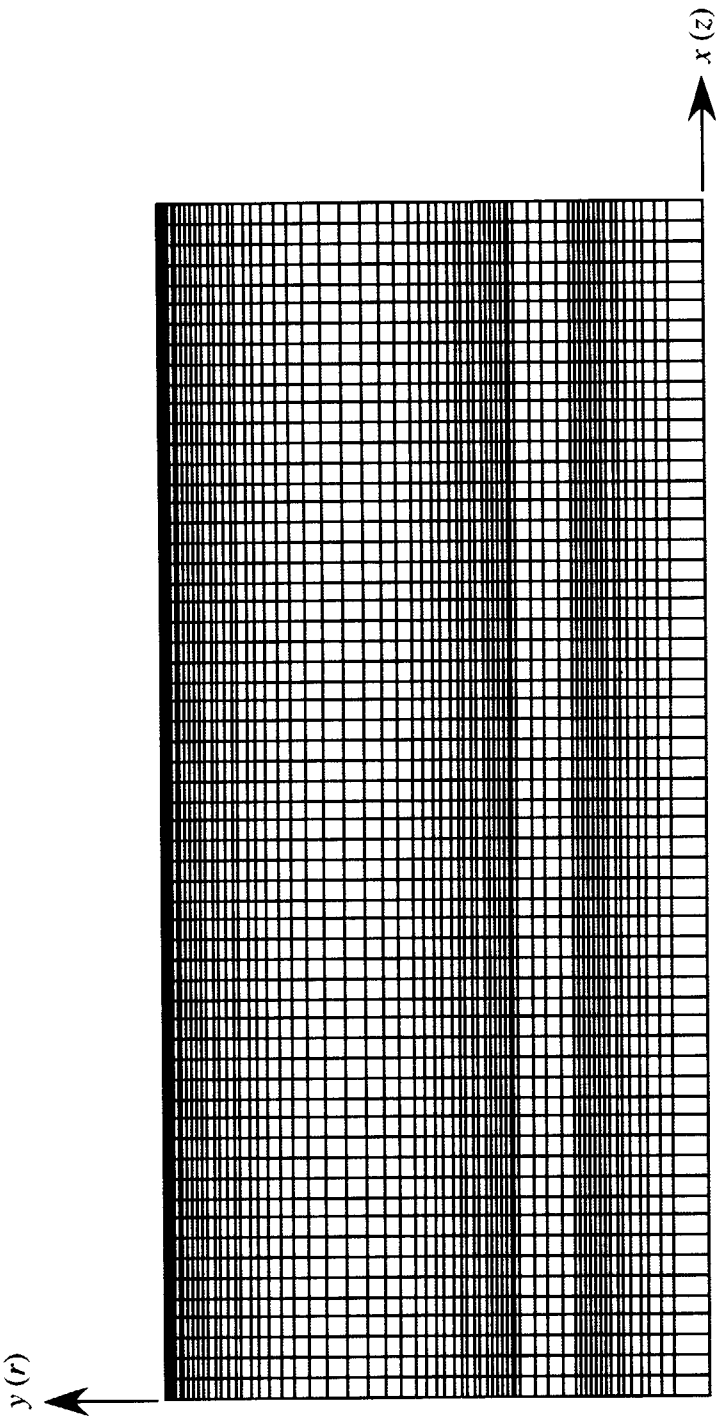

Fig. 27 Grids of the analytical model.

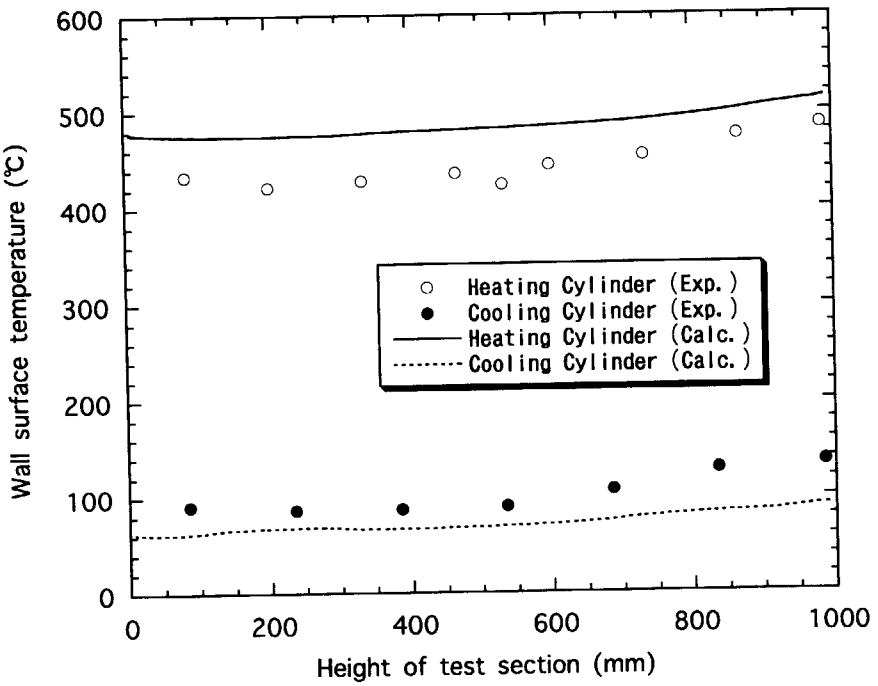

Fig. 28 Comparison of the calculated temperature on the heated and cooled wall surfaces with the experimental results for filling with He and the heat input of 12A.

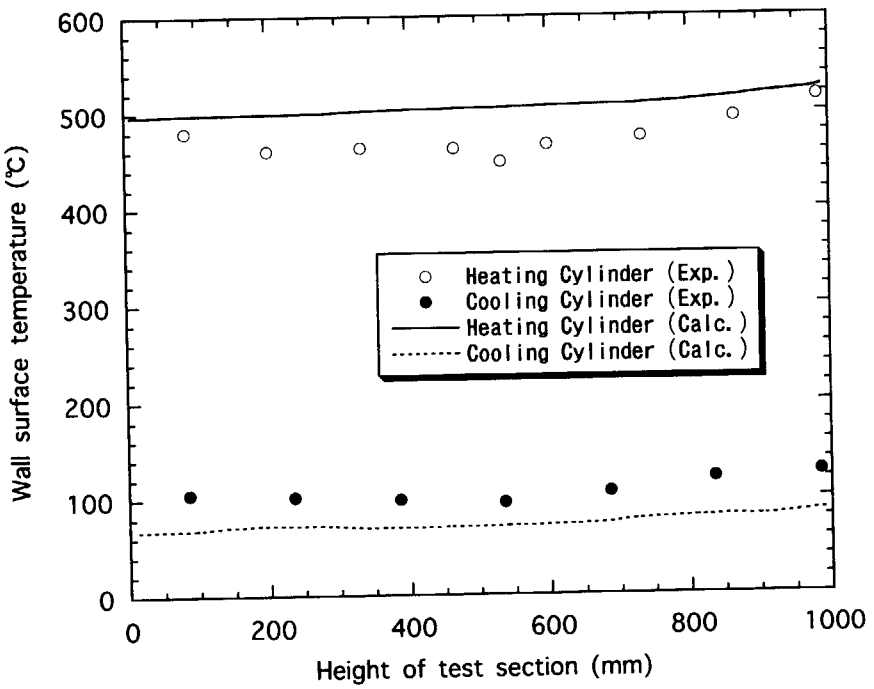

Fig. 29 Comparison of the calculated temperature on the heated and cooled wall surfaces with the experimental results for filling with N_2 and the heat input of 12A.

This is a blank page.

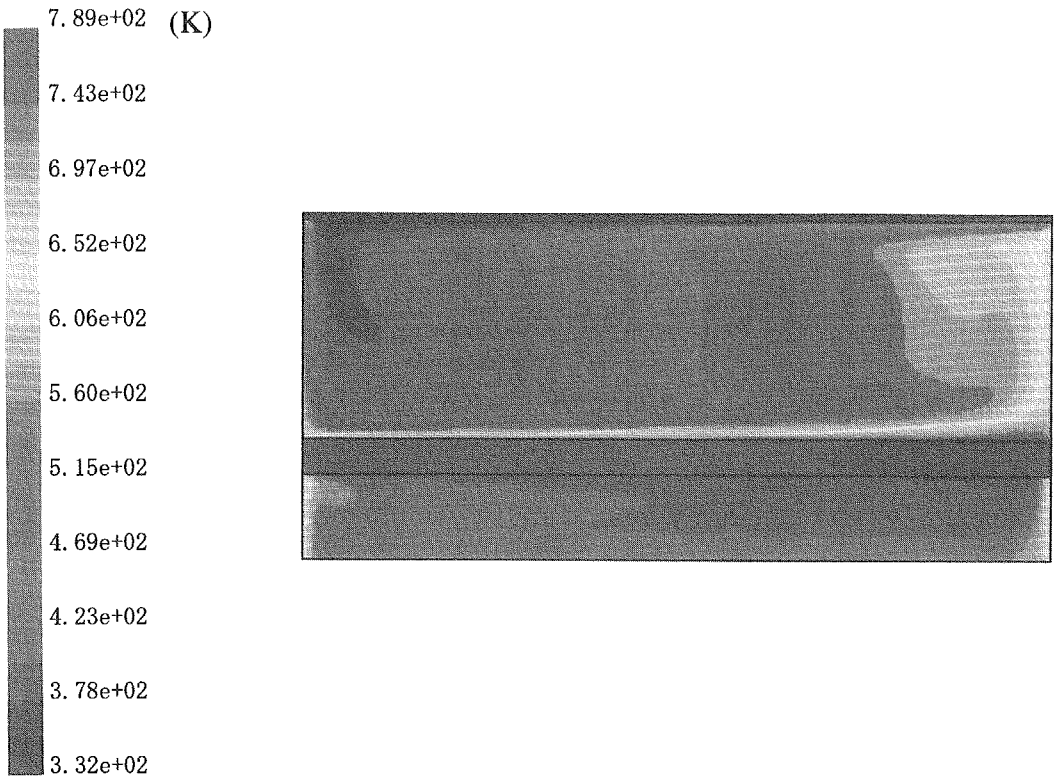

Fig. 30 Contours of static temperature for filling with He and the heat input of 12A.

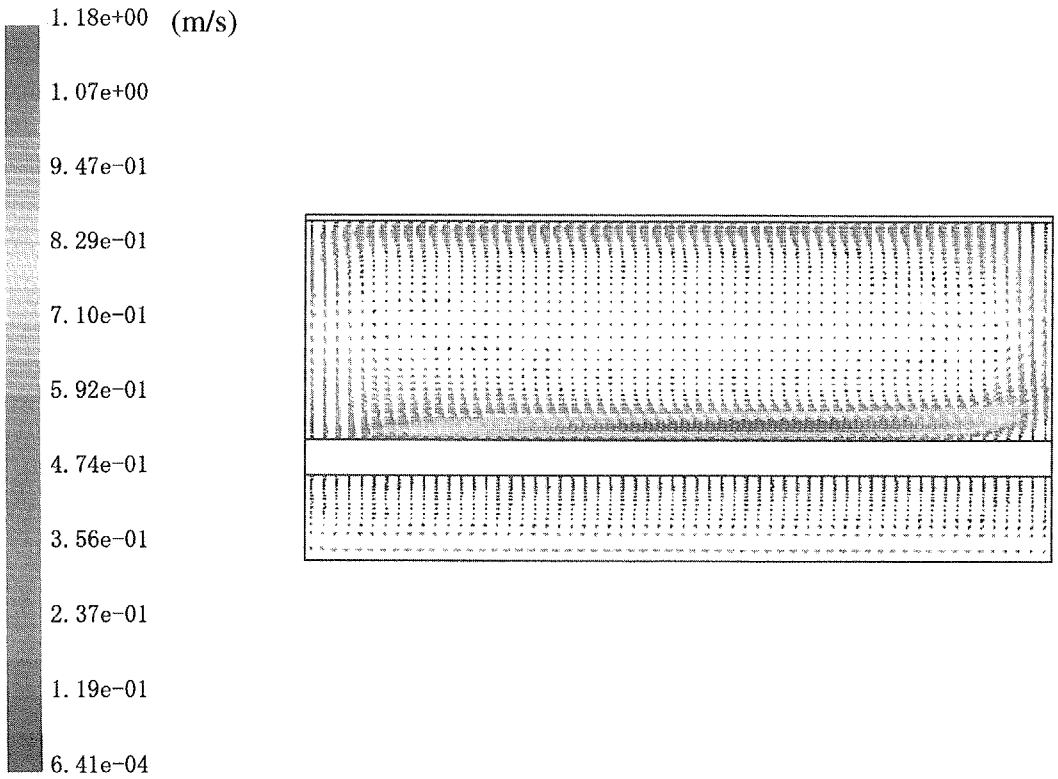

Fig. 31 Velocity vectors colored by velocity magnitude for filling with He and the heat input of 12A.

This is a blank page.

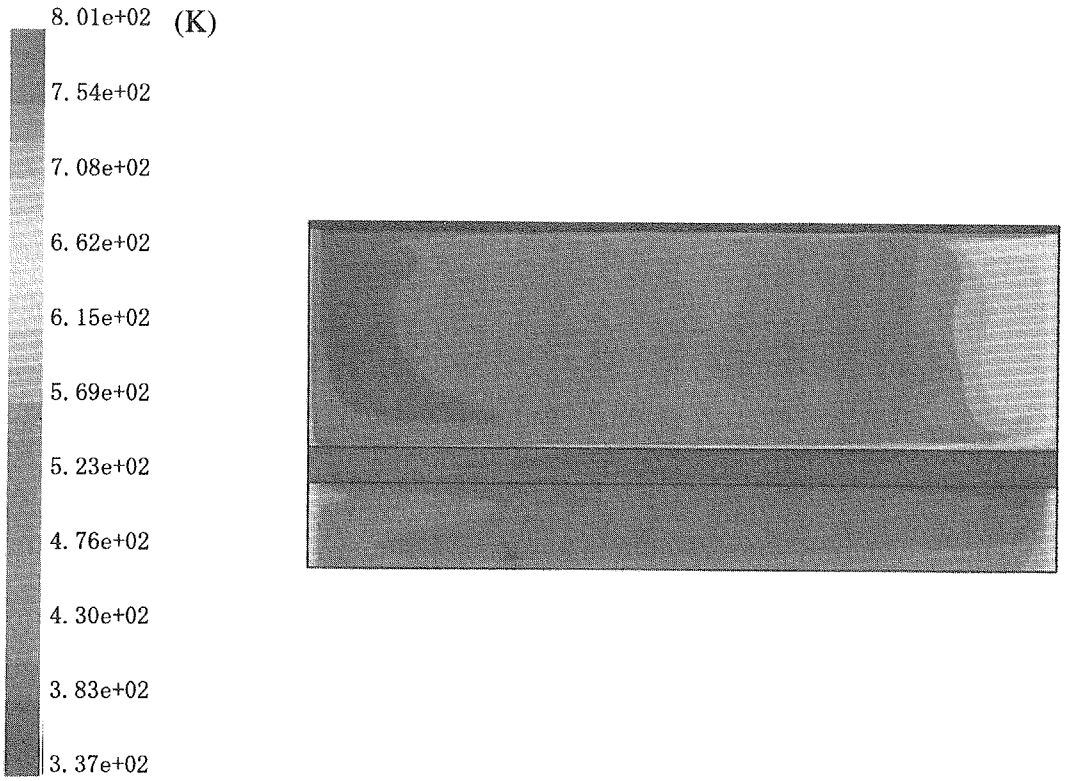

Fig. 32 Contours of static temperature for filling with N_2 and the heat input of 12A .

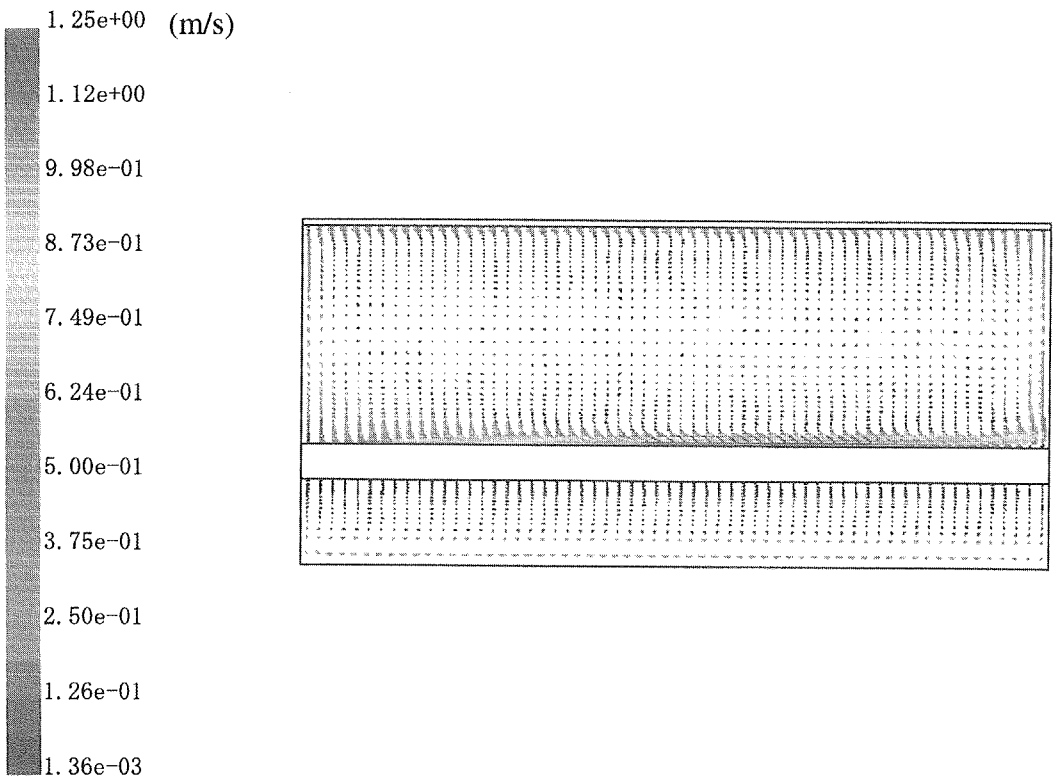

Fig. 33 Velocity vectors colored by velocity magnitude for filling with N_2 and the heat input of 12A.

This is a blank page.

5. Conclusions

We carried out the experiments and the numerical analyses on natural convection heat transfer coupled with thermal radiation in order to investigate heat transfer characteristics in vertical annular space of a double coaxial cylinder and the effect of the thermal radiation on the transferred heat. The following conclusions were obtained:

(1) The Nusselt number for natural convection without the effect of the thermal radiation was in agreement with the previous reported Nusselt number.

(2) The correlation about the Nusselt number coupled with thermal radiation in the vertical annular enclosure was proposed as the following relationship:

$$Nu_{all}(d) = \frac{Nu_c(d)}{1 - R_r} \qquad (6.8 \times 10^5 < Ra(d) < 1.0 \times 10^8) \ .$$

We gave the following equations for the present experimental conditions:

$$Nu_c(d) = 0.280\ Ra(d)^{0.25}(l/d)^{-0.25}$$

$$R_{r,exp.} = \frac{f_{r,exp.} \cdot (T_1^4 - T_2^4)}{q_{all}} = 3.204 \times 10^{-2} (T_1^4 - T_2^4)^{0.1235} .$$

We suggested the following equations as the general form for the vertical annular enclosure:

$$Nu_c(d) = 0.745\ Ra(d)^{0.25}(l/d)^{-0.25}$$

$$R_{r,calc.} = f_{r,calc.} \cdot (T_1^4 - T_2^4) / \left(\frac{Q}{A_2}\right) = A_1 \cdot \frac{1}{\frac{1}{\varepsilon_1} + \left(\frac{1}{\varepsilon_2} - 1\right)\frac{A_1}{A_2}} \cdot \sigma (T_1^4 - T_2^4)/Q .$$

(3) The ratio of the heat transferred by thermal radiation to the heat transferred by natural convection coupled with thermal radiation was 79% based on $f_{r,exp.}$ and 45% based on $f_{r,calc.}$ when the heated wall surface temperature was about 400°C.

(4) The numerical results were in good agreement with the experimental ones regarding the heated and cooled wall surface temperature.

(5) We carried out the numerical analyses under the same condition as the present experiments. However, in order to obtain the correct relationship between the Nusselt number and the Rayleigh number including the effect of thermal radiation under the high temperature condition, it is necessary to carry out the numerical analyses changed parameters such as the emissivities in future studies.

Acknowledgements

The authors would like to acknowledge the valuable discussions and comments provided by Dr. Shiina, Mr. Zhang and Mr. Miyamoto.

References

(1) Zhang, Y., Takeda, T. and Inaba, Y. : Study on natural convection heat transfer in a vertical enclosure of double coaxial cylinder —Cooling by natural circulation of air—. JAERI-Tech 2000-065 (2000).

(2) de Vahl Davis, G. and Thomas, R.W. : Natural convection between concentric vertical cylinders. *Phys. Fluids, suppl.*2 (1969), 198—207.

(3) JSME : *JSME Mechanical Engineers' Handbook* (1987), A6-127.

(4) JSME : *JSME Data Book, Heat Transfer*, 4th edition (1986), 328.

(5) Eckert, E. W. G. and Carlson, W. O. : Natural convection in an air layer enclosed between two vertical plates with different temperatures. *Int. J. Heat and Mass Transfer*, **2** (1961), 106—120.

(6) Elder, J. W. : Numerical experiments with free convection in a vertical slot. *J. Fluid Mech.*, **24** (1966), 823—843.

(7) Newell, M. E. and Schmidt, F. W. : Heat transfer by laminar natural convection with rectangular enclosures. *J. Heat Transfer*, **92** (1970), 159—168.

(8) Gill, A. E. : The boundary-layer regime for convection in a rectangular cavity. *J. Fluid Mech.*, **26** (1966), 515—536.

(9) Bejan, A. : Note on Gill's solution for free convection in a vertical enclosure. *J. Fluid Mech.*, **90** (1979), 561—568.

Appendix-1: Thermal conduction analysis of thermocouple

We carry out a numerical analysis in order to confirm that the deviation of the measured temperature caused by the method of fixing the thermocouples to the walls is small. The thermocouples are fixed to the walls by SUS bands.

In this numerical analysis, the CFD code FLUENT/UNS is used and only the energy equation Eq. (38) is solved. A thermocouple on the inner surface of the cooling cylinder is modeled for the analysis because the measurement error of the thermocouple may be a great influence on the experimental data arrangement.

(1) Analytical model and boundary conditions

Figure A-1 shows the analytical model and the boundary conditions in this analysis. The analytical model has two-dimension. The model consists of a SUS band, a thermocouple and a part of the cooling cylinder. The outer surface of the SUS-band is heated by constant heat flux, which is adjusted so that the temperature of the point 2 in Fig. A-1 is in agreement with the experimental value. The bottom surface of the cooling cylinder is a fixed temperature, which is in agreement with the experimental value. Thermal resistance between the SUS band, the thermocouple and the cooling cylinder is considered.

(2) Results and discussion

The numerical analysis is conducted for the experimental condition of 14A-heat input filled with He. The calculated temperature is 402.15K at the point 1, 401.75K at the point 2 (experimental value) and 401.35K at the point 3 in Fig. A-1. The temperature difference between the point 2 and the other points is 0.4K and it is very small.

Appendix-2: Comparison of crrelations

Comparison of Eqs. (31) and (34) with the correlation suggested in Ref. (1) is shown in Fig. A-2. The correlation is given by

$$Nu_{all}(d) = \frac{0.225\,Ra(d)^{0.25}(l/d)^{-0.25}}{1-5.442\times10^{-3}\left(T_1^4-T_2^4\right)^{0.191}} \qquad (5.6\times10^5 < Ra(d) < 1.04\times10^8)\ . \tag{A1}$$

Appendix-3: Calculated temperature in other conditions

Figures A-3 through A-10 compare the calculated temperature on the heated and cooled wall surfaces with the experimental results for filling with He or N_2 and the different heat input (6.5A, 8A, 10A, 14A), respectively.

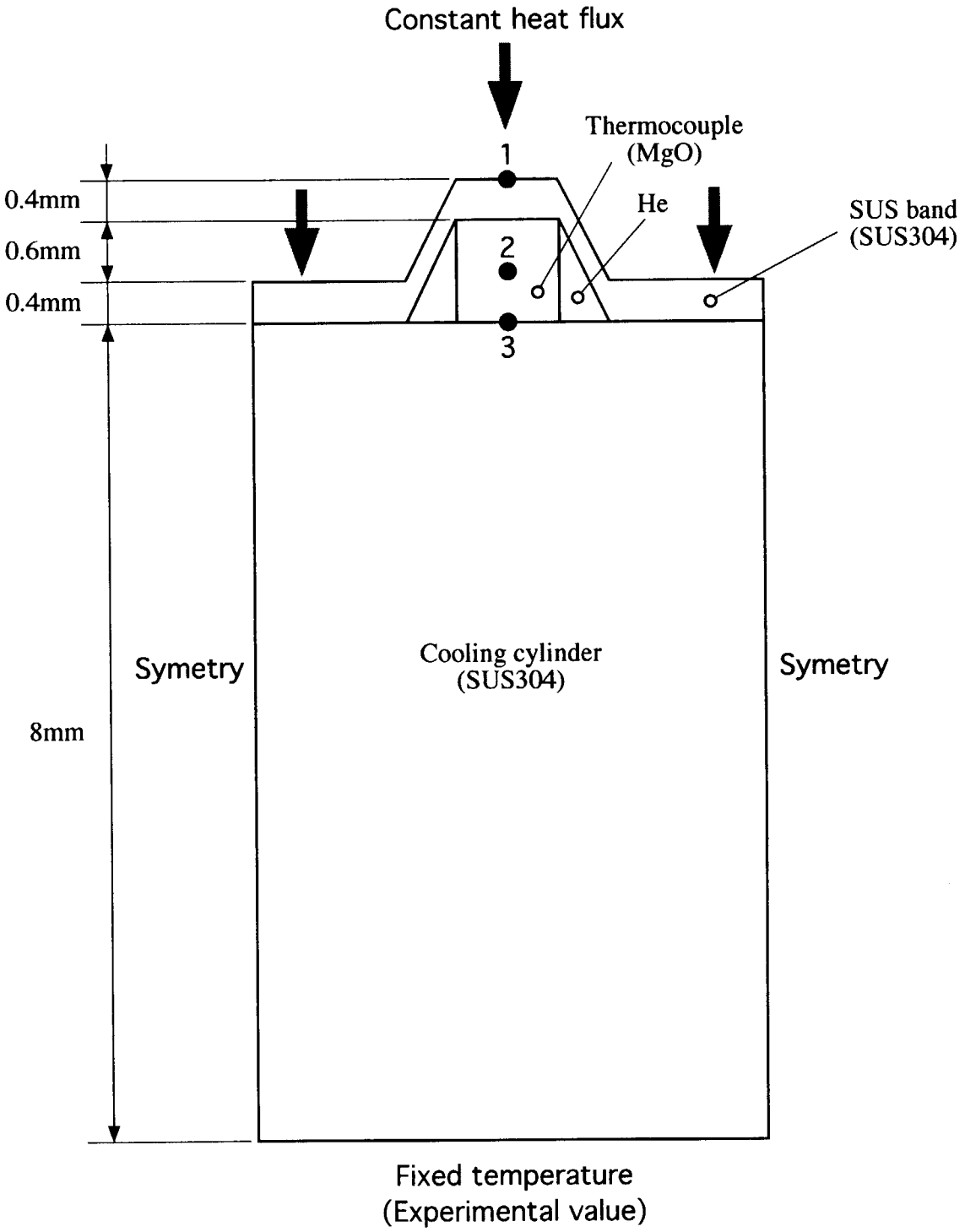

Fig. A-1 Analytical model and boundary conditions.

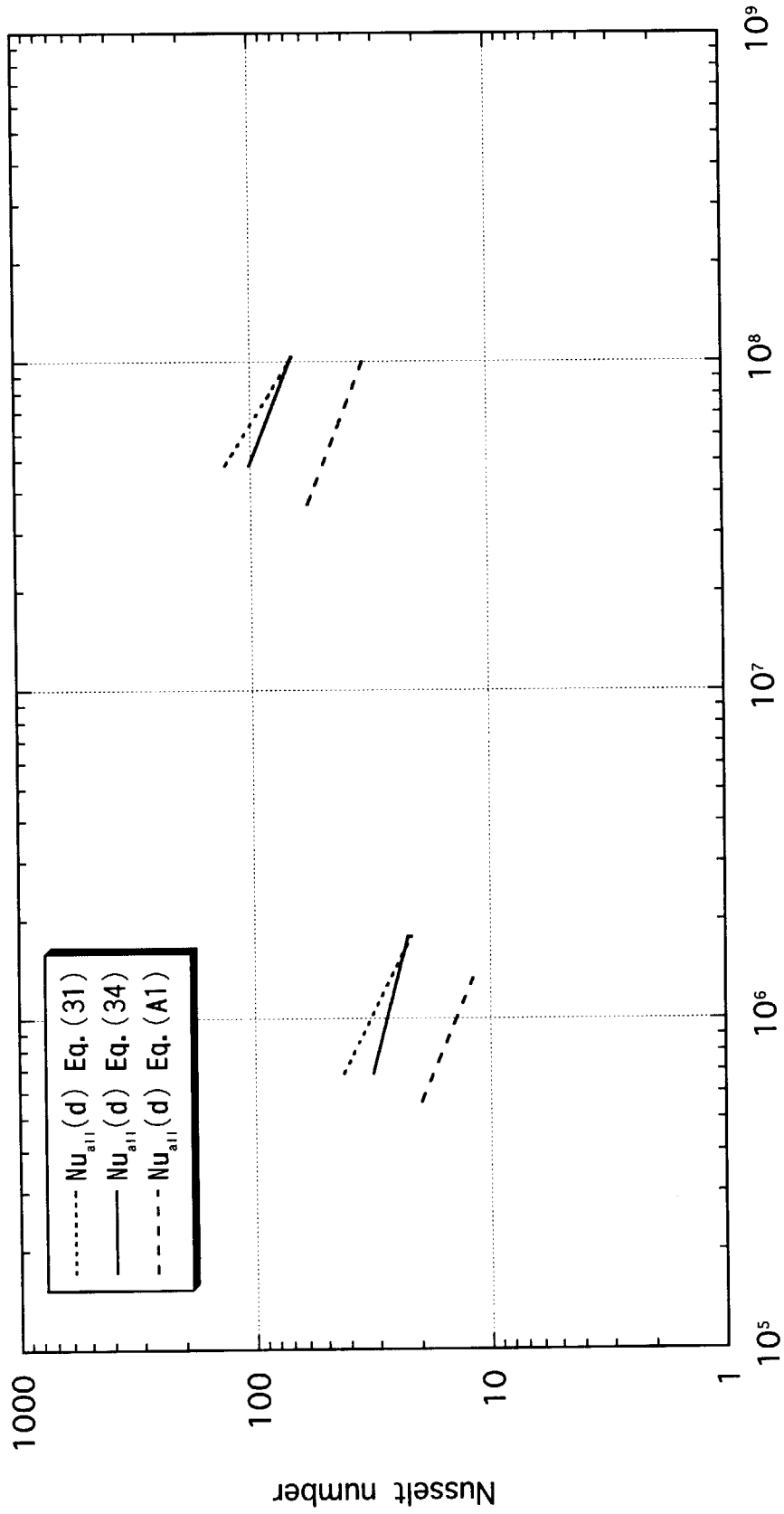

Fig. A-2 Comparison of the correlations between the Nusselt number and the Rayleigh number.

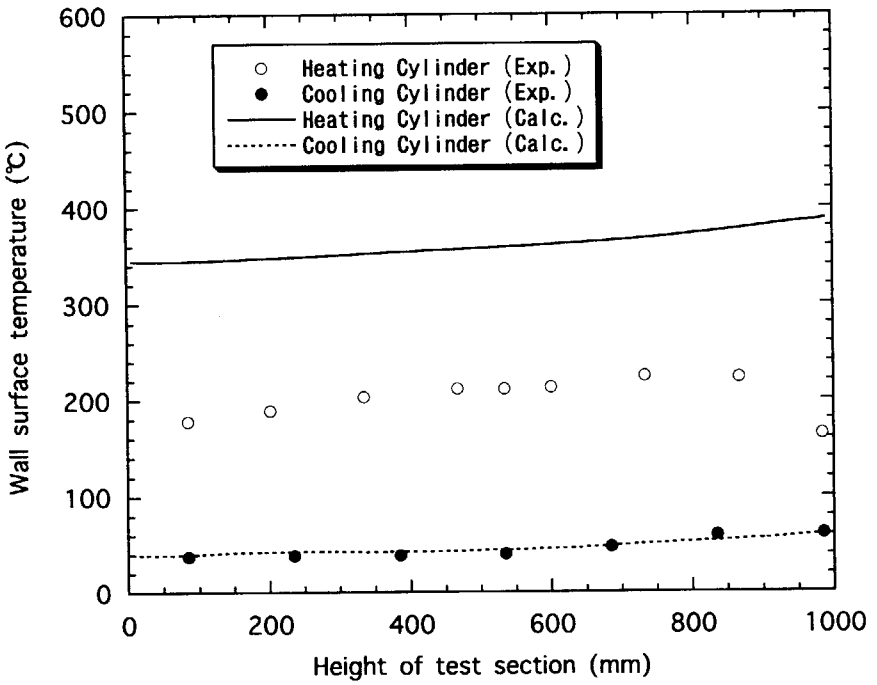

Fig. A-3 Comparison of the calculated temperature on the heated and cooled wall surfaces with the experimental results for filling with He and the heat input of 6.5A.

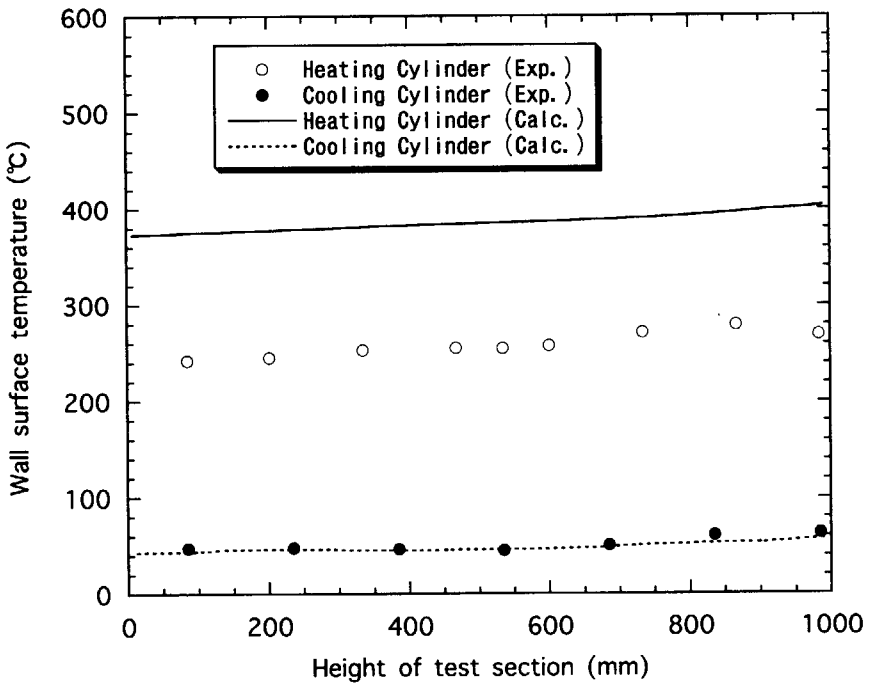

Fig. A-4 Comparison of the calculated temperature on the heated and cooled wall surfaces with the experimental results for filling with N_2 and the heat input of 6.5A.

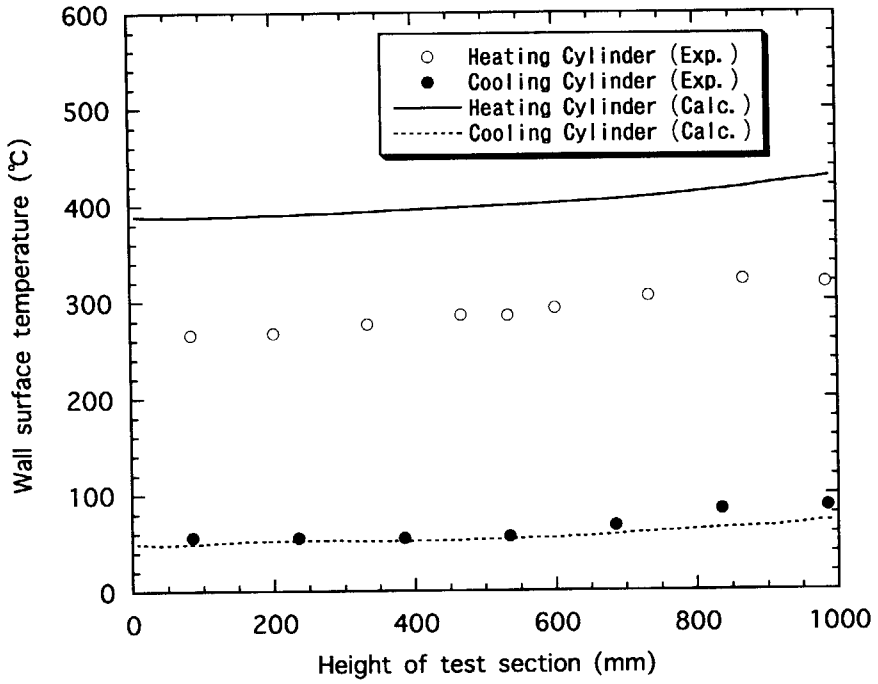

Fig. A-5 Comparison of the calculated temperature on the heated and cooled wall surfaces with the experimental results for filling with He and the heat input of 8A.

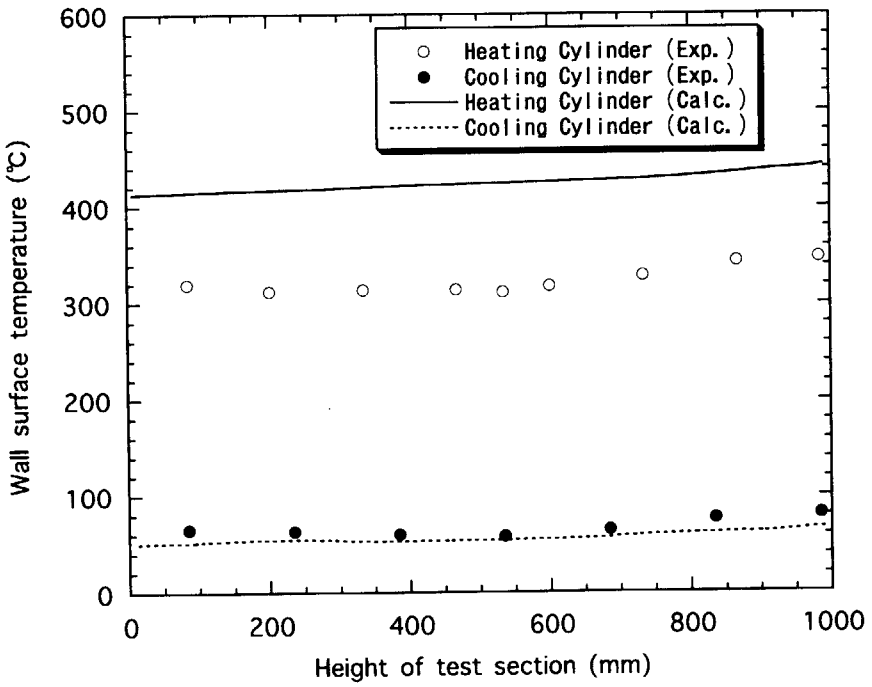

Fig. A-6 Comparison of the calculated temperature on the heated and cooled wall surfaces with the experimental results for filling with N_2 and the heat input of 8A.

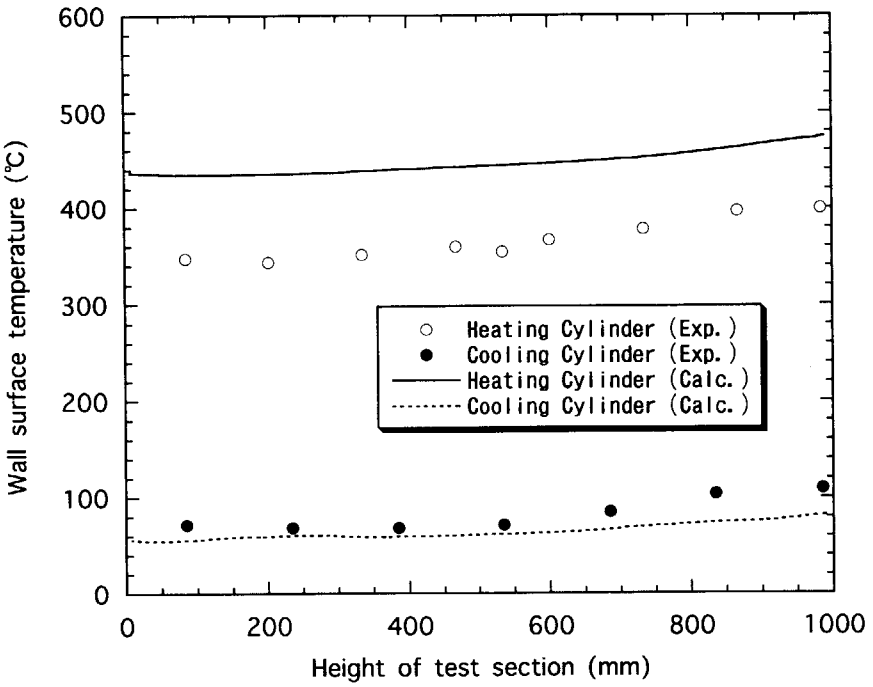

Fig. A-7 Comparison of the calculated temperature on the heated and cooled wall surfaces with the experimental results for filling with He and the heat input of 10A.

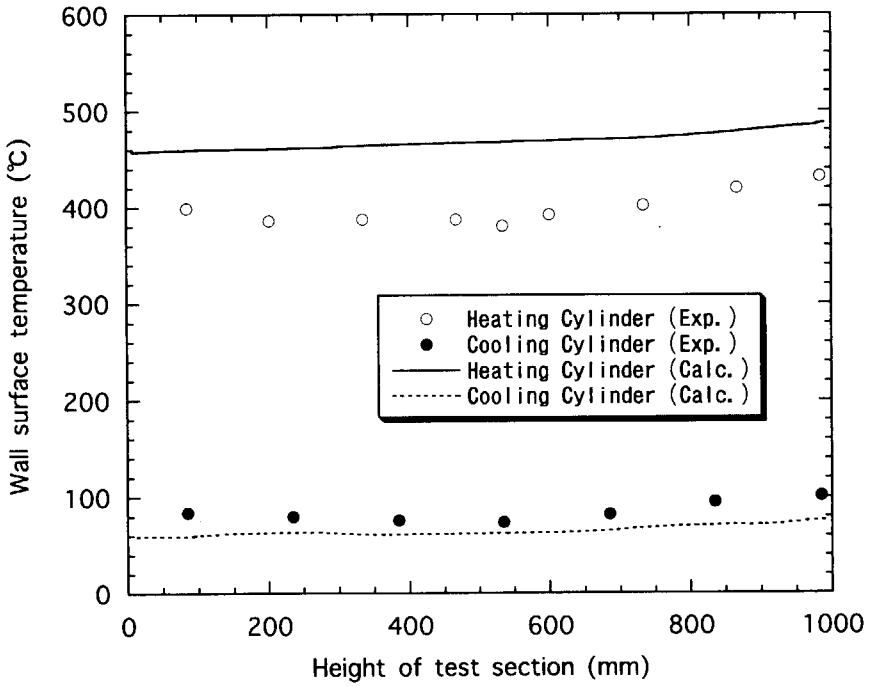

Fig. A-8 Comparison of the calculated temperature on the heated and cooled wall surfaces with the experimental results for filling with N_2 and the heat input of 10A.

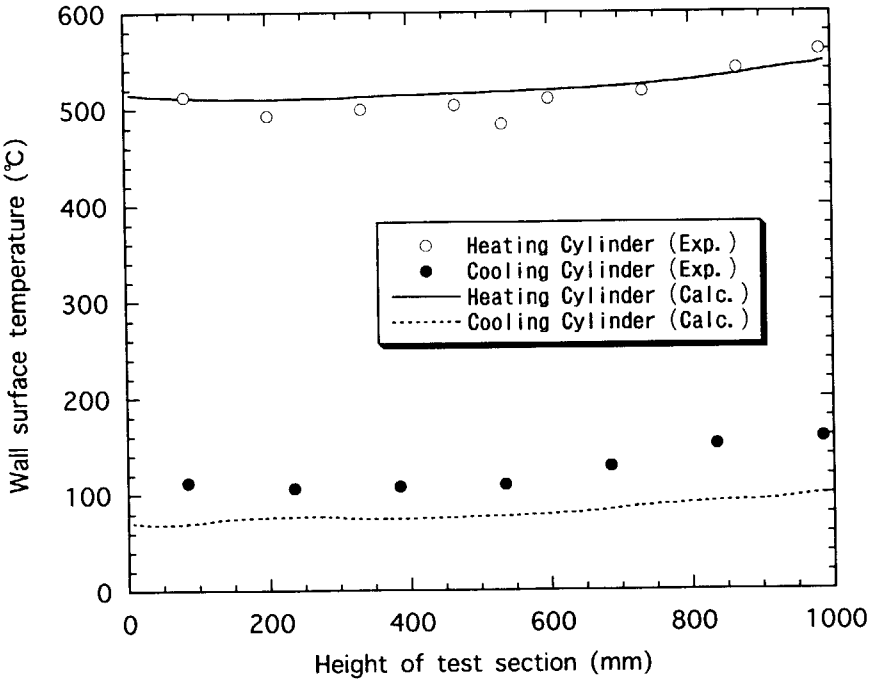

Fig. A-9 Comparison of the calculated temperature on the heated and cooled wall surfaces with the experimental results for filling with He and the heat input of 14A.

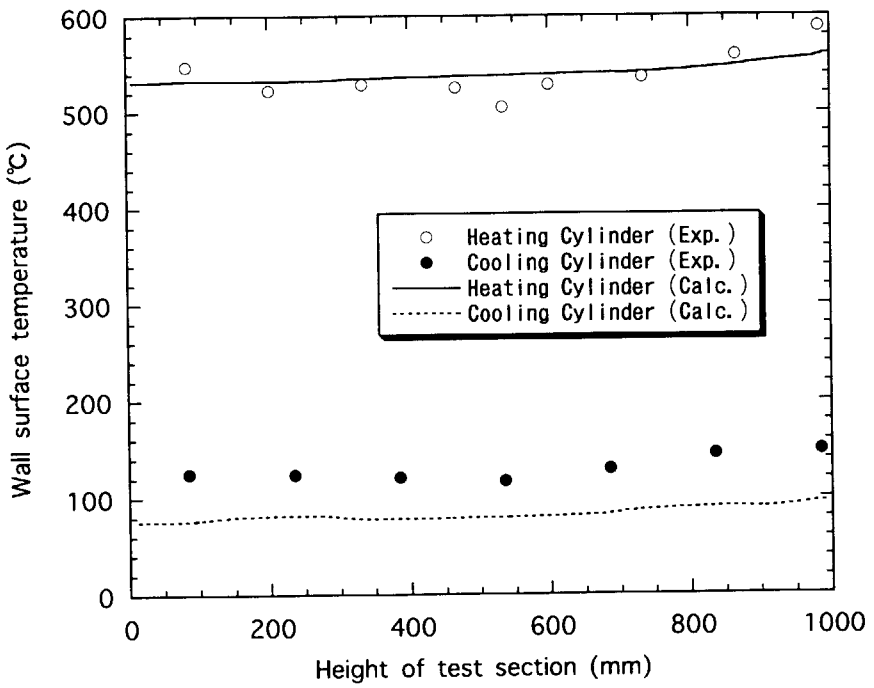

Fig. A-10 Comparison of the calculated temperature on the heated and cooled wall surfaces with the experimental results for filling with N_2 and the heat input of 14A.

This is a blank page.

国際単位系（SI）と換算表

表1　SI基本単位および補助単位

量	名称	記号
長さ	メートル	m
質量	キログラム	kg
時間	秒	s
電流	アンペア	A
熱力学温度	ケルビン	K
物質量	モル	mol
光度	カンデラ	cd
平面角	ラジアン	rad
立体角	ステラジアン	sr

表2　SIと併用される単位

名称	記号
分，時，日	min，h，d
度，分，秒	°，′，″
リットル	l，L
トン	t
電子ボルト	eV
原子質量単位	u

1 eV=1.60218×10^{-19}J

1 u=1.66054×10^{-27}kg

表5　SI接頭語

倍数	接頭語	記号
10^{18}	エクサ	E
10^{15}	ペタ	P
10^{12}	テラ	T
10^{9}	ギガ	G
10^{6}	メガ	M
10^{3}	キロ	k
10^{2}	ヘクト	h
10^{1}	デカ	da
10^{-1}	デシ	d
10^{-2}	センチ	c
10^{-3}	ミリ	m
10^{-6}	マイクロ	μ
10^{-9}	ナノ	n
10^{-12}	ピコ	p
10^{-15}	フェムト	f
10^{-18}	アト	a

表3　固有の名称をもつSI組立単位

量	名称	記号	他のSI単位による表現
周波数	ヘルツ	Hz	s^{-1}
力	ニュートン	N	$m\cdot kg/s^2$
圧力，応力	パスカル	Pa	N/m^2
エネルギー，仕事，熱量	ジュール	J	N·m
工率，放射束	ワット	W	J/s
電気量，電荷	クーロン	C	A·s
電位，電圧，起電力	ボルト	V	W/A
静電容量	ファラド	F	C/V
電気抵抗	オーム	Ω	V/A
コンダクタンス	ジーメンス	S	A/V
磁束	ウェーバ	Wb	V·s
磁束密度	テスラ	T	Wb/m^2
インダクタンス	ヘンリー	H	Wb/A
セルシウス温度	セルシウス度	℃	
光束	ルーメン	lm	cd·sr
照度	ルクス	lx	lm/m^2
放射能	ベクレル	Bq	s^{-1}
吸収線量	グレイ	Gy	J/kg
線量等量	シーベルト	Sv	J/kg

表4　SIと共に暫定的に維持される単位

名称	記号
オングストローム	Å
バーン	b
バール	bar
ガル	Gal
キュリー	Ci
レントゲン	R
ラド	rad
レム	rem

1 Å=0.1nm=10^{-10}m

1 b=100fm^2=10^{-28}m^2

1 bar=0.1MPa=10^{5}Pa

1 Gal=1cm/s^2=10^{-2}m/s^2

1 Ci=3.7×10^{10}Bq

1 R=2.58×10^{-4}C/kg

1 rad=1cGy=10^{-2}Gy

1 rem=1cSv=10^{-2}Sv

(注)

1．表1－5は「国際単位系」第5版，国際度量衡局1985年刊行による。ただし，1 eVおよび1 uの値はCODATAの1986年推奨値によった。

2．表4には海里，ノット，アール，ヘクタールも含まれているが日常の単位なのでここでは省略した。

3．barは，JISでは流体の圧力を表わす場合に限り表2のカテゴリーに分類されている。

4．EC閣僚理事会指令ではbar，barnおよび「血圧の単位」mmHgを表2のカテゴリーに入れている。

換算表

力	N(=10^{5}dyn)	kgf	lbf
	1	0.101972	0.224809
	9.80665	1	2.20462
	4.44822	0.453592	1

粘度　1 Pa·s(N·s/m^2)=10 P(ポアズ)(g/(cm·s))

動粘度　1m^2/s=10^{4}St(ストークス)(cm^2/s)

圧力	MPa(=10bar)	kgf/cm^2	atm	mmHg(Torr)	lbf/in^2(psi)
	1	10.1972	9.86923	7.50062×10^3	145.038
	0.0980665	1	0.967841	735.559	14.2233
	0.101325	1.03323	1	760	14.6959
	1.33322×10^{-4}	1.35951×10^{-3}	1.31579×10^{-3}	1	1.93368×10^{-2}
	6.89476×10^{-3}	7.03070×10^{-2}	6.80460×10^{-2}	51.7149	1

エネルギー・仕事・熱量	J(=10^7 erg)	kgf·m	kW·h	cal(計量法)	Btu	ft·lbf	eV
	1	0.101972	2.77778×10^{-7}	0.238889	9.47813×10^{-4}	0.737562	6.24150×10^{18}
	9.80665	1	2.72407×10^{-6}	2.34270	9.29487×10^{-3}	7.23301	6.12082×10^{19}
	3.6×10^6	3.67098×10^5	1	8.59999×10^5	3412.13	2.65522×10^6	2.24694×10^{25}
	4.18605	0.426858	1.16279×10^{-6}	1	3.96759×10^{-3}	3.08747	2.61272×10^{19}
	1055.06	107.586	2.93072×10^{-4}	252.042	1	778.172	6.58515×10^{21}
	1.35582	0.138255	3.76616×10^{-7}	0.323890	1.28506×10^{-3}	1	8.46233×10^{18}
	1.60218×10^{-19}	1.63377×10^{-20}	4.45050×10^{-26}	3.82743×10^{-20}	1.51857×10^{-22}	1.18171×10^{-19}	1

1 cal= 4.18605J（計量法）

= 4.184J（熱化学）

= 4.1855J（15℃）

= 4.1868J（国際蒸気表）

仕事率　1 PS(仏馬力)

= 75 kgf·m/s

= 735.499W

放射能	Bq	Ci
	1	2.70270×10^{-11}
	3.7×10^{10}	1

吸収線量	Gy	rad
	1	100
	0.01	1

照射線量	C/kg	R
	1	3876
	2.58×10^{-4}	1

線量当量	Sv	rem
	1	100
	0.01	1

(86年12月26日現在)

Study on Natural Convection Heat Transfer in Vertical Annular Space of a Double Coaxial Cylinder